UNIVERSITY OF INSUBRIA

VARESE

DEPARTMENT OF SURGICAL AND MORPHOLOGICAL SCIENCES

Coordination between intrinsic and extrinsic mechanisms in thoracic lymphatics

candidate:

ELEONORA SOLARI

matr. 612499

PhD PROGRAM IN CLINICAL AND EXPERIMENTAL PHYSIOLOGY

XXV CYCLE

SCHOOL OF BIOLOGICAL AND MEDICAL SCIENCES

tutor : PROF. DANIELA NEGRINI

academic Year 2011 – 2012

Table of Contents

Abstract

The lymphatic system runs in parallel with the blood vasculature, it plays a key role in maintaining tissue fluid homeostasis, as a tissue-drainage system, and it contributes to the immunosurveillance by providing a route for migrating cells. The lymphatic system is a highly branched network of thin-walled blind-ended vessels, which drain fluid, macromolecules and cells from the extracellular spaces within most organs, carrying them into larger thicker-walled collectors running deeper in the body. Fluid and solutes extravasated from vascular capillaries into the interstitial space enter blind-ended initial lymphatics, which are anchored to the interstitial matrix via anchoring filaments and possess overlapping endothelial cell-cell junctions behaving like valve structures, only permitting unidirectional lymph entry into the lymphatic vessel lumen. Valves in collecting lymphatics consist of two modified adjacent endothelial cell leaflets which meet in the vessel lumen forming a funnel inside the vessel and separating adjacent lymphangions, the functional units of the lymphatic system. Lymph is formed along a hydraulic pressure gradient developing between the interstitial tissue and the lumen of initial lymphatics. This pressure gradient depends upon both extrinsic and intrinsic pump systems. Tissue movements provide the extrinsic factor affecting lymphatic function, causing cycles of external compression/expansion of the lymphatic vessels lumen.. Lymphangions, segments of lymphatic vessel delimited by unidirectional valves and surrounded by smooth muscle cells, represent the functional units of the intrinsic pump mechanism. Their rhythmic active contraction is essential to guarantee the correct lymph flow either as the only source of pressure gradient formation or along with the extrinsic pump, where the mechanical features of the surrounding tissue are able to generate such an external pump action. During active contraction, lymphatic smooth muscle cells create an increase in intraluminal pressure and generate a local positive

pressure gradient which drives lymph propulsion. The subsequent relaxation of the smooth muscle layer generates a decrease in intraluminal pressure which drives lymph from the interstitial space into the vessel itself.

The aim of the present thesis was to study the interaction between the intrinsic and extrinsic mechanisms in a highly moving tissue such as the diaphragm. By *in vivo* fluorescence staining of diaphragmatic lymphatics we were able to identify vessels organized in loop structures and located both in the tendineous and in the peripheral muscle region. Lymphatic loops were classified into four groups (active, hybrid, passive and invariant) according to their functional behavior, forming functionally distinct regions. By whole mount immunostaining against smooth muscle actin we identified a dense smooth muscle mesh surrounding actively pumping sites, whereas in not contracting tracts smooth muscle fibers were more sparsely organized, showing a lot of large gaps around the vessel wall. Actively pumping lymphatic sites did not differ in diameter from all other classes of vessels. We found that their amplitude of contraction was independent on vessel size but strongly correlated to contraction frequency. By temporal analysis we were also able to identify trigger sites which controlled the diameter change of both other active and passive sites belonging to the same network. We then made an extensive study on the temporal correlation of activity among active, hybrid and passive sites belonging to the same network, and were able to identify trigger regions and follower regions whose behavior was dependent upon their respective trigger sites

Lastly, we started an ongoing project in order to understand the extrinsic pump effect due to respiratory and cardiogenic movements on diaphragmatic lymphatic function. By locally injecting KCl into the interstitium next to invariant longitudinal and/or transverse lymphatics we tested diameter and/or length changes and then intraluminal

pressure gradients due to extrinsic forces. Further analysis are required in order to define the actual contribution of intrinsic and extrinsic mechanisms in diaphragmatic lymphatics.

1. Introduction

1.1 The Lymphatic System

In vertebrates, two specialized vascular systems have been developed for effective circulation: the blood vasculature, which delivers oxygen and nutrients and carries away waste products for detoxification, and the lymphatic vasculature, which returns the interstitial protein-rich fluid (*lymph*) to the bloodstream (Fig 1.1). In fact, as the complexity of the blood circulatory system increased among higher species in the phylogenetic tree, an additional mechanism to clear the tissues from substances not absorbed by the blood vascular system has become necessary (1). In teleost fishes, two groups of lymphatic vessels can be identified, however, these vessels only occasionally have lymph hearts and lack lymphatic unidirectional valves. Lymph hearts, which are enlarged portions of lymphatic vessels, posses contractile elements in their vessel wall and consequently pulsatile function. The lymphatic vessels are endowed with unidirectional valves in their walls in order to prevent fluid backflow and to force lymph into the network and then in the veins. Similarly, amphibians and reptiles exhibit a pattern of longitudinal lymphatic vessels and most primitive amphibians also have a pair of lymph hearts per body segment. Advanced amphibians such as frogs have fewer lymph hearts, and amniotes, such as reptiles, birds and mammals, have a dramatically decreased number of these structures (1). Transient rudimentary lymph hearts are present in a few species of birds, but they are absent in most birds and mammals. Mammals and some birds which are mainly aquatic possess lymph nodes (2).

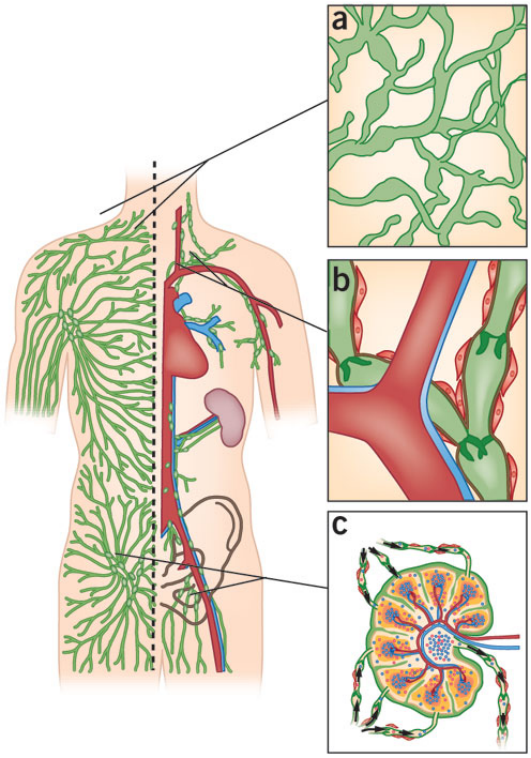

Figure 1.1 The lymphatic system. It consists of a complex network of blind-ended capillaries (**a**) which drain lymph and collecting vessels (**b**) which return it back to the venous system. Lymphoid organs are also very important, such as lymph nodes which act as filters. Redrawn from (3).

1.1.1 Embryogenesis of the Lymphatic System

The blood circulatory system is the first functional system formed during embryonic development. In vertebrates, the lymphatic vasculature appears once the blood vasculature has formed, thus supporting the hypothesis that lymphatics have a blood vascular origin (4; 5). During embryonic vasculogenesis angioblasts, the endothelial cells precursors which would form the line of blood vessels, originate from mesoderm-derived progenitor cells called hemangioblasts (6). They aggregate to form the primary blood islands: cells in the interior of the island differentiate into hematopoietic ones, and those in the periphery differentiate into angioblasts, which will further differentiate into the developing head mesenchyma. They then cluster and reorganize to form a network of primitive capillary-like structures, later remodeled during angiogenesis,

when new arteries and veins form. Angiogenesis consists in vessels sprouting, due to extracellular matrix disruption by endothelial cells migrating and proliferating into the perivascular space (7), or by splitting from preexisting capillaries and postcapillary venules (8). The newly formed blood vessels are stabilized by pericytes, smooth muscle cells and a basal lamina. The process of vasculogenesis is restricted to the early stages of embryonic development, whereas postnatal angiogenesis occurs during physiologic and pathologic neovascularization. In adults, physiologic angiogenesis occurs during the female reproductive cycle and in wound healing (9), whereas pathologic angiogenesis is involved in a variety of disorders, such as tumor growth and metastasis, diabetic retinopathy, rheumatoid arthritis, cardiovascular diseases and psoriasis (10). Two theories are proposed about lymphatic development: the first suggests that lymphatic endothelium derives from the blood venous one (*centrifugal theory*) whereas the latter suggests that lymphatic endothelium differentiates *in situ* from primitive mesenchyma (*centripetal theory*) and then acquires connections with the blood vascular system, at a limited number of sites (11). The most accepted model indicates that venous identity is the endothelial cells default status and, subsequently, VEGF (12; 13; 14; 15) and Notch (16; 17) signaling determine arterial fate, resulting in the separation of arterial and venous endothelium via ephrinB2/EphB4 signaling (18; 19). This model defines the lymphatic system developing from isolated primitive lymphatic sacs originating from venous endothelial cells, spreading by these cells which proliferate into the surrounding tissues, where peripheral lymphatic capillaries form (4; 5).

The blood vasculature system alone is not able to initiate lymphatic vasculature development and some additional gene products have to be expressed by venous endothelium to become progressively able to respond to local lymphatic-inducing signals (Fig 1.2). Although the molecular key defining the start of lymphatic endothelial

cells differentiation has not yet been clearly identified, the expression of the lymphatic vessel endothelial hyaluronan receptor 1 (Lyve1, a CD44 homologue and hyaluronan receptor; (20)) by a few cells of the endothelium lining the anterior cardinal vein (in mice at E9.0 – 9.5) is commonly considered the first molecular indication that venous endothelial cells are able to respond to a lymphatic-inducing signal (21). In fact, in mice a few hours after Lyve1 expression in the anterior cardinal vein, the transcription factor Prospero-related homeobox 1 (Prox1) can also be found (22). Then, the Prox1-expressing endothelial cells progenitors start to bud from veins in a polarized manner and, subsequently, these cells proliferate and migrate to form embryonic lymphatic sacs and the lymphatic vascular network. Indeed, Prox1 expression in the venous endothelium provides strong support for the model of a venous origin of the lymphatic vasculature (19). In fact, the critical role in lymphatic development played by Prox1 has been also confirmed by the evidence that $Prox1^{-/-}$ mouse embryos display multiple phenotypic abnormalities, including the complete absence of lymphatic vessels due to failure in lymphatic specification (23), and die around mid-gestation (22). Because endothelial cells budded from the anterior cardinal vein at E11.0 – 11.5 do not express lymphatic markers, whereas they express blood vascular ones (23), Prox1 activity is supposed to be required and sufficient to confer the lymphatic endothelial phenotype on progenitors cells located in the embryonic veins, which would otherwise remain as blood vascular endothelial ones (21; 23). Prox1 can be definitely considered as a master control gene inducing the lymphatic phenotype: in fact *in vitro* studies also show that Prox1 overexpression is sufficient to reprogram cultured blood endothelial cells into lymphatic ones (24; 25), acting as a repressor of about 40% of blood-specific markers and inducing the expression of about 20% of the lymphatic-specific genes.

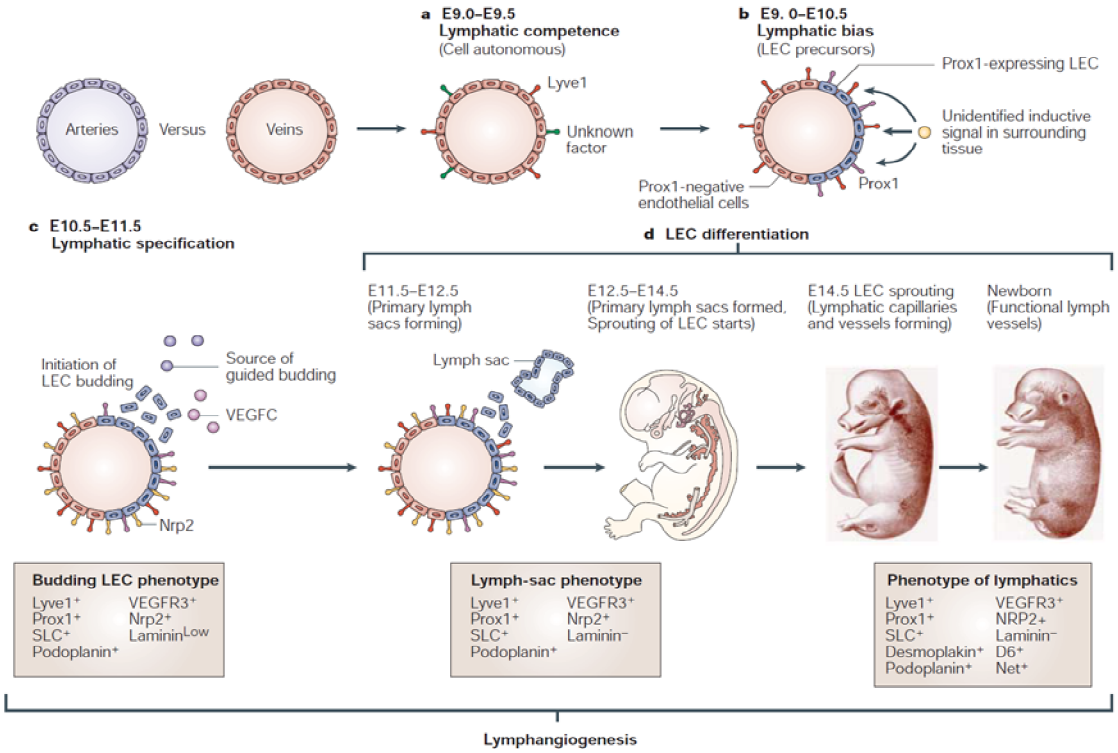

Figure 1.2 The model for lymphatic vasculature development. **A** Lymphatic competence is the autonomous ability of venous endothelial cells to respond to a specific, inductive signal; this stage is characterized, for example, by the appearance of Lyve1 expressing cells. **B** Lymphatic differentiation is eventually lost in other venous endothelial cells: Prox1 might be crucial for this step. **C** Lymphatic specification occurs independently to venous endothelial cells one. **D** Finally, lymphatic vessel differentiation and maturation occur in a stepwise manner leading to the synthesis of all of the main lymphatic system components. Redrawn from (21).

Early during mouse development, VEGFR-3 (Vascular endothelial growth factor-3, receptor for VEGF-C and VEGF-D, which are growth factors promoting lymphangiogenesis by interacting with VEGFR-3 and activating an intracellular tyrosine kinase-dependent signaling cascade) is widely expressed by both lymphatic and blood vascular endothelium, including the one of the anterior cardinal vein (26; 27), but is subsequently downregulated in blood vasculature (23; 27). VEGFR-3 gene-targeted mice exhibit a dramatic blood vascular phenotype, with embryonic lethality at E9.5 due to defective remodeling of the primary vascular plexus and incorrect hematopoiesis (26;

28). In fact VEGFR-3 inactivation causes cardiovascular failure and embryo lethality before the emergence of lymphatic vessels (26): in this case the lymphatic vasculature does not form and lymph fails to be drained causing the animal to die, thus highlighting the crucial role of this gene product.

Lymphatic and blood circulatory systems normally remain completely separated , with only a connection point, which is the junction between the thoracic duct and the left subclavian vein. Separation between the two vascular networks involves the adaptor protein SLP-76 and the tyrosine kinase SYK: in fact, mice in which any of these proteins have been functionally inactivated exhibit abnormal blood-lymphatic connections, embryonic hemorrhage and arteriovenous shunting (29).

By E14.5, the lymphatic vasculature has spread throughout most of the developing mouse embryo by budding and sprouting from the primary lymphatic sacs; however, these growing vessels have not yet become fully mature or terminally differentiated (21). Then, only near the time of birth, lymphatic vessels express the complete molecular markers profile typical of mature, completely differentiated lymphatics (21; 30).

1.1.2 Anatomy of the Lymphatic System

The lymphatic system is a highly branched network of thin-walled blind-ended capillaries which, in most of the organs, drain fluid, macromolecules and cells from the extracellular spaces. Through larger thicker-walled collectors the newly formed lymph is then carried centripetally (Fig 1.3) to form the two main lymphatic collecting trunks (the thoracic duct or, from the upper right quadrant of the body, into the right lymphatic duct) which empty into the venous circulation at the junctions of left or right internal

jugular veins and subclavian veins (31). Lymph nodes are interspaced in the collecting vessels and act as filters for the lymph as it passes through. At variance with the blood vascular system, lymph is transported unidirectionally from peripheral tissues back to the blood circulation (32). The lymphatic network is present in most body organs with the exception of the central nervous system, the meninges, the eyeball (except the conjunctiva), the orbit, the internal ear, the liver lobule, the spleen pulp, kidney parenchyma and avascular tissues, such as cartilage, nails and cuticle (33).

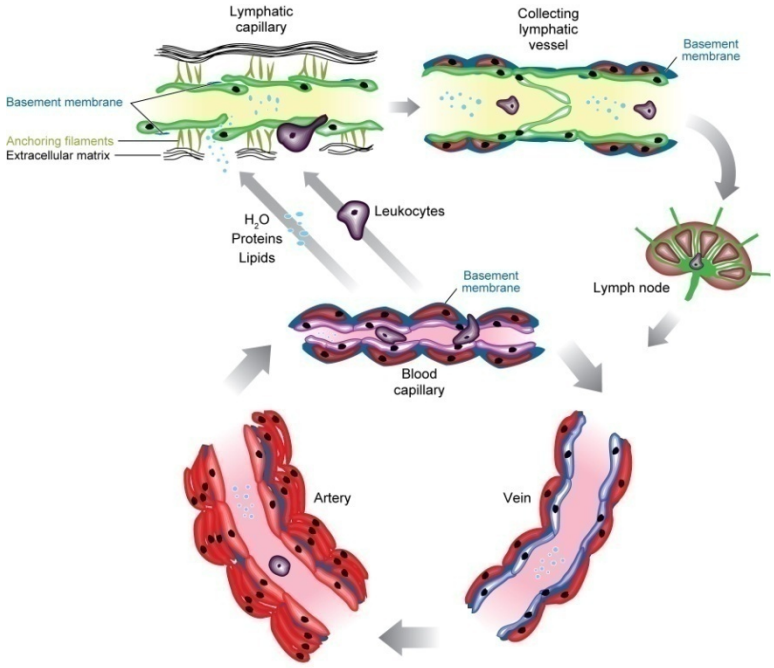

Figure 1.3 Structure of lymphatic vessels. Compared with blood vessels (red), lymphatic vessels (green) are thin walled and have a relatively wider lumen. The endothelial cells of lymphatic capillaries lack tight junctions, but neighboring cells partly overlap, forming valve-like openings, which allow easy access for lymph to the vessel lumen. Fibers known as anchoring filaments connect lymphatic capillaries to the surrounding extracellular matrix. The lymph then drains into collecting lymphatics, which eventually empty into veins in the jugular region. These collecting vessels have a basement membrane, are surrounded by vascular smooth muscle cells and contain intraluminal valves to prevent lymph backflow. On its way, lymph content is modified in its passage through lymph nodes. Redrawn from (34).

Fluid and solutes extravasated from vascular capillaries into the interstitial space enter blind-ended sacs lined by only a non-fenestrated endothelial layer, which displays

numerous invaginations and cytoplasmic vesicles on both luminal and abluminal surfaces (35; 36; 37; 38) and it is anchored to the interstitial matrix via anchoring filaments. These fibers (whose diameter is in the 6 – 10 nm range) tether the basal lamina to adjacent collagen fibers (39; 40) and possess a structure similar to that of elastin (41; 42; 43). The *initial lymphatics* are bulbous sacs (diameter 10 – 60 μm) which possess overlapping endothelial cell-cell junctions behaving like valve structures (primary valves), only permitting unidirectional lymph entry into the lymphatic vessel lumen (Fig. 1.4). They are usually found in a collapsed or partially collapsed state (44; 45). The lymph then moves into lymphatic vessels of a similar diameter, termed *lymphatic capillaries*, lined by an endothelial layer and a discontinuous basement membrane (46), with the exception of lymphatic capillaries in the bat's wings (47). The lymphatic capillary networks greatly vary in shape: anastomoses are usually numerous and blind-ends are especially common in the intestinal villi, the dermal papillae and the filiform papillae of the tongue. These structures are often organized in two layers: a superficial layer and a deeper one, the superficial being of smaller caliber than the deep layer. Also, lymphatic capillaries rely on tethering anchoring filaments, to couple them to the framework of the extracellular matrix and thus facilitating fluid convection and lymphatic drainage (39; 40).

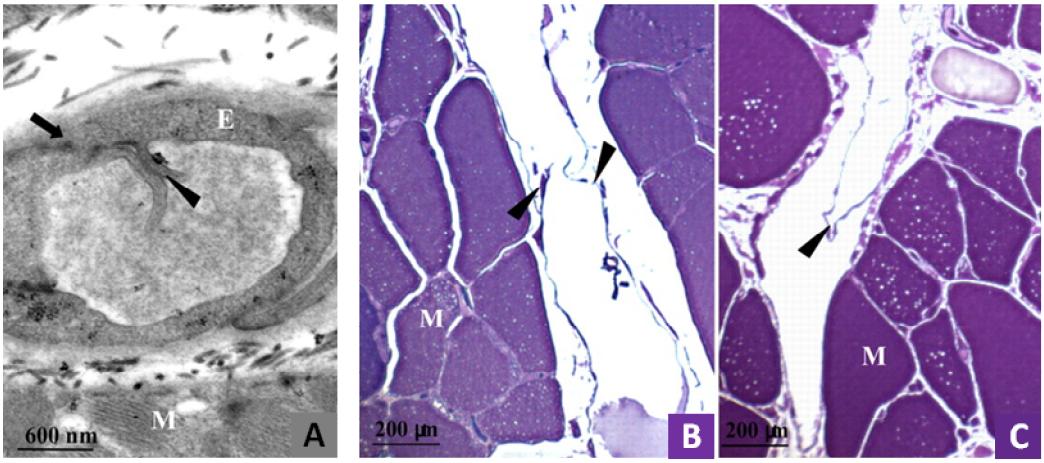

Figure 1.4 Lymphatic valves. **A** Primary valves in a diaphragmatic initial lymphatic formed by two adjacent endothelial cells (E) showing overlapping cytoplasmic extensions (arrowhead) at their junction (arrow); M, muscle. **B and C** Transverse lymphatic ducts showing open (B) or closed (C) secondary valves, formed by two leaflet (arrowheads) attached at opposite sides to the lymphatic vessel wall. Modified from (48).

Collecting lymphatics (whose diameter is in the 50 – 200 µm range) vessel wall is composed by a monolayer of endothelial cells and a basement membrane, but they are also surrounded by lymphatic smooth muscle cells and pericytes, not enveloping the smaller vessels (49), and possess endothelial intraluminal valves (secondary valves) which prevent lymph backflow along the vessel major axis (49; 50). Valves in collecting lymphatics differ from the initial lymphatics ones, in fact they consist of two modified adjacent endothelial cell leaflets which meet in the vessel lumen (Fig 1.5), not unlike bicuspid valves of the larger mammalian venous system. They are made up of a thin collagen sheet sandwiched between two endothelial layers and are relatively long (about twice the length of the lymphatic vessel cross-section), forming a funnel inside the lymphatic and separating adjacent lymphangions, the functional units of the lymphatic system. Also, the lymphatic smooth muscle layer is unique, because it possesses both tonic and phasic contractile activity (44; 50); in particular, phasic spontaneous contractions of lymphatic muscle are involved in lymph propulsion along

the intervalvular segments of the lymphatic network. The collecting lymphatics can be further classified as prenodal (afferent) or postnodal (efferent), to better specify whether they carry lymph to or from the lymph node.

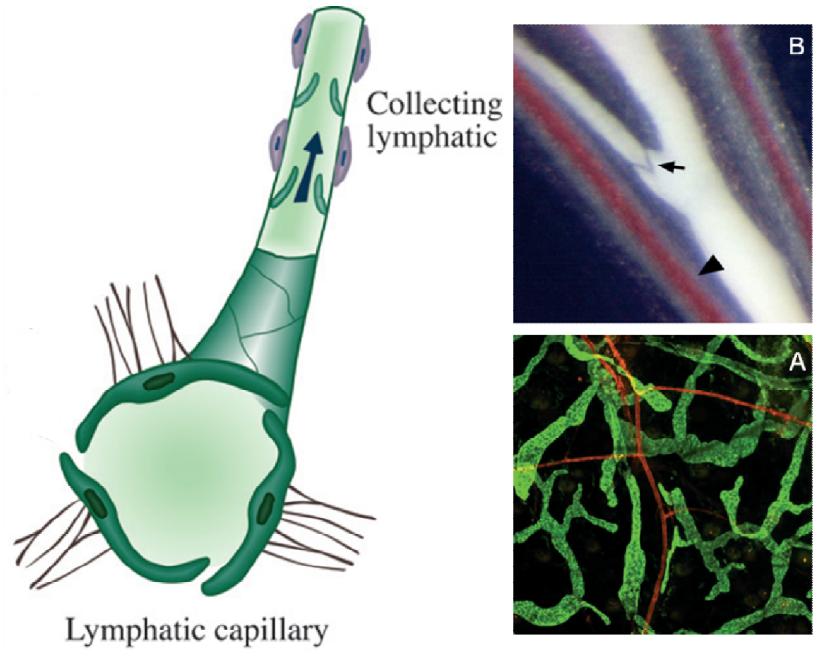

Figure 1.5 Lymphatic vessels: **A** Blind-ended lymphatic capillaries in adult mouse ear whole mount stained for Lyve 1 (green) and smooth muscle actin (red), which identifies smooth muscle cell-covered blood but not lymphatic vessels. **B** Chyle-filled collecting lymphatic vessel in mouse mesentery: arrow indicates lymphatic intraluminal valve; arrowhead indicates the blood vessel. Modified from (51).

The *thoracic duct* has a more complex structure than other collecting lymphatic vessels, in fact it presents a distinct subendothelial layer of branched corpuscles, similar to that found in the arteries; in the middle coat there is, in addition to the muscular and elastic fibers, a layer of connective tissue with fibers arranged longitudinally (33). On its way lymph passes through *lymphoid organs* such as lymph nodes, which consist of a fibrous capsule, from which the trabeculae proceeds inward imperfectly dividing the gland into open spaces freely communicating with each other, the lymphoid tissue occupying these spaces without completely filling them, a free supply of blood vessels, which are

supported in the trabeculae and the afferent and efferent vessels communicating through the lymph paths in the substance of the gland. Another lymphoid organ is the *cisterna chyli*, which receives the right and left lumbar lymphatic trunks and the intestinal lymphatic trunk. The lumbar trunks are formed by the union of the efferent vessels from the lateral aortic lymphatic glands: they receive the lymph from the lower limbs, from the walls and viscera of the pelvis, from kidney and suprarenal glands and the deep lymphatics of the greater part of the abdominal wall (33).

1.1.3 Functions of the Lymphatic System

The lymphatic system runs in parallel with the blood vasculature, and it plays a key role in maintaining tissue-fluid homeostasis, as a tissue-drainage system, and it contributes to the immuno-surveillance by providing a route for migrating cells. The terminal vessels of this network collect fluid, macromolecules, lymphocytes and antigen-presenting cells extravasated from the tissues and return them unidirectionally to the blood circulation via larger collecting lymphatic vessels (34). Lymphatics are also essential for the absorption of long-chain dietary triglycerides and lypophilic compounds released in the intestine in the form of chylomicrons. Impairment of the lymphatic transport because of abnormal vessels development or damaged vessels causes water and proteins stagnation in the interstitial space leading to edematous conditions. Moreover, the abnormal function of the lymphatic system contributes to a large number of diseases, such as lymphedema, different inflammatory disorders and cancer metastasis. In fact, the lymphatic system is also a major transport route for immune cells and disseminating tumor cells: while traveling in lymphatic vessels, cells and particles undergo lower flow rates and smaller shear stresses than they would

experience in the blood circulatory system. Furthermore, the lymph nodes act as holding reservoirs where white blood cells can proliferate and disseminating tumor cells form metastatic tumors. Indeed, tumor cells more easily penetrate lymphatic vessels than blood ones (Fig. 1.6), since the former have looser endothelial cell-cell junctions and possess a discontinuous basement membrane (52). On the other hand, for all these reasons the lymphatic route might provide several targeting advantages over the blood circulation for drug delivery. In particular, there might be a great potential for concentrating immunomodulators, chemotherapeutics, and imaging agents to specified lymph nodes, avoiding dose-limiting systemic side effects, systemic dilution, and liver degradation.

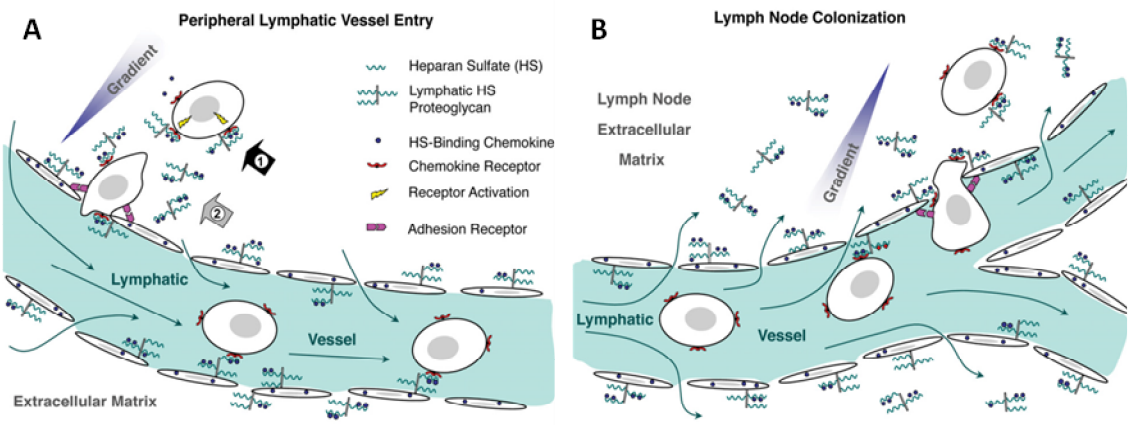

Figure 1.6 Lymphatic invasion by cancer metastasis. **A** In peripheral lymphatic vessels, or in tumor lymphatics, spatial gradients of chemokine-scaffolded extracellular matrix macromolecules interacting with lymphatic endothelium may facilitate tumor-cell migration into lymphatic vessels, affecting the intra-lymphatic flow (arrows). **B** Also in the lymph node, a spatial chemokine gradient is present; however, both its and trans-lymphatic flow direction are reversed, facilitating extravasation (colonization) of lymph node by trafficking tumor cells. Redrawn from (53).

1.1.4 Lymph formation

From a structural point of view, the organization of lymphatic vessels into different vascular compartments, such as capillaries, precollecting, and collecting lymphatics, reflects the dual role of lymphatic system in fluid absorption and lymph transport. In fact, two components contribute to the net flow rate in lymphatic vessels, which are lymph formation and lymph propulsion. The first describes fluid drainage from the interstitium into initial lymphatics, while the second refers to the forces driving lymph from initial lymphatics to collecting vessels, through the nodes and ducts, and eventually back to the blood.

The lymphatic system plays an important role in the maintenance of normal interstitial fluid volume and fluid protein concentration. Lymph formation is driven by local forces, which are interstitial hydrostatic and oncotic pressures and strain of the ECM, which can be affected by skeletal motion as well as the slight strains associated with pressure oscillations caused by arterial pressure pulsations and vasomotion of neighboring arterioles. Lymphatic endothelial cells, like vascular ones, have cytoskeletal proteins which permit a variety of active cell shape changes, such as pseudopod projection or phagocytosis. But there is no evidence that such cytoplasmic motions translate into a contractile mechanism for the entire lymphatic vessel, as in collecting ducts equipped with smooth muscle cells within their vessel wall. Thus, the compression/expansion cycle depends upon periodic displacement of the tissue surrounding initial lymphatics, like that due to skeletal muscle contraction (54).

The fluid distribution between vascular and interstitial compartments is regulated by forces operating across the microvascular wall and the surface area of a permeable structure, comprising the endothelial barrier to fluid and solutes, as well as within the

extracellular matrix and lymphatic vessels. Under normal conditions the balance of these forces favors the net fluid flux from the bloodstream to the interstitial space, a process called *capillary filtration*. Also plasma proteins may cross the microvascular barrier and enter the interstitium, thus the lymph flow provides the only route to return back these extravasated macromolecules to the blood circulatory system. But if extravasated proteins accumulate in the interstitium the balance of forces regulating transcapillary fluid filtration is disrupted, resulting in a redistribution of fluid and plasma proteins from the vascular space into the interstitial compartment, which is not compatible with life. Alterations in the forces acting across the vessel wall and/or the surface area and permeability of this barrier allow for moment-to-moment regulation of transcapillary fluid flow and thus vascular volume.

Fluid movement across the vascular capillary wall is driven by the difference in the hydrostatic pressure (ΔP) generated by the circulating blood fluid and the oncotic pressure ($\Delta\pi$) exerted by plasma proteins within the capillary lumen relative to that of the interstitial space, as stated by the Starling's Law

$$J_v = L_p \cdot A_m \cdot \left[(P_c - P_{in}) - \sigma \cdot (\pi_p - \pi_{in})\right] \qquad (1.1)$$

where J_v is the fluid volume filtration rate (nl/sec), A_m is the endothelial exchange surface area (cm^2), P_c is the blood capillary hydrostatic pressure (cmH_2O), P_{in} is the interstitial hydrostatic pressure (cmH_2O), π_p is the plasma oncotic pressure (cmH_2O) and π_i is the interstitial oncotic pressure (cmH_2O). In addition, L_p is the hydraulic conductivity, a coefficient describing the permeability of the capillary wall to water ($cm/sec \cdot cmH_2O$), and σ is the unitless reflection coefficient, which describes the molecular sieving property of the capillary wall ($\sigma = 0$ means completely permeable without solute reflection back; $\sigma = 1$ means completely impermeable with 100%

reflection back). For example, the albumin reflection coefficient in subcutaneous capillaries is ~ 0.7, meaning that only 30 % of plasma proteins may cross the capillary wall. The major source of capillary transmural oncotic pressure is albumin, with less contribution from globulins. Hence, there is an inward-directed oncotic pressure gradient across the capillary wall, as well as an outward-directed hydrostatic pressure gradient (55; 56).

The Starling' Law, derived through thermodynamic analysis from the original formulation by Sir Eernest starling (57) is commonly summarized as:

$$J_v = L_p \cdot A_m \cdot [\Delta P - \sigma \cdot \Delta\pi] \qquad (1.2)$$

where $\Delta P = P_c - P_{in}$, determined by capillary blood pressure relative to the tissue interstitial one and $\Delta\pi = \pi_p - \pi_{in}$, set by the different concentration of plasma proteins inside and outside of the vascular capillary.

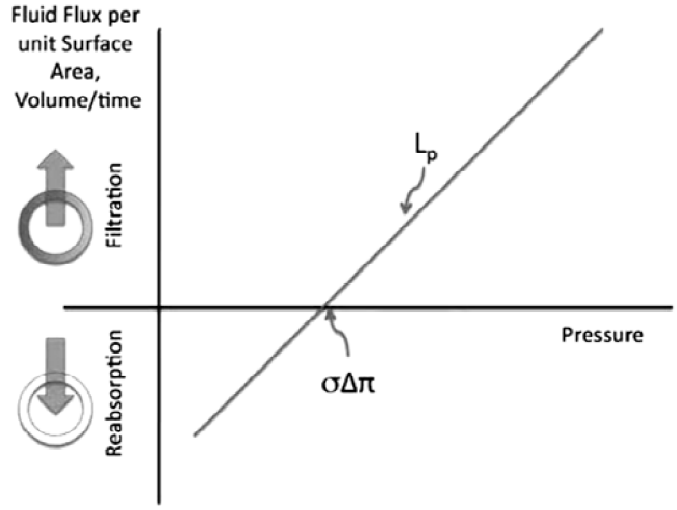

Figure 1.7 Forces affecting fluid filtration/reabsorption. Hydrostatic pressure above the oncotic pressure gradient results in fluid filtration into the tissue. When the hydrostatic pressure gradient across the vessel barrier equals the oncotic pressure gradient there is no net fluid flux (intercept with x axis). If the pressure falls below that point, fluid is reabsorbed from the interstitium into the vascular space. The slope of the relationship between fluid flux per unit surface area and pressure is the hydraulic conductivity (L_p, redrawn from (58)).

A positive P_c a negative P_{in} and the π_{in} favor fluid filtration from the vascular to the extravascular compartment; conversely π_p and positive P_{in} tend to retain fluid into the vascular space. The graph in Fig 1.7 describes the volume flux per unit of surface area (J_v/A) as a function of the difference in hydrostatic pressure, ΔP, which defines a straight line with slope equal to L_p and pressure (x axis intercept) equal to oncotic pressure, π. In the microvasculature, the P_c is higher at the arteriolar end (35 – 45 mm Hg) than at the venular one (12 – 15 mm Hg, (55). Thus, upstream of the capillary network near the arterioles $\Delta P > \Delta\pi$ and fluid exits the vessel. However, under pathological conditions where L_p is increased and σ decreases, large quantities of proteins accumulate in the interstitial space producing an oncotic force which drives fluid into the interstitial tissue and prevents fluid reabsorption into the blood circulation, leading to edema.

In most tissues, supplied by the lymphatic network, P_{in} tends to be subatmospheric (between ~ -10 to ~ - 1 cmH_2O) promoting fluid filtration both at the arteriolar and at the venular end of the capillary walls, the filtered fluid being subsequently removed by lymphatic drainage (Fig 1.8).

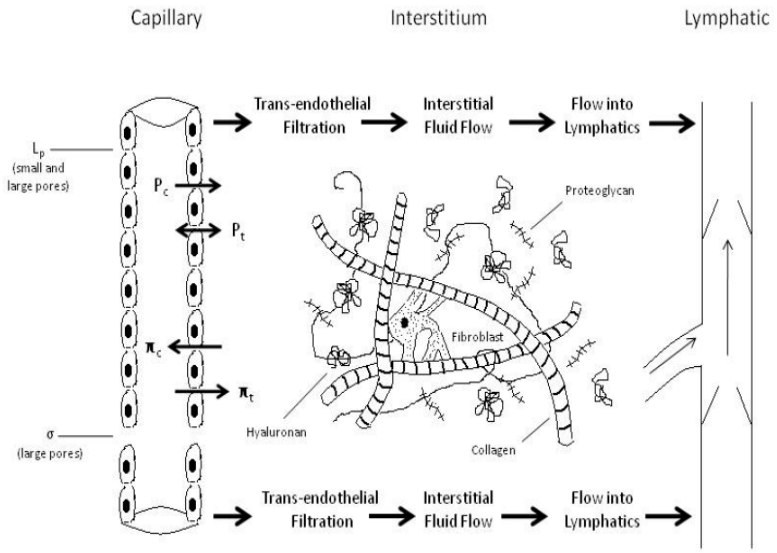

Figure 1.8 Hydrodynamic forces governing fluid flow across the microvessel wall. Fluid movement across the capillary wall is driven by Starling's forces, due to the difference in hydrostatic pressure (ΔP) and oncotic pressure ($\Delta\pi$) between the capillary lumen (c) and the interstitial compartment (i). Fluid and proteins filtered out of the capillary accumulate in the interstitial space, decreasing both P_c and π_c and increasing interstitial pressure. On the contrary, interstitial pressure is decreased by lymphatic outflow. L_p is the hydraulic conductivity and σ is the oncotic reflection coefficient. Redrawn from (59).

Instead, in tissues not supplied by lymphatics, such as the nervous system, retina, renal medulla and salivary glands, P_{in} is generally > 0 cmH_2O, so that fluid is filtered from the arteriolar side of the capillary and reabsorbed into the blood stream at the venular end.

Fluid and macromolecules which cross the microvessel wall and are not reabsorbed back into the plasma tend to accumulate in the interstitial space to be removed by lymphatic vessels. Starling's Law also explains the net fluid movement between the interstitial tissue compartment and lymphatic vessel lumen.

Indeed, lymph flux (J_l, ml/min) can be expressed as:

$$J_l = L_p \cdot A_m \cdot \Delta P_{lymph} = L_p \cdot A_m \cdot \left[\left(P_{in} - P_{lymph}\right) - \sigma \cdot \left(\pi_{in} - \pi_{lymph}\right)\right] \qquad (1.3)$$

ΔP_{lymph} depends upon hydraulic and oncotic pressures of the lymphatic capillary (P_{lymph} e π_{linf}) and of the interstitial space (P_{in} e π_{in}). The reflection coefficient σ which varies between 1 and 0 in lymphatics is ~ 0, thus none of the solute is reflected at the barrier. Hence, the hydraulic pressure gradient alone drives fluid movement

$$J_l = K_l \cdot \Delta P_{TM} = K_f \cdot \left(P_{int} - P_{lymph}\right) \qquad (1.4)$$

where K_l is the lymphatic conductance). Consequently, a positive ΔP_{TM} gradient resulting from P_{in} higher than P_{lymph}, drives fluid flux from the interstitial space into the initial lymphatic lumen, opening primary flap valves (Fig 1.9).

On the contrary, a negative ΔP_{TM} gradient due to higher lymphatic hydraulic pressure ($P_{lymph} > P_{in}$), for example during lymphangion contraction, would favor the lymph backflow in the interstitial space, which is prevented by primary valves closure.

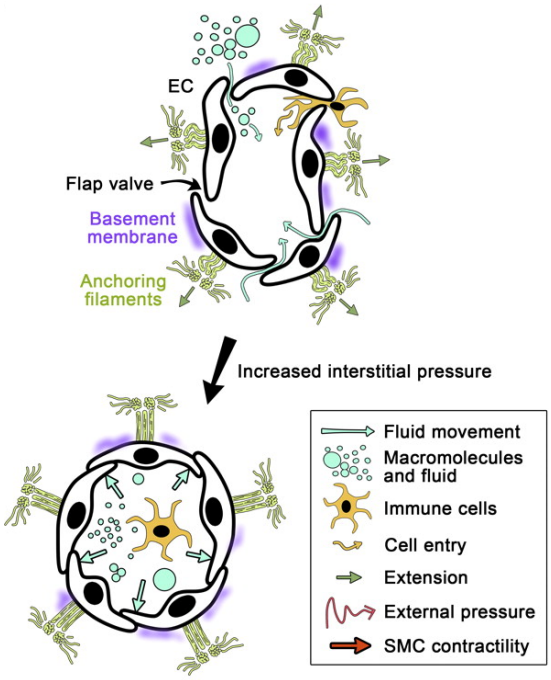

Figure 1.9 Mechanism of lymph formation in initial lymphatics. Initial lymphatics drain interstitial fluid and macromolecules via openings between lymphatic endothelial cells (LECs), preventing lymph backflow into the interstitium. Anchoring filaments attach LECs to the extracellular matrix, preventing the vessel to collapse under conditions of increased interstitial pressure (black arrow). Redrawn from (60).

This transient pressure gradient coupled with the presence of primary and secondary valves allows lymph formation and propulsion due to the compression/relaxation cycle of either extrinsic or intrinsic lymphatic pumps, both in initial and in collecting lymphatics.The transient change in interstitial and lymphatic pressure in initial lymphatic capillaries is sustained by tissue movements, an important factor affecting lymphatic function, causing cycles of external compression/expansion of the lymphatic vessels lumen. The pressure gradients developed across the lymphatic vessel wall favor both fluid drainage from the interstitial space and/or progression of the lymph along the lymphatic network (45; 44). A good model to study the initial lymphatic-extracellular tissue interaction in the formation and progression of lymph is represented by the diaphragmatic lymphatic network, which provides peculiar and unique features, being

exposed to complex tissue displacements and stresses during the cardiac and respiratory cycle.

1.2 The Diaphragm

The diaphragm is the primary ventilator muscle in humans and consists in a dome-shaped structure, with a central tendineous region surrounded by a ring of striated muscle fibers radially oriented, which except in pathological conditions, completely separates the pleural from the abdominal cavities. The central tendineous region extent changes with growth, with a more muscular diaphragm in children than in adults. Interestingly, the central tendon is reduced or lacking in certain species, such as the polecat and the porpoise (61). From a functional point of view, the diaphragm forms an elliptical cylinder (the muscle region) covered by an almost flat dome (the central tendineous region). The cylindrical, vertical part of the muscle is in contact with the inner face of the lower rib cage, over a "zone of apposition" which occupies approximately one third of the total height of the rib cage. The lower ribs are therefore exposed to the abdominal pressure and not to the pleural one (62; 63).

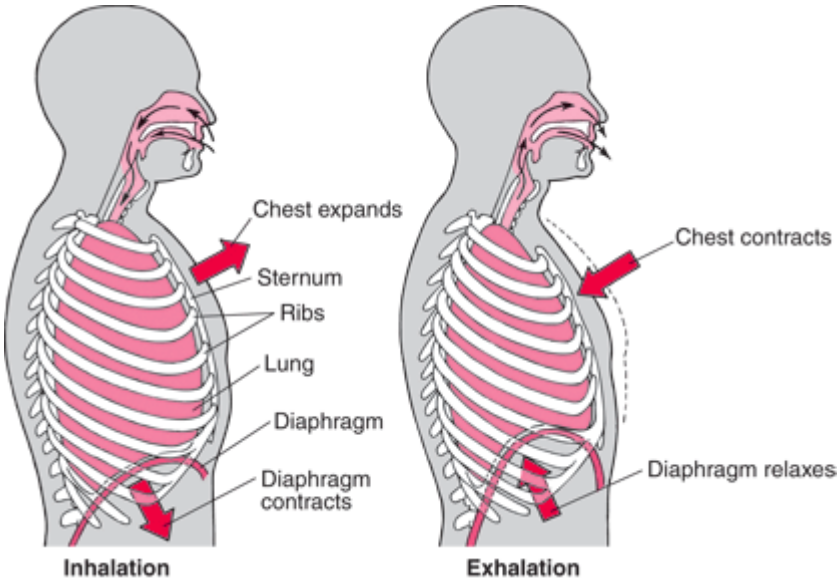

Figure 1.10 Diaphragmatic contraction/relaxation. During breathing the thorax volume changes and the diaphragmatic contraction compresses the abdominal viscera, causing also the abdominal shape modification. Redrawn from (64).

The diaphragmatic muscle contraction causes the muscular fibers shortening and the diaphragmatic dome descending towards the abdomen (65). At the same time, shortening of the diaphragmatic fibers exerts a cranially oriented force on the lower ribs (66; 67), allowing their upward movement (68). Together with the contraction of the external intercostal muscle, this expands the thoracic cavity by increasing both its cranio-caudal and trasverse axis.(Fig 1.10) As a consequence, the pleural pressure decreases, thus increasing transpulmonary pressure, decreasing alveolar pressure and driving air into the lungs. In addition, the abdominal viscera are pushed caudally, increasing the abdominal pressure. The positive abdominal pressure exerts an external force to the internal face of the lower ribs. During the expiration phase the diaphragmatic muscular fibers passively relax and return to their initial length, thus shifting the diaphragm upward towards its end-expiratory state.

1.2.1 Anatomy of the Diaphragmatic Lymphatic System

The diaphragmatic lymphatic network drains fluid, solutes of large molecular weight, and cells from the pleural and the peritoneal cavities, mainly through the peripheral vessels located in the parietal mesothelial and submesothelial tissues covering thoracic and abdominal walls and both diaphragmatic surfaces (69; 70; 71; 72). Diaphragmatic lymphatics depart from pleural and peritoneal cavities through the so called *stomata,* which are mesothelium discontinuities formed at the confluence between mesothelial cells (73; 74), and submesothelial *lacunae* (75) which, for their morphological and functional features, may be considered as large initial lymphatics. This extended mesh of vessels is hierarchically organized with submesothelial lacunae located within the interstitial space beneath the mesothelium (48; 75), lymphatic capillaries located among the skeletal muscle fibers, transverse ducts, running perpendicularly from the

submesothelial lacunae through the skeletal muscle fibers, and deeper collecting vessels which receive the newly formed lymph and eventually empty into larger ducts (Fig 1.11) functioning as collectors for the lymph to be carried out of the diaphragm through extra diaphragmatic trunks, mostly the right and partly the left lymphatic duct.

Initial lymphatic vessels in the submesothelial interstitium or lymphatic capillaries (with a diameter of 1–10 μm) dispersed among muscle fibers display primary unidirectional valves in their vessel wall, formed by two adjacent endothelial cells linked by overlapping junction, with cytoplasmic extensions partially protruding into the vessel lumen. On the contrary, unidirectional intraluminar valves, formed by two endothelial cells leaflets attached at opposite sides of the lymphatic vessel wall, are commonly detected in collecting and transverse lymphatic ducts departing from both submesothelial lacunae (48).

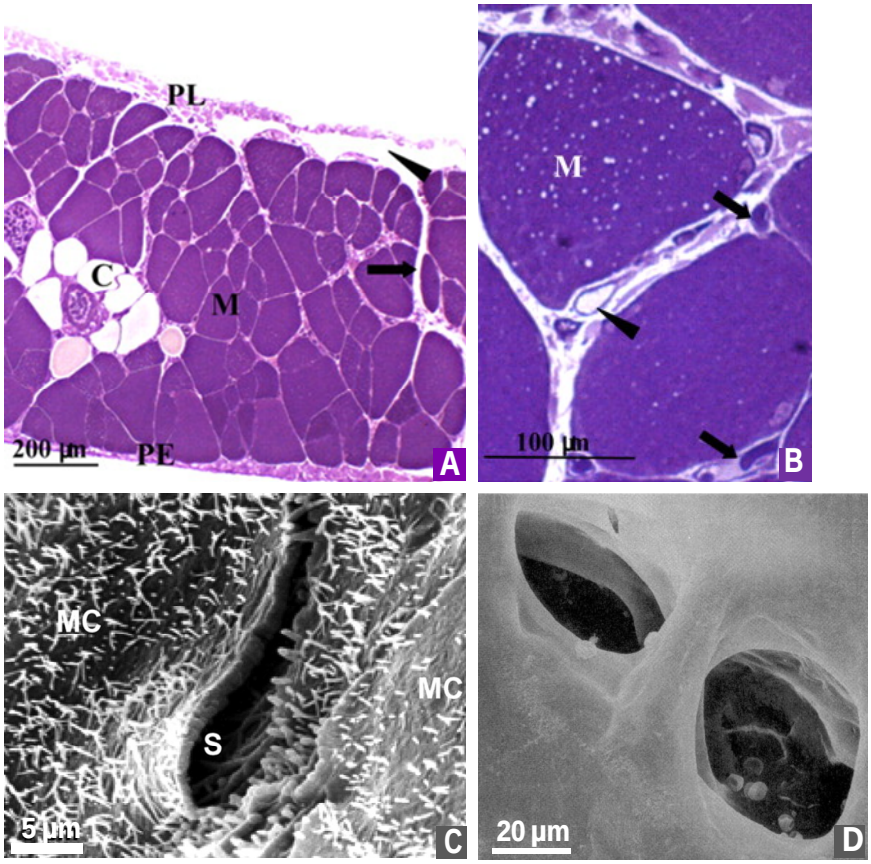

Figure 1.11 Diaphragmatic lymphatics anatomy **A** Semithin cross section of rat diaphragm showing diaphragmatic lymphatic network arrangement from pleural (PL) to peritoneal (PE) surfaces. Submesothelial lacunae (arrowhead) are located within the interstitial space beneath the mesothelial layer, whereas transverse ducts (arrow) run perpendicularly to the lacunae through the muscular fibers (M) and central collectors (C) are located in the deep interstitial space. **B** Small nonerythrocyte-filled lymphatic vessels (arrowhead) surround muscle fibers (M) and are distinguishable from blood capillary vessels (arrows), which are erythrocyte-filled. Modified from (48). **C** Scanning electron photomicrograph of a lymphatic stoma on the tendineous pleural surface of the rat diaphragm. The stoma (S), delimited by a net border, opens at the confluence between adjacent mesothelial cells (MC), which are characterized by a mesh of microvilli protruding from the cell surface. Modified from (76). **D** Cluster of lymphatic stomata on the muscular pleural diaphragmatic surface, yet again delimited by a net border. Modified from (73).

Pleural diaphragmatic lymphatics are typically organized into planar submesothelial linear vessels or complex loops, where linear tracts merge, forming a bidimensional mesh laying on top of the muscular or tendineous diaphragmatic plane (77). The loop conformation of lymphatic vessels can also be found in other tissues, such as skeletal

muscle (78), where lymphatics run along vascular arteriolar arcades (44), or in the mesentery (79).

Diaphragmatic lymphatic vessels on the pleural side are anatomically distinguishable not only for their arrangement, but also for their distribution. In fact, submesothelial lymphatic loops are mainly located in the peripheral ventrolateral regions of the diaphragm, whereas linear lymphatics are dispersed over the whole diaphragmatic surface, apparently connecting different regions and no loops can be found in the medial tendineous diaphragmatic region (77). Lymphatics can be visualized under white light epi-illumination stereomicroscope beneath the transparent parietal pleura covering the diaphragmatic surface and appear as darker-than-background conduits delimited by faint white borders. As reported in Fig 1.12, from a single linear vessel, the loop branches into shorter ducts placed in parallel and/or in series with each other. Therefore, at variance with linear tracts, loops offer multiple paths for fluid recirculation. This kind of arrangement seems to be finalized at exploiting the contraction/relaxation phases of diaphragmatic muscle fibers to alternatively enhance lymph formation or propulsion along the lymphatic network, thus contributing to optimize fluid and solute removal from the pleural and peritoneal cavities throughout the entire respiratory cycle (77).

Unlike the pleural side, on the peritoneal diaphragmatic surface lymphatic vessels are organized in distinct areas, which consist of saw-toothed vessels extending radially from the central tendon to the thoracic wall. Each area forms a relatively distinct functional unit with respect to fluid draining from the serous cavities and the lymphatic vessels of the tendineous portion connect either with the serrated lymphatic vessels or with peri-esophageal ones (80).

The rat diaphragm thickness is almost constant on the whole extent, measuring ~ 750 μm (48). Similarly, the thickness of the mesothelial monolayers is uniform throughout the whole surface, whereas the pleural submesothelial interstitial tissue is significantly thicker (~ 35 μm) compared to the peritoneal (~ 20 μm) one (48). Studies on the submesothelial lymphatic network immersed into the interstitial space indicate that lacunae width and length are comparable when measured on the pleural or on the peritoneal side, but their density is higher over the peritoneum compared with the pleural one and the $area_{lacunae}$-to-$area_{tissue}$ (the percentage-wise cross-sectional area occupied by the lacunae per unit of submesothelial tissue area) is higher in the tendineous compared to the muscular regions of both the ventral and dorsal part of the pleural side and in the ventral region of the diaphragmatic peritoneal side of the diaphragm (48). These morphological differences between the peritoneal and pleural side of the diaphragm might related to the fact that, although the mechanisms supporting lymph formation and progression from the two serous cavities into the diaphragmatic network are the same, the amount of fluid removed from the peritoneal side is much larger than from the pleural side (81; 72; 75; 73).

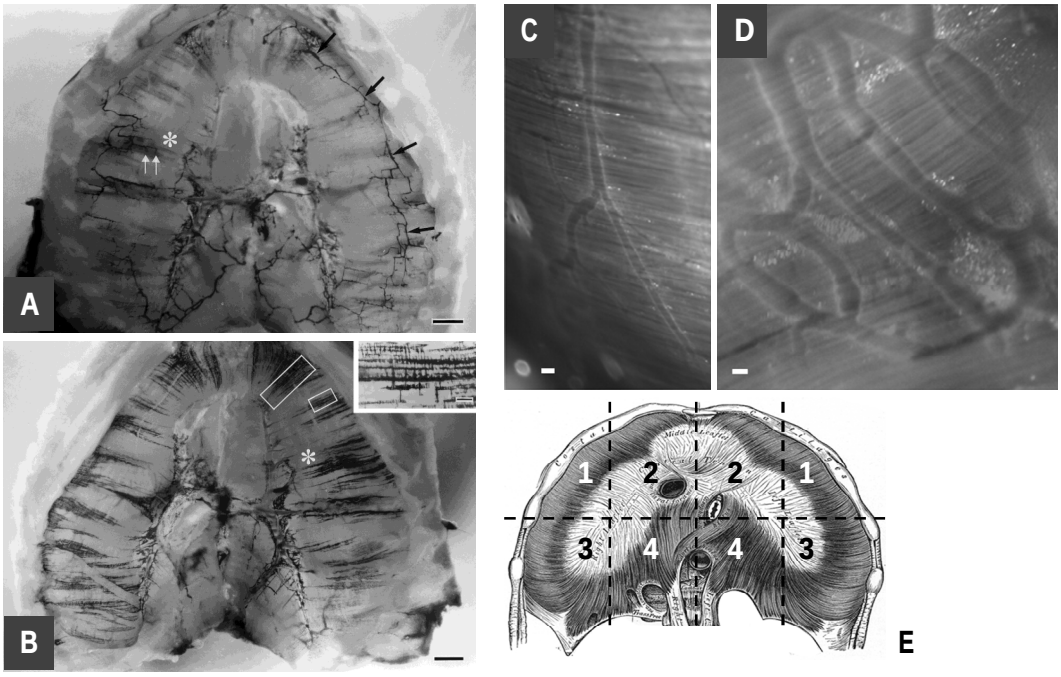

Figure 1.12 Diaphragmatic lymphatic system. **A and B** Pictures showing different diaphragmatic lymphatic vessels arrangement on both pleural (A) and peritoneal (B) side of an ink-stained rat diaphragm. Peritoneal submesothelial vessels extend radially and parallel to one another from the central tendon to the thoracic wall, with numerous connecting branches, forming distinct areas of lymphatics. On the pleural side, lymphatics are arranged in radial and reticular patterns. The radial arrangement is clearly evident from the tendon–muscle border to the mid-muscle portion. As they approach the thoracic wall, lymphatic vessels extend transverse branches which traverse muscle fibers and interconnect with adjacent lymphatics (scale bars = 1 mm). Modified from (80). **C and D** Stereomicroscope images of pleural lymphatics, which are mainly organized into linear vessels (C) or complex loops (D), showing both anatomical and functional divergence. Underneath the lymphatic loop, the diaphragmatic muscular fibers are clearly distinguishable and cross the loop almost perpendicularly (scalebars: C = 100 µm, D = 200 µm). Redrawn from (77). **E** Picture of the diaphragmatic frontal view. The shaded areas correspond to the medial tendineous tissue (light shading) and the peripheral skeletal muscle (dark shading). The dashed superimposed lines identify four different regions: (a) ventrolateral area corresponding to ventral peripheral muscular portion, (b) medial ventral portion corresponding to ventral tendineous area, (c) dorsolateral muscular region and (d) dorsomedial tendineous region. Redrawn from (82).

The different diaphragmatic lymphatics are probably involved in different functions, even within the same hierarchical order of vessel, with lymphatic loops acting as a low-resistance pathway for direct fluid drainage from the serous cavities, and the subsequent lymph redistribution into linear vessels running toward the tendineous medial portion or

to transverse and deeper collecting ducts (48; 77). Indeed, recent studies on the fluid distribution within the diaphragmatic submesothelial lacunae suggest that lymphatic loops in the muscular periphery may be the preferential sites of fluid entrance into the diaphragmatic lymphatic network.

In thoracic tissues, lymph formation and progression seem to mostly depend upon compressive or expansive external forces, squeezing and enlarging lymphatic vessel lumen, due to the tissue displacement by the beating heart or by the contraction/relaxation of respiratory muscles (83; 84; 85). In the pleural diaphragmatic lymphatic network lymph formation depends upon the pressure gradient between pleural fluid (P_{liq}) and intraluminal hydraulic lymphatic pressure (P_{lymph}). At end-expiration, the peripheral diaphragmatic muscular fibers are relaxed and passively stretched by the pulling action of the stiffer central tendon fibers. This condition, coupled with the sub-atmospheric diaphragmatic P_{liq}, might distend the superficial lymphatics oriented transversally to the muscular fibers and reduce P_{lymph}, favoring end-expiratory lymphatic filling. Then, on inspiration, the muscular fibers contract and shorten and the central tendineous fibers are stretched while diaphragmatic P_{liq} decreases (86), a condition that, by limiting lymph formation, might instead favor lymphatics squeezing and lymph propulsion along the network. On the other end, in lymphatics running through soft compliant tissues, a well-developed vessel wall equipped with a smooth muscle layer is required to generate the transmural pressure gradients affecting lymph formation and intraluminal pressure waves to correctly propel the lymph through the entire network, and also the phasic changes of wall stiffness favoring lymphangion filling, smooth muscle diastole and lymph propulsion along the vessel during the smooth muscle systole.

1.2.2 Mechanical features of the diaphragmatic lymphatics

Two populations of diaphragmatic lymphatics, not distinguishable on the basis of their orientation over the diaphragmatic surface, but all running perpendicularly to the underlying muscular fibers, have been identified on the diaphragmatic pleural surface, having high compliance (index of vessel wall distensibility, indicated as volume change for a given pressure range; H-C_{lymph} amounting ~ 7 nl/mmHg) or low compliance (L-C_{lymph} amounting to ~ 2 nl/mmHg). Based on these data, three ideal initial diaphragmatic lymphatics can be modeled: a superficial lymphatic laying over the muscular/tendineous plane and delimited almost entirely by the mesothelium, an intermediate lymphatic still partially delimited on one side by the mesothelium, but surrounded by the muscular/tendineous tissue over most of its lateral surface, and a lymphatic completely immersed in the muscular/tendineous tissue. $C_{lymph\text{-}M}$ for a deep vessel with ellipsoidal cross-sectional shape is extimated ∼100- and ∼20-fold smaller than measured H-C_{lymph} and L-C_{lymph}, respectively. The model suggests that tensile stress is higher in the more compliant wall of the submesothelial superficial and intermediate lymphatics, compared to the one of deeper initial lymphatics (Fig 1.13). The highest tensile stress can be found in intermediate lymphatics, at the edges between the compliant wall and the stiff diaphragmatic tissue basement which undergoes the greatest deformation, whereas in deep, stiffer lymphatics, in particular with a circular shape, wall tension is lower and more homogenously distributed over the entire surface. According to these models, the mechanical properties and functions of initial lymphatics may depend upon surrounding tissue stiffness. Submesothelial lacunae delimited by a compliant wall probably serve as reservoirs of drained fluid, while deeper vessels running in the stiffer tissue, particularly those with a circular cross-sectional shape like the large vessels in the deep diaphragmatic interstitium (48) present

an homogeneous wall stress distribution which, combined with the low compliance and with unidirectional valves, provides a more efficient structure able to propel fluid along the network (76). In relaxed isolated mesenteric lymphatics C_{lymph} is intermediate (87) between submesothelial and deep diaphragmatic vessel, suggesting that the smooth muscle layer may not only sustain active lymphatic pumping, but also provides a relatively stiff mechanical support to lymphatic vessels immersed in soft tissues.

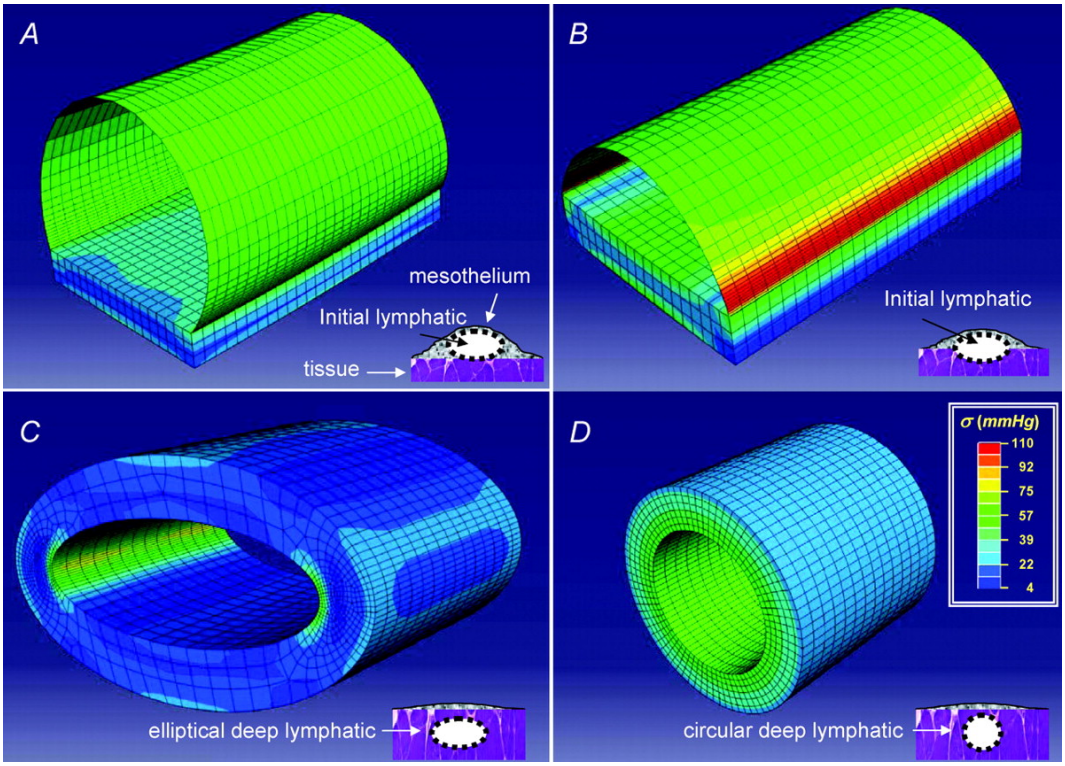

Figure 1.13 Three-dimensional modeling of the diaphragmatic lymphatic vessel wall highlighting the stress distribution map. **A** Ellipsoidal superficial vessel located immediately beneath the mesothelium, which is delimited mostly by a thin wall of lymphatic endothelium plus pleural mesothelium and lays on a diaphragmatic muscular/tendineous support. **B** Intermediate lymphatic duct deeper in the submesothelial tissue, which is only partially delimited by a thin wall, but most of the lateral surface is surrounded by the muscular/tendineous tissue. **C** Ellipsoidal deep lymphatic located among the diaphragmatic muscular/tendineous fibers and surrounded by an isotopic tissue. **D** Circular deep lymphatic vessel among the diaphragmatic muscular/tendineous fibers surrounded by an isotopic tissue. The circumferential stress distribution is represented by color key from blue (low stress) to red (high stress. Redrawn from (76).

Consequently, cyclic contraction and relaxation of either skeletal and/or smooth muscle cells in the vessel wall may support lymphatic function by favoring the development of transmural pressure gradients, which sustain lymph formation and propulsion along the network, and by modifying the mechanical features of the lymphatic vessel wall, increasing the efficiency of the lymph formation/lymph propulsion phases.

The transmission of forces and displacement from the perivascular tissue to the wall of the initial lymphatic is guaranteed by the mechanical links provided by the anchoring filaments (88; 89) which connect the outer endothelial cell surface to the extracellular matrix fibers (90; 91; 92) Indeed, in skeletal muscles such as the diaphragm, the lymphatic endothelium runs at close proximity with the interstitial collagen fibers and with the skeletal muscle fibers (Fig1.14), thus optimizing the anchoring filament function and the force transmission to the lymphatic lumen.

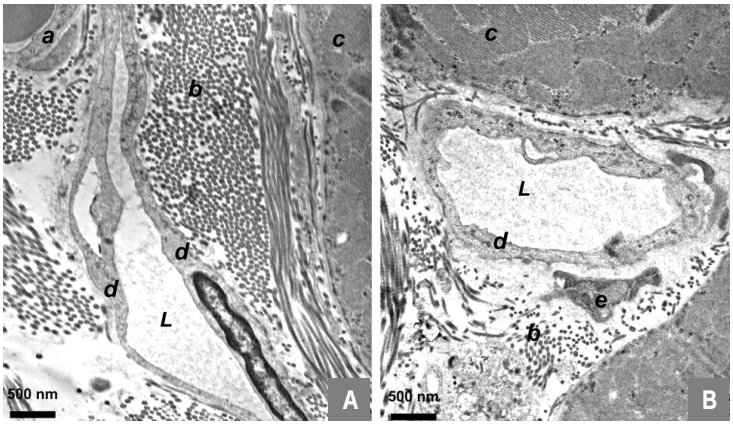

Figure 1.14 Pictures highlighting the anatomical proximity of initial lymphatic lumen and interstitial fibrillar structures. **A and B** Transmission electron microphotographs of rat diaphragm. Initial lymphatics (L) run through connective tissue composed of loose collagen fibers which are organized in bundles (b) adjacent to the skeletal muscular fibers (c). These vessels are characterized by thin endothelial wall (d), tight junctions or overlapping leaflets and anchoring filaments linking the endothelial cells to the adjacent collagen fibers and to the muscle fiber sarcolemma. a, vascular capillary endothelium; e, fibroblast. Modified from (76).

Based on the peculiar arrangement and experimental accessibility of the pleural diaphragmatic lymphatic network, it has been possible to directly measure P_{in} and P_{lymph} in rodents to verify, *in situ* and *in vivo,* the existence of a net ΔP_{TM} supporting lymph formatin from the diaphrgamtic interstium to the initial lymphatics (Fig.1.15) .

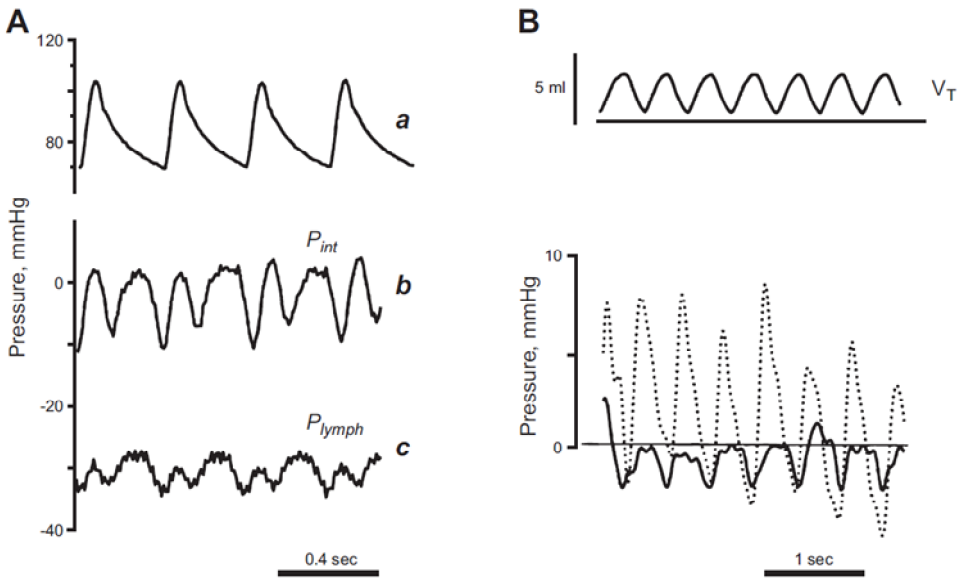

Figure 1.15 Effect of cardiac and respiratory activity on interstitial (P_{int}) and lymphatic (P_{lymph}) fluid pressure. **A** cardiogenic oscillations of diaphragmatic interstitial (b, P_{int}) and intraluminal lymphatic pressure (c, P_{lymph}), measured in rats under neuromuscular blockade. Both diaphragmatic P_{int} and P_{lymph} oscillate almost in phase with systemic arterial pressure (a), shifting from a minimum to a maximum value during cardiogenic oscillations. Taken from (83; 93). **B** simultaneous recording of respiratory tidal volume (V_T, top panel) and lymphatic (P_{lymph}; continuous lines) and interstitial (P_{int}; dashed lines) pressures obtained in intercostal lymphatics of anesthetized and spontaneously breathing rats showing a variable pressure gradient from the interstitium to the lymphatic vessel. Redrawn from (93; 84).

Data show that both P_{lymph} and P_{in} oscillates in phase with the cardiac activity and that, since P_{lymph} is physiologically lower than P_{in}, a net ΔP_{TM} does exist sustaining lymph formation. Therefore, the extrinsic mechanism supported by to the tissue displacement associated to the cardiac motion can , per se, provide a source of lymphatic flux in the diaphragm.

1.3 Lymph propulsion

Lymph propulsion through lymphatic vessels is affected by local forces but, on the other hand, it also depends upon systemic forces such as respiration (44; 81; 94; 95) blood pressure (96), exercise (97), and massage (98; 99; 100). In addition, lymph formation rates may indirectly affect lymph propulsion since the lymphatic smooth muscle contraction of collecting vessels is stretch-sensitive (97; 101; 102).

Since the lymphatic transport is not circuitous and the prevailing steady-state pressures do not support lymph formation or lymph flow along the lymphatic network, intraluminal unidirectional valves play a pivotal role preventing lymph backflow (Fig 1.16).

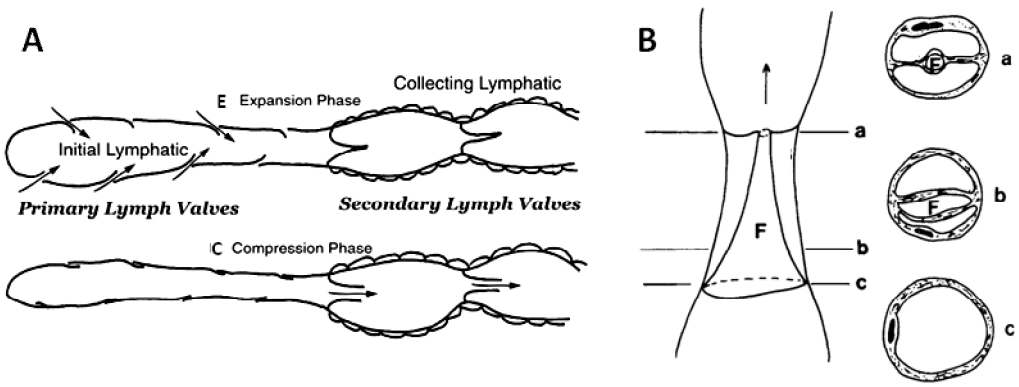

Figure 1.16 Lymphatic valves functioning. **A** Schematic diagram of primary and secondary valve opening during the expansion (E) and a compression (C) phase of a lymphatic vessel. Primary valves in the initial lymphatic open during the filling phase (E), facilitating interstitial fluid to enter the vessel. But the secondary (intralymphatic) valves in the collecting lymphatic are closed to prevent lymph backflow. During the compression phase primary valves close to prevent lymph backflow into the interstitium while the secondary valves open to facilitate lymph propulsion towards the entire network. Redrawn from (103). **B** Schematic diagram of the intraluminal valve funnel arrangement. Funnel (F) consists of a thin connective tissue sheet covered by lymphatic endothelium. Funnel inversion is prevented by the attachment to the lymphatic wall via two buttresses. Flow is in direction of the arrow. Schematics of cross-sections a, b, and c are shown at the right. Redrawn from (104).

In fact, there is no single pump in the lymphatic system as there is in the cardiovascular system where the energy of the heart's contractions is enough to propel blood through the entire circulatory system. On the other hand, the lymphatic system possesses numerous intrinsic pumps, called lymphangions, which contract to guarantee the correct lymph flow in the majority of mammals, and represent the functional units of the lymphatic system (Fig1.17). Since the driving force created by a single lymphangion is not enough to propel the lymph through the entire lymphatic system, lymphatic vessels are organized in chains of these kind of pumps.

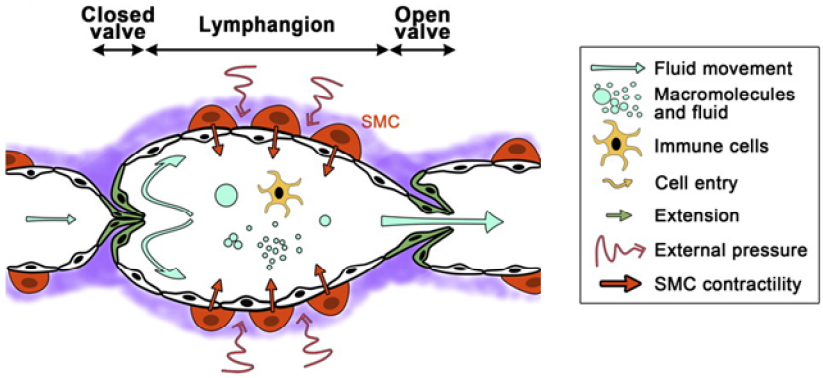

Figure 1.17 Mechanism of lymph propulsion in collecting vessels. Coordinated opening and closure of lymphatic valves is important for efficient lymph transport. Smooth muscle cells covering each lymphangion possess intrinsic contractile activity. EC, endothelial cell. Redrawn from (60).

There is no evidence that in any regional lymphatic network lymphatic tracts contract simultaneously along all of their length from capillaries to the local collecting output. On the contrary, numerous reports demonstrate the propagation of coordinated peristaltic-like pumping waves along the lymphatic network (105; 106). Moreover, in some regional lymphatic networks (as those in the lower limbs), the presence of an interrupted fluid column in lymphatic vessels has been demonstrated during the normal contractile activity of lymphangions; in such situations adjacent lymphangions contract in counter-phase fashion (107). Consequently, each lymphangion can be described as a

short-distance local pump whose primarily task is to drive a bolus of lymph only to fill the adjacent or few next ones. However, all together the pumps chains are able to guarantee the correct long-distance lymph transport.

1.4 Intrinsic and extrinsic lymphatic pumps

The lymphatic system function relies upon a combination of intrinsic and extrinsic pumps, which act in order to generate lymph flow and changes in lymphatic tone to modulate lymph flow resistance. There are several forces affecting lymphatic functions. Traditionally, they are divided into two groups based on their motive force. The active, or intrinsic, lymphatic pump refers to the forces generated by the active spontaneous phasic contractions of smooth muscle cells in the lymphatic vessels wall. On the contrary, the passive, or extrinsic, lymphatic pump combines together all the forces generated in the tissue outside the lymphatic vessels wall.

The lymphatic system possesses multiple *intrinsic short-distance pumps* (lymphangions), the contraction of which is essential to guarantee the correct lymph flow. In general, it appears that lymphatic vessels not encased in a parenchymal tissue that undergoes regular periodic oscillations in tissue pressure demonstrate regular, strong, fast phasic contractions, which drive lymph through the lymphatic network. During the active contraction, lymphatic smooth muscle cells create an increase in intraluminal pressure and generate a local positive pressure gradient which, aided by the unidirectional valves, drives lymph propulsion (Fig 1.18). As a result of such intrinsic pumping activity, a positive pressure gradient occurs near the downstream propagating zone, whereas at the upstream edge of the contracting tract a negative pressure gradient develops between the active lymphangion and the upstream one. This gradient generates the short-lasting local reversed flow, which pushes cell leaflets against each other closing the valve (105). The majority of the contraction-derived energy is used to produce the correct intraluminal pressure gradient and propel the lymph flux, but some part of this energy takes part in lymphatic wall tension generation and produces deformations in extracellular matrix components such as collagen and elastic fibers.

Afterward, during the diastolic phase, these fibers release their stored energy and allow the lymphatic vessel to re-expand. Actively driving forces are greatly influenced by extra-lymphatic events, which sometimes have a bigger impact on lymph flow than the active pump, and the force sum vector is not always favorable to lymph flow.

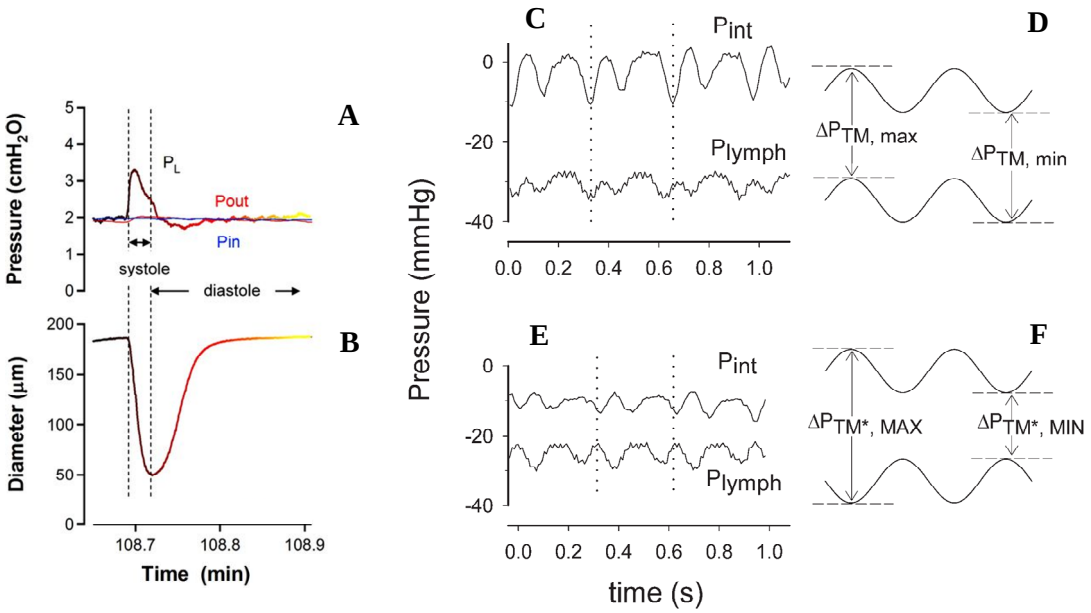

Figure 1.18 Intrinsic and extrinsic lymphatic pumps. Time course of PL (pressure recorded by the servo-null pipette in the central chamber, A) and diameter changes (B) during a complete contraction cycle. Graphs also show the phase delay between the diameter changes and velocity. Modified from (108). **C** P_{int} and P_{lymph} in phase oscillation during the cardiogenic cycle delimited by the vertical dotted lines. **D** The net transmural hydraulic pressure gradient (ΔP_{TM}) affecting lymphatic function may be calculated in correspondence of the tracings minimum (ΔP_{TM}, min) and maximum (ΔP_{TM}, max) values. **E and F** represent tracings like the ones in C and D respectively, but oscillations are clearly in opposite phase. Redrawn from (83).

The *extrinsic lymphatic pump* refers to all the extra-lymphatic forces influencing lymph flow, not related to the active contraction of the lymphatic vessels wall, but generated by other forces in the tissue surrounding the vessels. Extrinsic forces include the influence of cardiac and arterial pulsations on neighboring lymphatic vessels, the contraction of skeletal muscles adjacent to lymphatics, central venous pressure

fluctuations, gastrointestinal peristalsis and respiratory movements. All of these forces may generate hydrostatic pressure gradients in the lymphatic network, to propel the lymph flux even without intrinsic contractility (83; 84; 81).

For example, looking to Fig 1.18, during cardiogenic cycle P_{int} and P_{lymph} recorded in the same vessel can oscillate both in phase (C-D) or in opposite phase (E-F). When they oscillate in phase (C), ΔP_{TM} gradient remains constant (D) giving rise to a constant lymph flux. On the contrary, when P_{int} and P_{lymph} oscillate out of phase (E), ΔP_{TM} gradient varies with time (F) giving rise to a pulsatile lymph flux.

1.5 The Lymphatic Smooth Muscle

Interstitial fluid and macromolecules enter into the lymphatic system through initial lymphatics, which are usually devoid of smooth muscle elements. Lymphatic smooth muscle cells appear in the lymphatic network at the level of collecting vessels in most tissues and animals (109; 110) with the exception of the bat's wings (111) where they are also found in initial lymphatics. The smooth muscle cells are loosely organized where they first appear in the lymphatic network but become oriented into more organized layers (Fig 1.19) in the larger collectors (112; 113). In fact, there, they are strategically arranged into one to three layers, intermixed with collagen and elastic fibers and surrounded by an adventitia made of fibroblasts, connective elements and nerve terminals. Generally, from periphery to progressively larger vessels, the amount of smooth muscle cells increases and they become more ordered with distinguishable layers. The smooth muscle layer may be sometimes interrupted where unidirectional valves divide the vessel into lymphangions and exhibits spontaneous phasic brisk and strong contractions, leading in some vessels to the complete but transient obstruction of the lumen. In fact, the contraction of these cells leads to a rapid reduction of the lymphatic diameter, an increase in the local lymph pressure, the closure of the upstream intraluminal valve, the opening of the downstream valve and the lymph ejection, propagating along the entire network and resulting in a pulsatile lymph flow.

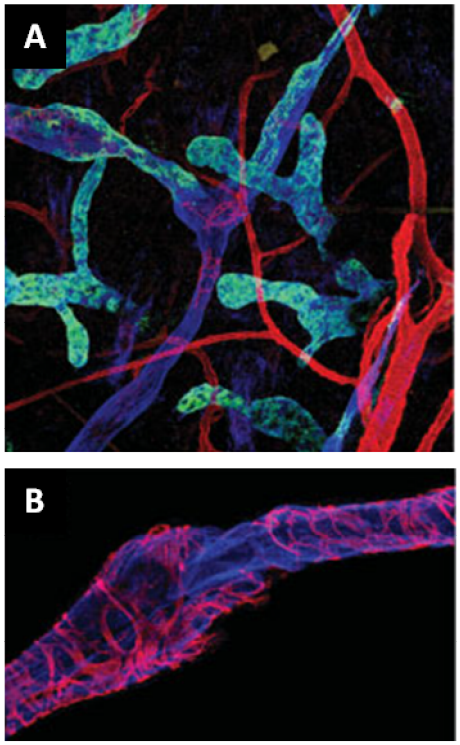

Figure 1.19 Lymphatic smooth muscle. **A** Immunofluorescence staining of dermal lymphatic vessels using antibodies against lymphatic markers, such as Lyve1 (green) and podoplanin (blue). Taken from (114). Red staining shows the α-smooth muscle actin (αSMA), which indicates the smooth muscle cells around blood vessels (not counterstained) and collecting lymphatic vessels, but not lymphatic capillaries, which are devoid of smooth muscle cells. **B** Higher magnification of a lymphatic valve, visualised by podoplanin (blue) and αSMA (red) double-staining. The smooth muscle mesh is interrupted where the intraluminal lymphatic valve divides two adjacent lymphangions. Redrawn from (115).

1.5.1 Lymphatic Smooth Muscle development

It is likely that the lymphatic endothelium is crucial for smooth muscle recruitment and differentiation, regardless of the exact muscle cell origin. In fact, during lymphatic system development, endothelium-derived signals probably mediate the recruitment of lymphatic muscle cells to the developing vessel, resulting in the maturation of the functional lymphatic. If lymphatic smooth muscle development follows the course of the vascular one, the cells generally have a mesodermal origin with local variations (116). For example, vascular smooth muscle cells of the great arteries and cardinal veins

differentiate from cells of the cardiac neural crest (117). One of the few studies documenting lymphatic smooth muscle development has provided evidence that lymphatic muscle cells arise from mesenchymal progenitors (118) in this fashion. Another possible route for lymphatic smooth muscle development in cardiac lymphatics may follow that of the vascular smooth muscle cells of the coronary circulation, where they differentiate from proepicardial ones (116; 119). This development route fits with the similarities seen in the molecular features of cardiac and lymphatic muscle as well as the role of lymphatic muscle in the phasic contractile lymphatic pump. This potential route of lymphatic development may also be related to the primitive lymphatic hearts that are seen in lower vertebrate species, showing both smooth and striated muscle elements (120).

1.5.2 Lymphatic Smooth Muscle intrinsic contractility

The main function of the lymphatic smooth muscle is to rhythmically contract to allow the lymphatics to efficiently propel the lymph, using an unusual array of contractile proteins. In fact, these cells express isoforms of myosin heavy chain (MHC) and actin which parallel the phenotypic features of vascular, cardiac and visceral myocytes (121). The lymphatic smooth muscle contractions are brisk when compared to typical vascular smooth muscle ones, with estimated cellular shortening velocities of 2 cell lengths/second (101). Yet these same vessels can have long term, tonic changes in lymphatic diameter to control flow resistance. Thus lymphatic smooth muscle contractions have similarities to both vascular smooth muscle cells and cardiac myocytes. In fact, lymphatic smooth muscle cells express different isoforms of myosin heavy chain: for example SMB, SM1, and SM2 in rat mesenteric lymphatics and SMA,

SMB, SM1 and SM2 in rat thoracic ducts. SM1 and SM2 isoforms differ in their carboxy terminus, whereas the SMA and SMB isofroms vary at the region of the ATP binding domain of the myosin head (122; 123; 124; 125). Studies have shown that the SMB isoform is typically expressed in smooth muscle with faster contractile properties and has nearly two times higher ATPase activity than SMA (126; 127; 128). The mesenteric lymphatics also express slow-skeletal/fetal cardiac β-MHC, a faster non-smooth muscle MHC isoform. Because of the strong phasic contractile nature of the mesenteric lymphatics, this MHC profile matches the function of the mesenteric lymphatics which are stronger pumps than the thoracic duct. In both the thoracic duct and mesenteric lymphatics also sarcomeric (cardiac) α-actin and non vascular smooth muscle actin proteins are present, demonstrating that lymphatic smooth muscle expresses different isoforms of both striated and nonstriated muscle and correlates the nature of lymphatic vessels functional similarities to both vascular smooth and cardiac muscle cells with the contractile protein isoforms found in these tissues (Fig 1.20). These data also explain the regional variations in both functionality and the contractile elements observed within the lymphatic system.

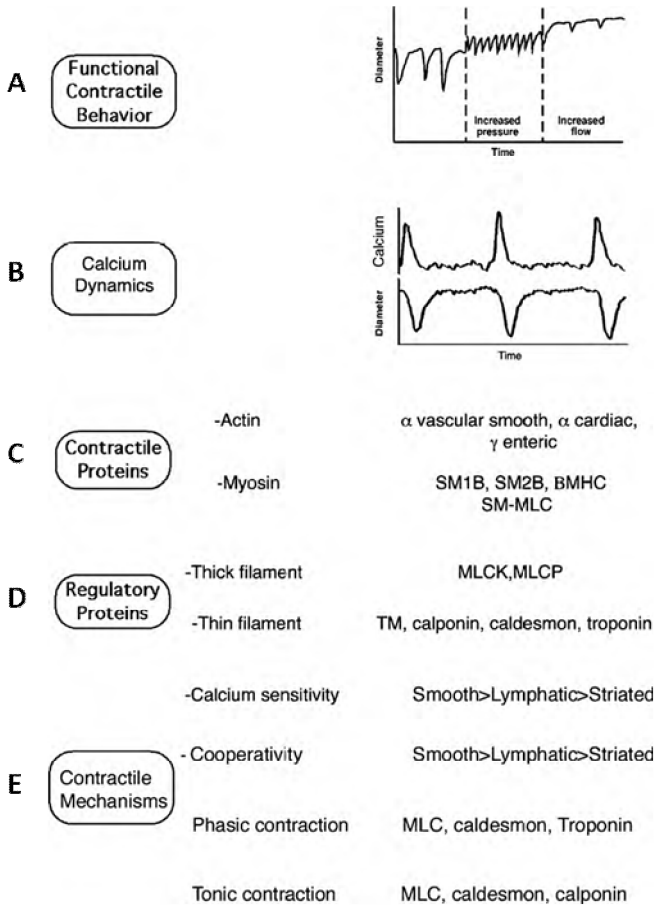

Figure 1.20 Diagrams reporting lymphatic vessel diameter profiles and calcium tracing, and proposed regulatory mechanisms for lymphatic smooth muscle. **A** Changes in vessel diameter due to increased pressure or flow. **B** Example of spontaneous contractions and calcium transients in rat mesenteric lymphatic vessel. **C and D** Lists of both smooth and striated muscle-specific contractile and regulatory elements in lymphatic smooth muscle. **E** The combination of smooth and striated muscle contractile and regulatory proteins is involved in modulating tonic and phasic pumping mechanisms. SM smooth muscle, MHC myosin heavy chain, MLC myosin light chain, MLCK myosin light chain kinase, MLCP myosin light chain phosphatase, TM tropomyosin. Redrawn from (129).

Lymphatic smooth muscle contractions are consequent to action potentials (130) and the spontaneous and intrinsic origin of these events suggests that each action potential, or group of action potentials, must be preceded by a pacemaker event, evoking the transient constriction (131; 132). The action potentials are composed of at least two components and, as demonstrated by their sensitivity to blockers of voltage-dependent calcium channels, are the consequence of the influx of Ca^{2+} ions through L-type Ca^{2+}

channels (133; 134). They propagate through gap junctions connecting adjacent lymphatic smooth muscle cells, as they have been detected in bovine mesenteric lymphatic smooth muscle (135). L-type Ca^{2+} channels are strictly voltage-gated and their opening requires the depolarization of lymphatic smooth muscle membrane potential, which should be generated by an electrical event (pacemaker potential, Fig 1.21). Some evidences support these findings: first, studies on large lymphatic vessels, such as bovine mesenteric lymphatics, demonstrate that the pacemaker mechanism relates to a slow depolarization, leading to the generation of regularly occurring action potentials (132), which has been suggested to be due at least in part to the activation of an ionic current with properties resembling those of the cardiac pacemaker current (I_f) of sinoatrial nodal cells (136). Moreover, recordings of lymphatic smooth muscle membrane potential highlights the existence of small spontaneous transient depolarizations, which, either individually or through summation, have been suggested to generate action potentials and smooth muscle constriction (137) In fact, the initial phase of the spontaneously generated action potential has the same time course as the rising phase of spontaneous transient depolarization (137) and also noradrenaline (10 – 100 nM range) or vessel distention, which both increase lymphatic pumping rate, enhance spontaneous transient depolarization activity (137; 138). Furthermore, spontaneous transient depolarizations occur independently of both the innervation and the endothelium. Therefore, these events are likely to be generated by the smooth muscle cells (137).

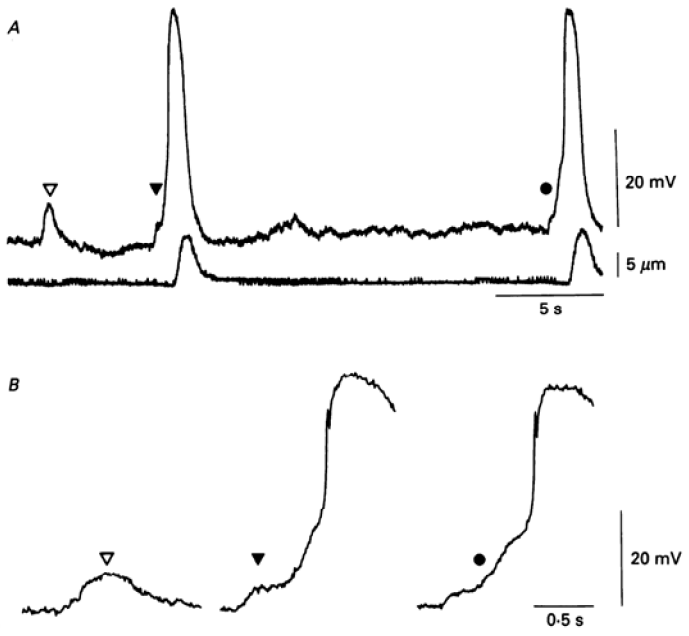

Figure 1.21 Records of membrane potential and associated constriction of a short segment of lymphatic vessel undergoing spontaneous constrictions. **A** The smooth muscle exhibited spontaneous transient depolarizing potentials and action potentials. STDs (Δ) were monophasic and did not cause constriction whereas action potentials (▲, ●) were biphasic and induced vessel constriction. **B** the STD and the action potentials marked in A are shown on an expanded time scale. Redrawn from (137).

Thus, in large mammals, such as bovine and sheeps mesenteric lymphatics, the pacemaker mechanism leading to the action potential onset is thought to be a slow depolarization, due in part to activation of an ionic conductance (136). In guinea-pig mesenteric smooth muscle cells, pacemaking seems to be related to spontaneous transient depolarizations (STDs), which underlie the rising phase of the action potential (130). STDs, also recorded from sheep mesenteric lymphatic smooth muscle are due to a calcium-activated chloride (Cl_{Ca}) current (130; 139), generated by brief release of calcium from intracellular stores. If of sufficient amplitude, STDs generate the action potential and consequently the contraction (130). Vessel distension and agonists, which increase lymphatic pumping, also enhance STD activity, whereas substances that decrease lymphatic pumping reduce STD activity (130).

Lymphatic smooth muscle is variably innervated in different tissues and species and neural activation can have different effects on lymphatic muscle contraction, depending upon the nerve type. The lymphatic smooth muscle contractile activity can be modulated in an inotropic (change in the contraction strength) and/or chronotropic (change in the contraction frequency) fashion by chemical agents like neurotransmitters, circulating hormones or substances released by surroundings cells (endothelium, immune cells) into the interstitial space, but also by physical factors such as transmural pressure, luminal flow and shear stress, which can alter lymphatic tone (Fig 1.22). The lymphatic vessels tone can be evaluated as the difference between the systolic and completely relaxed (diastolic) lymphatic vessel diameters, expressed as percentage of the completely relaxed diameter. The phasic contractile activity is pressure/stretch sensitive (101; 140): in fact, increasing in vessel wall stretch induces enhancement both in lymphatic contraction frequency and in contraction strength. Particularly, humoral substances such as α-adrenergics, β-adrenergics, prostaglandins, bradykinin and substance P can also affect both the tone of lymphatics as well as alter the active pumping activity. The modulation of lymphatic smooth muscle tone is probably exerted by guanylyl cyclase, cyclic GMP, cyclic AMP, protein kinase A, protein kinase G and nitric oxide (141; 142; 143; 144; 145; 146; 147; 148). The prevailing hypothesis from most studies indicates that numerous factors can inhibit lymphatic contractions through the production of cGMP and cAMP, which then lead to the activation of cGMP- and cAMP-dependent protein kinases and act to reduce the frequency and strength of the contractions.

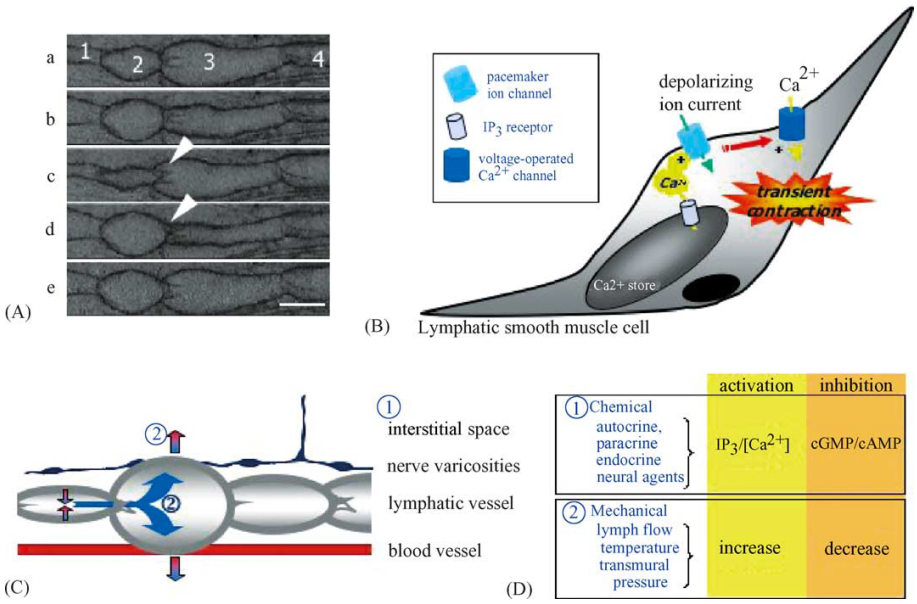

Figure 1.22 Mechanism and modulation of lymphatic smooth muscle contractile activity. **A** Image sequence of a pumping lymphatic vessel, showing four chambers contracting in a sequential fashion. In (c) for example, chamber 2 which has been filled by chamber 1 contracts and fills chamber 3. The unidirectional valve (arrowhead) visible between chambers 2 and 3 is open. In (d), chamber 2 is filled by chamber 1, while chamber 3contracts: the valve is now closed to prevent lymph backflow (scale bar 100 µm). **B** Schematic illustration of hypothesis for lymphatic smooth muscle contraction. **C** Schematic illustration of the flow induced modulation and the structures involved in pumping activity modulation. **D** Mechanisms and signaling pathways involved in lymphatic pumping activation/inhibition. Redrawn from (50).

Transmural pressure (eq. 1.1 and 1.2) may itself be considered an important lymphatic pumping modulatory agent, which alters both strength and frequency of lymphatic contractions. Some studies, performed both *in vivo* and *in vitro*, report that an increased transmural pressure causes positive inotropic and chronotropic effects on lymphatic vessels pumping activity; obviously, lymphatics from different tissues and species have different hydrostatic pressures at which they reach their maximum pumping activity, but increasing lymph pressure beyond these values results in diminished pumping (101; 105; 149; 150; 151; 152; 153). On the other hand in bovine mesenteric lymphatics it has been demonstrated that there is little or no correlation between lymphatic vessels

contractions and distension/stretch stimuli (154). Moreover, isolated bovine and rat mesenteric lymphatic vessels show stable spontaneous pumping activity even when held at an intraluminal pressure of zero cmH_2O and in the absence of either radial or axial distension, leading to the conclusion that lymphatic vessel wall distension by intraluminal pressure is a key factor which is able to modulate the lymphatic pumping activity, but it is not a mandatory factor for pacemaking.

Lymph flow usually shows not only great changes in magnitude, but also transient changes in its direction. Thus, if lymphatic active pumping activity is sensitive to the *shear stress* exerted by lymph flow, also lymph flow itself is not only generated by the lymphatic pump but can provide a feedback, even influencing the pump activity. In fact, in isolated bovine mesenteric lymphatics an inhibition of both amplitude and contraction frequency (Fig 1.23), due to the controlled increase in imposed flow has been found (155). Moreover in isolated mesenteric lymphatics or thoracic duct from the rat the imposed-flow caused the inhibition of the active lymphatic pumping activity (148). The active pump of the thoracic duct appears much more sensitive to flow than the mesenteric lymphatic one (156): imposed-flow decreases both the frequency and amplitude of contraction and consequently the lymphatic flow itself is reduced. The flow-induced inhibition of lymphatic pump causes a rapidly developing inhibition of contraction frequency, dependent on the magnitude of imposed flow but not on its direction, and a slowly developing inhibition of the amplitude of the lymphatic contraction, dependent on the direction of the imposed flow but not on its magnitude.

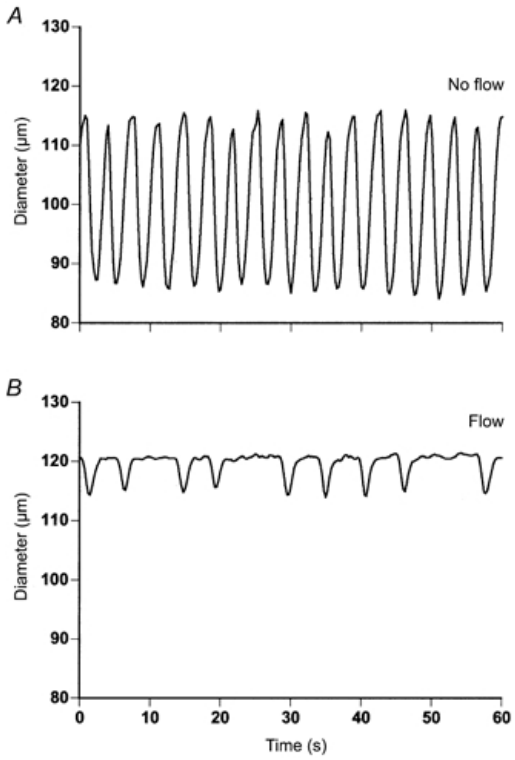

Figure 1.23 Effect of imposed flow on the active pumping activity in rat mesenteric lymphatic vessels. **A** Input and output pressures are 5 cm H_2O, and imposed flow gradient is 0 cm H_2O. **B** Input pressure is 8.5 cm H_2O, output pressure is 1.5 cm H_2O and imposed flow gradient is 7 cm H_2O. The increased imposed flow decreases the contraction frequency and increases the systolic diameter length. Redrawn from (148).

1.5.3 Pharmacological modulation of intrinsic lymphatic function

The release of inflammatory mediators is thought to increase vascular permeability, leading to possible edema formation. Once in the inflamed tissue environment, inflammatory mediators and cells producing them can enter initial lymphatic vessels, to reach the lymph nodes. Following this path, inflammatory mediators can potentially play an additional role in altering lymphatic vessel contractility and hence lymph flow. Due to the multi-target action of inflammatory mediators, it is difficult to determine whether lymphatic phasic pumping activity is affected by the edema-mediated filling of the vessel and subsequent constriction and/or directly by the inflammatory mediators themselves. Systemic administration of histamine has been shown to induce a

significant increase in lymph flow (157; 158; 159), which seems to be due to the histamine-induced increase in transvascular efflux of fluid and protein, at the level of the transcapillary venule (158; 160). Pre-treatment with a H_1-antagonist suppresses the histamine-induced increase in lymph flow and protein concentration, suggesting that the increase in lymph flow caused by stimulation of H_1-receptors can be affected by the increase in lymph formation (161). On the other hand, histamine decreases lymph flow when delivered to the thoracic duct of dog through the *vasa vasorum* (151). Topical application of histamine on mesenteric lymphatic vessels of anaesthetized rats causes an increasing in vessel diameter length and contractility, while contraction frequency is unaffected (162). Because histamine is also present in the interstitium during inflammation and has been detected in lymph drained from injured tissues, it is conceivable that histamine directly stimulates lymphatic vessels function (163).

The effect of serotonin (5-HT) on lymphatic vessels pumping activity has been investigated in isolated longitudinal bovine mesenteric lymphatic segments, where it evokes tonic contractions (164). The effect of serotonin on lymphatic vessels contractile activity has also been described in canine thoracic duct and in porcine tracheobronchial and hepatic vessels (165; 166; 167). However, when vessels are pre-constricted, it has been reported that serotonin causes a vessel relaxation (168). Pharmacological characterization of the receptor subtypes revealed that vessel contractions are mediated by 5-HT_2 receptors, whereas 5-HT_4 receptors mediate the vessel relaxation, both receptor types being located on the smooth muscle (168). In spontaneously contracting sheep mesenteric vessels, serotonin primarily causes an inhibition of the spontaneous constriction; an increase in contraction frequency has been observed only when the inhibition has been blocked by the 5-HT_4 inhibitor DAU 6285 (169; 170).

Acetylcholine administration to lymphatic vessels shows a relaxation of pre-constricted thoracic duct and tracheobronchial lymphatics in dogs and induces a slowing of spontaneous transient contraction in bovine, porcine and guinea-pig mesenteric lymphatics and in afferent lymph microvessels from iliac lymph nodes in rats (141; 143; 171; 172; 173; 174). These effects have been shown to be mediated, at least in part, by the endothelial release of nitric oxide, because nitric oxide-donors mimick the acetylcholine-induced response. Moreover, nitric oxide-synthase (NOS) inhibitors slightly affect lymphatic phasic contractility, as reported in isolated mesenteric lymphatic vessels. Thus, the physiological role of the lymphatic endothelium in the regulation of spontaneous lymphatic pumping activity involves the endogenous production of nitric oxide by the constitutive endothelial nitric oxide synthase (eNOS), which for example decreases the lymphatic pumping activity in the rat mesentery (175). Moreover, during inflammation, also macrophages produce nitric oxide (176). The result of nitric oxide-mediated effects is an inhibition of lymphatic function and consequently result in a facilitation of the edema formation.

Arachidonic acid products are amongst the most important modulatory molecules of inflammation acting, as they are non-steroidal anti-inflammatory drugs, at least in part by inhibiting prostaglandin synthesis. Studies in which the effects of inhibitors of cyclo-oxygenase and other arachidonate metabolism pathways on lymphatic vessels have been investigated show that the spontaneous pumping activity is suppressed in their presence (177; 178), suggesting the ability of lymphatic vessels to generate arachidonate products in order to modulate their spontaneous activity. Moreover, non-contracting lymphatic vessels can be induced to rhythmically contract with a variety of derivatives, the most potent being the stable receptors for prostaglandin H2 and thromboxane A2 (PGH_2/TXA_2) mimetic (compound U46619), and the leukotrienes B4, C4 and D4.

Arachidonic acid by itself induces a variety of contractile responses in bovine mesenteric lymphatics, this probably due to the fact that it may be converted by the lymphatic vessel to stimulatory and inhibitory metabolites.

In guinea-pig mesenteric lymphatics, substance P and ATP enhance contraction frequency. These responses are prevented by the cyclo-oxygenase inhibitor, indometacin, the TXA_2 synthase inhibitor, imidazole and the PGH_2/TXA_2 receptor antagonist, SQ29548, suggesting that substance P and ATP both induce the endothelium to release the prostanoid PGH_2/TXA_2, which serves as a diffusible activator (179; 180). Indometacin or SQ29548 have also been shown to inhibit the perfusion-induced vessel constriction and increase the vasomotion frequency in microlymphatics of rat iliac lymph node with an intact endothelium, further suggesting that the lymphatic endothelium is able to release the constrictor prostanoid PGH_2/TXA_2 in response to an increase in intraluminal flow (174).

Cyclo-oxygenase (COX) metabolites and prostaglandins have been extensively demonstrated to directly affect lymphatic pumping and induce powerful excitatory and inhibitory responses on isolated mesenteric lymphatic vessels (147; 181; 182). The source of COX metabolites was proposed to be the endothelium because lymphatics with an intact endothelium are able to release the dilator prostaglandins PGE_2 and/or prostacyclin when stimulated by PAR-2 activation (183) or arachidonic acid (174) or the constrictor prostanoid TXA_2 in response to increase in intraluminal flow (174) and stimulation with substance P (179), suggesting that lymphatic production of prostaglandins should be altered during inflammation.

Bradykinin increases lymphatic vessels contraction frequency and lymph flow, in a dose-dependent manner, but it does not affect the spontaneously pumping lymphatic

vessels tone. In fact a B1 antagonist (Des-Arg9-[Leu8]-bradykinin) has no effect on the baseline of lymphatic pumping but completely inhibits the bradykinin-induced increase in contraction frequency; on the contrary a B2 antagonist (N-acetyl-D-Arg-[Hyp3,Thi5,8,D-Phe7] bradykinin) significantly depresses lymphatic contraction frequency in baseline conditions but shows no effect on bradykinin-induced increasing in contraction frequency, suggesting that bradykinin induces positive chronotropic but not inotropic effects on lymphatic pumping activity through the stimulation of B1 receptors (184).

Heparin is one of the major endogenous substances with potent anticoagulant activity and is extensively used in medical practice. In fact, as a natural anticoagulant heparin is used for the prevention and therapy of thromboses. It's anticoagulant activity is associated with the activation of antithrombin, contributing to the decrease in platelet adhesion and aggregation. Heparin has a strong relaxing effect on lymphatic smooth muscle, decreasing both amplitude and frequency of spontaneous phasic contractions. Also the tone of lymphatic smooth muscle decreases after heparin exposition: it has been reported that the inhibitory effect of heparin on lymphatic smooth muscle is mainly endothelium-dependent, by constitutive NO synthase activation (185).

The alpha receptor antagonists prazosin (alpha 1) and yohimbine (alpha 2) not significantly alters lymphatic vessels tone or contractile activity in mesenteric lymphatics, suggesting that lymphatics do not possess basal adrenergic tone. On the other hand, norepinephrine and phenylephrine administration produce dose-dependent effects both in increasing contraction frequency (and consequently lymphatic flow) and in decreasing diastolic diameter length. The changes in lymphatic pumping activity induced by norepinephrine is completely blocked by prazosin or phentolamine and only partially by yohimbine, whereas the $alpha_2$-adrenoceptor agonist (alpha-methyl-

norepinephrine) induces no changes in lymphatic function, supporting the hypothesis of the existence of alpha-adrenoceptors on lymphatic smooth muscle. Thus conditions characterized by increased sympathetic outflow may increment lymphatic function through alpha $_1$- but not alpha $_2$-adrenoceptors. (186).

1.6 Lymphatic safety factors

Interstitial pressure affects the transmural pressure gradient driving lymph formation. The potential of the initial lymphatic lumen to collapse under a positive pressure difference is minimized by their unique anatomy, as initial lymphatics endothelial cells are tethered to the interstitium by anchoring filaments (40) responsible for holding the lumen open during conditions of increased tissue pressure or swelling, creating large (~2 μm diameter) interendothelial non selective pores. Those pores are a consequence of the "button"-like pattern of endothelial cell-cell junctions, in contrast to the contiguous expression of these molecules in blood vessels and collecting lymphatics endothelium (187). Therefore, interstitial fluid is able to access the initial lymphatic lumen especially during edematous states when tissue pressure becomes positive.

Possibly as a result of direct communication between interstitial fluid and lymphatic lumen, interstitial pressure and lymph flow are positively related (188). In dog hind leg, the rise of lymph flow is quickest at tissue pressures of ~0 − 1 cmH_2O and attains a sustained maximal value when tissue pressure reaches 2 cmH_2O. The relevance of this relationship is that it maintains a constant interstitial fluid volume due to the tight correlation between interstitial volume and interstitial pressure shown in Fig 1.26 B (189). Two edema safety factors are evident from Fig 1.26, assuming that interstitial pressure is normally negative: a) since interstitial pressure must rise above 2 cmH_2O to lead lymph flow to plateau, large changes in interstitial pressure can be accommodated before edema develops, and b) an elevated lymph flow will quickly return the interstitial volume back to the normal value, as long as the excess fluid volume does not exceed the capacity of the lymphatic circulation. Thus, a small increase in interstitial fluid volume significantly increases its hydrostatic pressure, promoting lymph flow which acts restoring the interstitial volume to the normal condition.

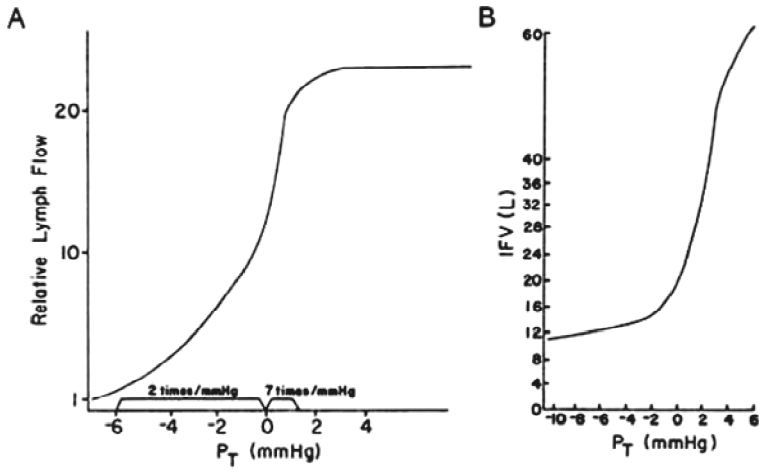

Figure 1.24 Relationship between lymph flow and interstitial fluid pressure. **A** shows the relative increase in lymph flow in response to changes in tissue hydrostatic pressure (P_T, mmHg) during edematous conditions induced by intravascular infusion of Ringer's. **B** shows interstitial fluid volume (IFV, L) in response to changes in tissue hydrostatic pressure. Redrawn from (190).

In fact, during the rapidly rising phase of interstitial fluid pressure reported in Fig 1.24 A, lymphatic vessels becomes progressively more filled, thereby stretching their vessel walls and also increasing lymphatic pumping activity. However, when interstitial fluid pressure reaches the atmospheric value interstitial fluid begins to compress the outer lymphatics wall, preventing a further increase in lymph flow, thus explaining the plateau phase. Therefore, a great increase in lymph flow mainly occurs in negative to slightly positive interstitial fluid pressure range.

1.7 Pathologies associated to the Lymphatic System

Malfunction of the lymphatic vasculature can result in congenital or acquired disorders such as edema, which is a disfiguring and disabling disorder often characterized by swelling of the extremities, tissue fibrosis, accumulation of subcutaneous fat, and susceptibility to infections (191; 192). Impairment of lymphatic drainage caused by dysfunction of the lymphatic vasculature leads to fluid and solutes accumulation into the interstitial space, and eventually to lymphedema, a chronic progressive swelling of the affected tissues (Fig 1.25). Lymphedema can be either hereditary (primary lymphedema) or a consequence of a disease, trauma, surgery, or radiotherapy (secondary or acquired lymphedema).

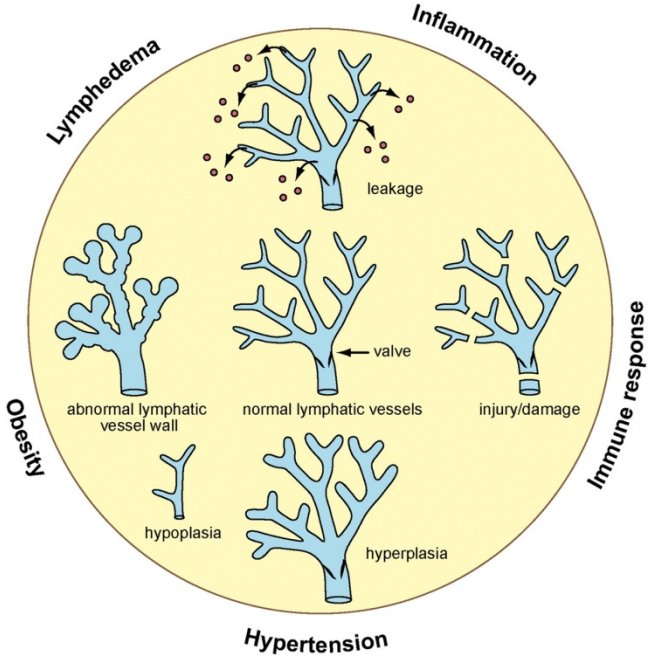

Figure 1.25 Pathologies associated to the lymphatic vasculature failure. Different alterations in the lymphatic vascular network can lead to a variety of pathologies: hypoplastic, hyperplastic, leaky or damaged lymphatics can result in different types of primary or secondary lymphedema. Redrawn from (193).

Lymphedema is also a disabling and disfiguring condition severely affecting the quality of life and at the moment and no cure exists: traditional supporting management of this disease includes manual lymphatic drainage, massage, and external compression. In the past few years the growth of new functional lymphatic vessels has been successfully induced in a mouse model of lymphedema as well as in healing diabetic and surgical wounds (194; 195; 196). The VEGFR-3-specific mutant form of VEGF-C, VEGF-C_{156S}, is effective in stimulating the growth of lymphatic vessels without having effects on blood vascular vessels, such as increase of leakiness caused by wild-type VEGF-C, which also activates VEGFR-2 (197).

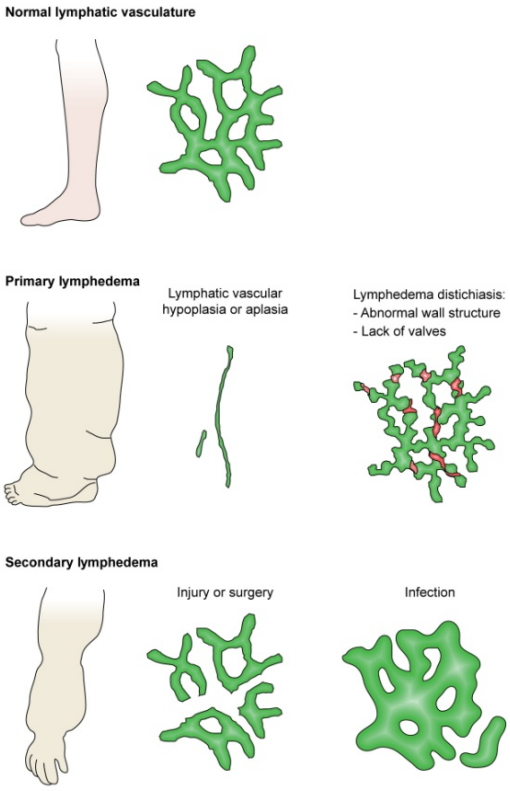

Figure 1.26 Lymphedema. Failure in lymphatic vascular function can be caused by various developmental or acquired structural defects. Hereditary or primary lymphedema can be caused either by total absence or severe reduction of lymphatic vessels or by abnormal lymphatic vessel morphology. Secondary or acquired lymphedema is usually due to disruption or trauma of lymphatic vessels by injury, surgery, or infection. From (34).

Primary lymphedemas (Fig 1.26) are estimated to affect approximately 1 in 6000 people, with a sex ratio of approximately one male to three females. Hereditary lymphedema type I (*Milroy's disease*) is an early-onset form of lymphedema, which becomes apparent at birth affecting primarily legs and feet: in these patients the lymphatic vessels are absent or extremely hypoplastic in the affected areas, but not in the unaffected ones (198). Hereditary lymphedema type II (*Meige disease*) is a late-onset form of primary lymphedema, commonly detected around puberty. Studies on its inheritance has linked this disease to an inactivating mutation in the FOXC2 gene (the transcription factor Forkhead box protein C2, (199)). In general, both these diseases are characterized by dilated lymphatic vessels and accumulation of lymph fluid. *Lymphedema-distichiasis syndrome* is a multisymptoms disorder characterized by edema of the limbs, with pubertal or variable age of onset, associated with a variety of congenital abnormalities. In several families with this pathology, inheritance has been linked to mutations in the FOXC2 gene (200).

In the thorax primary lymphedema may lead to both chronic pulmonary interstitial edema (201; 202) and pleural effusion. An increase in pulmonary interstitial fluid volume impairs the diffusion of respiratory gases at the alveolus-capillary membrane, while an increased pleural fluid volume and pressure strongly reduces lung expansion, both these events severely impairing respiratory function.

Secondary lymphedema (Fig 1.26) may develop in upper or lower extremities or in external genitals as a consequence of invasive surgeries, radiation or traumas and represents the primary form of lymphedema in industrialized countries. Its incidence, approximately 6 % to 30 % of operated patients, is increased by radiotherapy but its

etiology and pathophysiology are still not fully understood and appears to be multifactorial (191). Worldwide, the most common cause of lymphedema is *filariasis*, currently affecting over 120 million people, mostly in tropical areas. It is caused by mosquito-transmitted infection with the parasitic nematodes *Wuchereria bancrofti*, *Brugia malayi*, or *Brugia timori*. These parasites live and reproduce in the lymphatic system, causing a massive dilation of lymphatic vessels and eventually a complete and permanent disruption of lymphatic transport, which leads to a predisposition to long-term recurrent bacterial infections and a condition known as elephantiasis (203).

Common complications of lymphedema include progressive dermal fibrosis, accumulation of adipose and connective tissue, impaired wound healing, decreased immune defense and thus increased susceptibility to infections (191). In rare cases, long-term lymphedema can also place the patient at risk of developing lymphangiosarcoma.

2. Aim

Lymph formation and propulsion are mainly driven by hydraulic pressure gradients developing between the interstitium and the initial lymphatic vessels lumen, or between adjacent lymphangions, which represent the functional units of the lymphatic system. Lymphatic vessels immersed in highly moving tissues such as the diaphragm, which is the experimental model of this study, or more generally all thoracic tissues, undergo cyclic displacement which consist of compression and expansion of the vessels lumen imposed by local stresses resulting as a consequence of cardiac and respiratory activities. Therefore, historically most of the forces affecting diaphragmatic lymphatics function have been considered to be generated by extrinsic pumps. On the other hand, some recent evidences underlined that passive pressure gradients measured *in vivo* are not always able to correctly predict the lymph flow direction in lymphatic loop structures, suggesting the existence of at least another kind of force affecting lymph flow. However, although the intrinsic and extrinsic mechanisms are recognized as important factors in the formation and propulsion of the lymph from the tissues to the vascular venous stream along the lymphangions chain, the intimate integration of factors leading to accurate modulation of the lymphatic flow to cope with the requirements of each tissue are at present far from being clarified. Indeed, a combined study of the simultaneous effects of spontaneous lymphangion contraction and tissue motion under physiological condition in normal tissues has not been performed yet due to the difficulties of the experimental approach.

To fill in this gap of knowledge on the function of initial lymphatic, we developed a series of targeted studies to try to characterize the mechanical behavior of initial lymphatic and the specific role of the intrinsic and the extrinsic mechanism in fluid formation and propulsion in the **initial lymphatics** of the diaphragmatic lymphatic network.

We planned:

1. to verify, and eventually characterize, the intrinsic contractility, never accurately investigated before, of the initial diaphragmatic lymphatics and its ability to generate lymph flow
2. to locally and in a controlled manner modify the extracellular tissue stress and displacement to verify its effect on the development of transmural pressure gradients.

In analogy with the cardiac mechanics the contractile cycle of lymphatics can be divided into periods of lymphatic systole and diastole (204; 205). The determination of mechanical parameters such as contraction frequency, stroke or compliance volumes, ejection fraction and lymph flow has been used to evaluate the extent and role of lymphatic intrinsic pumping mechanism using the cardiac mechanics formalism (101; 206; 207).

3. *Materials and Methods*

Part I

3.1 *In vivo* experiments

The experiments of this study were performed on the pleural submesothelial diaphragmatic lymphatic network of adult Wistar rats (mean body weight: 327 ± 33 g, n = 11) which were housed and handled following the guidelines of the University of Insubria ethical research committee. Rats were anaesthetised with an intraperitoneal injection of 75 mg/kg ketamine (Sigma Aldrich, Milan, Italy) and 0.5 mg/kg medetomidine (Domitor, Pfizer) cocktail. Half-boluses of the same anesthetic cocktail were administered every hour until the end of the experiments, when animals were euthanized via an anesthesia overdose. The maintenance of a deep surgical anesthesia level was assessed on the basis of the lack of the hind-paw avoidance reflex.

Once deeply anesthetized, rats were turned supine on a warmed (37°C) blanket and were tracheotomised, inserting a T-shaped cannula into the trachea: this surgical procedure was performed using a T-cannula in order to alternatively connect the animal to the mechanical ventilator or the continuous oxygen line. Afterwards, the diaphragmatic lymphatic network was *in vivo* stained by an intraperitoneal injection (Fig 3.1) of 2% FITC-dextran conjugate (FD250S – Sigma Aldrich) in saline plus 10% microspheres (F8813 – FluoSpheres® Carboxylate-Modified Microspheres, 0.1 µm, Yellow-Green Fluorescent (505/515)) which provides a stable long-term labeling of diaphragmatic lymphatics. The injecting cannula was inserted through the lateral wall of the abdomen and it was driven along the cranial surface of the liver in order to correctly position the tip in the subdiaphragmatic medial region. To facilitate the right cannula allocation and not to scratch the peritoneal surface of the diaphragm, the cannula tip was shaped to adapt to the diaphragmatic dome curvature.

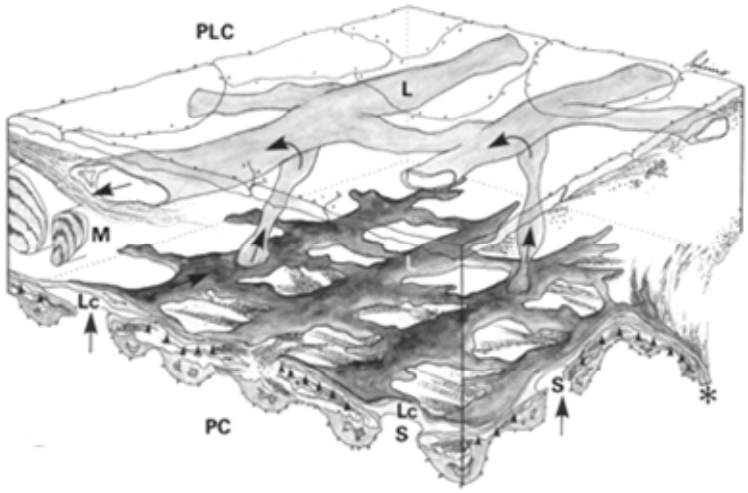

Figure 3.1 FITC-conjugated dye drainage from peritoneal cavity (PC). Subperitoneal lymphatics vessels (darker vessels) are extremely flat (arrowheads) for the most part and drain lymph fluid from the peritoneal cavity through the stomata (S). Lymphatics immersed in muscle fibers (M) are connected to some subpleural ones (lighter vessels), allowing their FITC-filling. Arrows indicate FITC-dextran path in the diaphragmatic lymphatic system. PLC, pleural cavity. From (80).

After 1 hour of *in vivo* staining in the prone position, the animals were turned supine again, the jugular vein and carotid artery were exposed. a PE60 plastic saline-filled catheter was inserted in the right carotid artery and connected to physiological pressure transducers (Model P23XL, Gould Electronics) in order to monitor arterial pressure and heart rate. Animals were paralyzed with a single bolus of 0.3 ml pancuronium bromide (Sigma Aldrich) solution (2 mg/ml in saline) administered in the jugular vein. Immediately after paralysis, the tracheal cannula was connected to a mechanical ventilator (Harvard Apparatus, model Inspira ASV DC1-7058, USA) and rats were ventilated in room air at a tidal volume and frequency automatically set by the ventilator on the basis of rat weight. The mechanical ventilation is required for the chest wall opening: in fact, when pleural pressure becomes atmospheric lung inflation needs to be supported by positive end-inspiratory alveolar pressure. Subsequently the chest wall was opened by mid-sternal thoracotomy and the four to five most caudal ribs were

removed in order to expose the right pleural diaphragmatic dome, taking care to not pierce the diaphragmatic surface, and dehydration was prevented by frequently rinsing with a gentle flush of warm saline solution (37°C).

The pleural submesothelial lymphatic mesh was visualized under a stereomicroscope equipped with a black-and-white CCD camera (ORCA ER, Hamamatsu, Milan, Italy) connected to a personal computer running SimplePCI software (Hamamatsu). Lymphatic vessels filled with FITC-dextran were identified due to the FITC excitation with an optic fiber epi-illuminator equipped with a 425 ± 65-nm bandpass filter (Carl Zeiss Italy) and fluorescence emission was collected by the stereomicroscope fitted with a two-bandpass filter (FITC/TRITC, catalog no. 56918, Chroma Technology, Rockingham, VT). Images were collected at 1 – 10 Hz to optimize the spatial and temporal resolution of the contracting vessels kinetic and lymph flow. The exposure time was routinely set to 0.2 s or lower. During the recording periods, rats were temporarily disconnected from the ventilator and oxygenated with a continuous intra-tracheal flux of 50% O_2 in nitrogen at a continuous positive airway pressure of 7 mmHg, in order to minimize the field oscillations due to the ventilator-supported inflation/deflation lung displacement.

3.2 Whole mount assay

The most commonly used techniques for vessels imaging are (a) immunolabeling of endothelial cell using specific markers, (b) intravital perfusion of a not specific label, and (c) casting of the network by intravascular injection of a filling agent, followed by corrosion of the surrounding tissue for imaging by scanning electron microscopy (SEM). In this case we used the three-dimensional stacks of vessels images, which revealed the detailed architecture of the microvascular network. The presence of smooth muscle elements in the vessel wall of diaphragmatic lymphatics was assessed by whole mount immunofluorescence assay. Therefore, after contracting vessels were *in vivo* video recorded for further offline analysis, the diaphragm was fixed *in situ* for ten minutes with 4% Paraformaldehyde (PFA, Sigma Aldrich), immediately after the animal had been suppressed. Then specimens were excised and post-fixed for twenty minutes with 4% PFA; they were then rinsed in Phosphate buffered saline (PBS, Euro Clone) three times for five minutes each and subsequently permeabilised in ice cold 100% methanol and 0.5% Triton X-100 (Sigma Aldrich) in PBS. Diaphragmatic tissue samples were rinsed with PBS three times, five minutes each and then incubated in blocking solution (1% bovine serum albumin ,BSA, , and 5% goat serum in PBS) for one hour in order to saturate nonspecific binding sites. Specimens were then cut into two pieces: one section was incubated overnight with primary mouse anti α-smooth muscle actin antibody (1:25 – Actin Alpha 2 Smooth Muscle Antibody (1A4) – Novus Biologicals) in blocking solution at 4°C. The second section was incubated for the same amount of time in blocking solution, at 4°C. Both sections were then rinsed three times with PBS for five minutes each, followed by an incubation with the secondary goat anti-mouse antibody conjugated to Alexa Fluor® 647 (1:100 – goat anti-mouse IgG2a – Molecular Probes) for one hour at room temperature. The diaphragmatic specimens

were finally washed three times with PBS for five minutes each and then mounted onto a coverslip glass with Fluoroshield (F6057, Sigma Aldrich) for confocal microscope (Leica TCS SP5, Germany) observation.

Laser scanning confocal microscopy permits to collect high resolution digital images from a series of optical sections through the whole thickness of the sample. Epifluorescence microscopy is widely used in vascular imaging, but excitation and emission light scattering usually limits the depth to which high-resolution images can be collected to < 40 μm and further error may be introduced as 3D structures are projected onto a 2D plane (208). Confocal microscopy, which reduces out of focus light via a pinhole, can image to greater depths and is routinely used to collect 3D image data. Stained vessels were confocally scanned throughout the entire diaphragmatic depth in 0.5-μm *z*-axis steps, using a 20X dry objective and a pinhole corresponding to one Airy Unit. The negative controls for all experiments were produced and analyzed via similar procedures, except that the control samples were not incubated with primary antibody (see above). In addition, aorta specimens were processed as illustrated above and used as positive controls. Negative and positive controls were scanned with the same instrument settings as the specimens for a valid comparison of relative fluorescence intensities. Photobleaching, the loss of the fluorescent signal due to the exposure to the laser light, was not prominent during scanning.

The analysis of confocal images was performed using Image J (MBF package, version 1.46j – http://rsbweb.nih.gov/ij/; http://www.macbiophotonics.ca/imagej/) and Adobe Photoshop software. Pleural diaphragmatic lymphatic network overviews were obtained *in silico* by aligning and superimposing consecutive images into a continuous panorama using Adobe Photoshop software. Serial sections were recorded beginning at the top surface of the specimen (placed pleural side up) and the resultant stacks of individual

lymphatic vessels and intraluminal valves were rendered in three dimensions using 3D projection function with brightest point projection and a complete rotation around the y axis method of Image J. Lymphatics cross sections were obtained using Reslice function of Image J software on the previously merged z-stacks.

3.3 Offline analysis

3.3.1 Diameter vs time profiles

Measuring diameter length is a standard technique in vascular research. Initially light microscopy with graded eyepieces was used, and then video microscopy allowed taping and analysis in time (209; 210). Later, multi-sites simultaneous measures were performed on digital images, both online and offline (211; 212). Eventually, automatic measures of diameter profile at sites of interest was reported for many medical applications, including coronary angiography, b-mode ultrasound, CT and MRI data (213; 214; 215; 216).The vessel diameter of a structure can also be determined manually, which is extremely time-consuming and allows only a small number of images to be processed. In fact, the human observer, although excellent in pattern recognition, has further deficits which give rise to reduced reproducibility (217).

Video *in vivo* recorded were transformed from the Simple PCI proprietary *.cxd format to a multipage TIFF stack and then the open source package ImageJ (NIH) was used for offline image analysis. The "Diameter" (218) plug-in uses an algorithm to estimate the inner diameter, based on the FITC-fluorescent dye filling the vessel (Fig 3.2): the contrast of the lymphatic vessel is produced by the FITC-conjugate emission, which results in a homogenous light structure in front of a dark background.

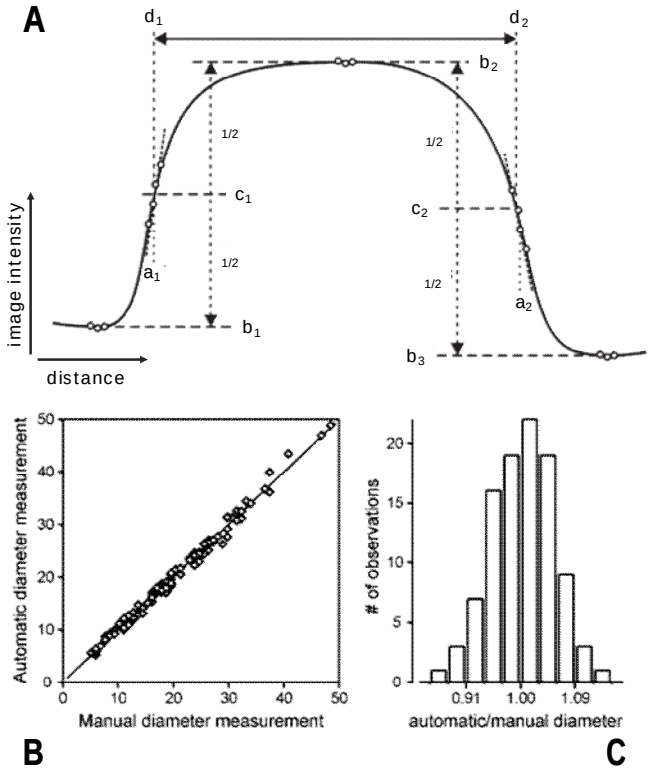

Figure 3.2 Image J's Diameter Plugin. Panel **A** shows Diameter plug-in algorithm intermediates, which estimates boundary (a – maximum intensity changes), reference intensities (b) in the three resulting areas, threshold (c – mean of adjacent reference intensities) and finally vessel boundary (d), where the linear trend around the boundary estimates crosses the threshold (circles represent the raw data used for calculation). The bottom panels demonstrate the concordance of manual and automatic measurements at the same position: The product-momentum correlation is $R^2 = 0.991$, and results can be fitted by a linear trend (**B**).The ratios of automated/manual results are provided in a histogram (mean 1.004, **C**). Modified from (218).

In detail, the algorithm requires a line selection, which has to cross the vessel and to exceed the maximum vessel diameter during the recorded period on both sides. This is why ROI were plotted on the z-stack maximum projection image. The "Dynamic Profiler" function of ImageJ showed the pixel intensities profile along the selected line in real time. The estimate borders (a_1 and a_2 in Fig. 3.2) are the two positions with the maximum difference between the mean intensity of the three adjacent points to both sides. This separates the profile in three parts. Reference intensities (b_1, b_2 and b_3 in Fig.

3.2) are the darkest areas outside the blood vessel, separately for both sides, and the brightest area within the vessel, determined by the average of three consecutive points. The intensity threshold (c_1 and c_2 in Fig. 3.2) is the average of the adjacent reference intensities, calculated separately for both sides to account for different surroundings of the vessel. The intensities of the two positions left and right of the border estimates are fitted with a linear trend. The points of intersection (d_1, d_2 in Fig. 3.2) of the fit with the intensity threshold give the precise vessel edges. Half of maximal vessel thickness correspond to sqrt (3/4) of the radius; therefore the diameter length of the vessels is [d_1,d_2] * sqrt (4/3). The diameter and both ends of the full width at half-maximum of the vessel (in pixels, then transformed in µm) of the five adjacent measurements and for every loaded ROI were eventually copied to the system clipboard and subsequently analysed with Origin 5.0 software.

3.3.2 Fluorescence vs time profiles

Fluorescence intensity profiles were obtained by Image J multi-measure function on a single ROI placed within the vessel borders (ROI were placed on the minimum intensity projection in order to avoid possible artifacts). Then results were copied on an Origin 5.0 worksheet an plotted vs time.

3.3.3 Data analysis

The contractile cycle of lymphatic vessel can be divided into periods of lymphatic systole and diastole (Fig 3.3), in close analogy with the cardiac cycle. Contraction frequency, stroke volume, ejection fraction and lymph flow can be determined to evaluate lymphatic pumping function by means of this cardiac analogy (101; 205).

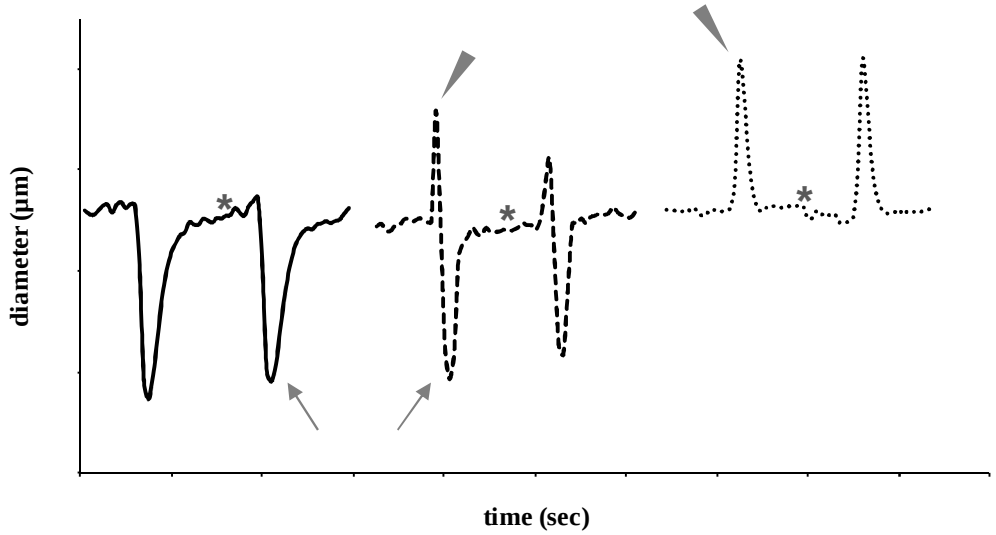

Figure 3.3 Typical diameter vs time profiles of lymphatic vessels showing active (continuous line), hybrid (dashed line) or passive (dotted line) mechanical behavior throughout the intrinsic lymphatic contraction cycle Details of their behavior are illustrated below in the "Results" section. Lymphatic pumping parameters are defined in a fashion similar to the cardiac cycle. Diastolic diameter (*, µm); systolic diameter (arrows, µm); fully expanded diameter (arrowheads, µm); pumping frequency (F) = contractions/minute or expansion/minute; stroke volume (SV) = diastolic volume (or peak volume) − systolic volume; ejection fraction (EF) = SV (or CV)/diastolic volume; lymph flow (LF) = SV (or CV) × F.

The mean value of five diameter measurements was transformed to the corresponding microns value and then plotted vs time using Origin 5.0 Software, taking care to exclude data causing SD >2 pixels. Table of results was then copied to a Clampfit 10.2 Software free sheet, setting the correct sampling interval per signal (1 – 10 Hz).

Systolic and fully expanded diameters were obtained by manually placing cursors at the lowest/highest value in the plot profile of the cyclical pumping activity (for 1 Hz profiles) or as the mean value of 0.5 seconds sampling interval (for 10 Hz profiles), to reduce the higher noise proper of this kind of traces. Also diastolic diameter length was measured as the mean value of at least five seconds sampling interval recorded as a stable trace reaching plateau, immediately before the next downward/upward deflection, both for pumping vessels or not contracting ones, in order to be subsequently compared.

Cyclic active contraction or passive expansion period (sec) was estimated using Autocorrelation function of Clampfit 10.2 Software. The Autocorrelation function (Fig 3.4 A)provides time series analysis, looking for cycles within data: traces are shifted along themselves incrementally (in "lags") and the output is an "autocorrelation function estimate" (ACFE) calculated at each lag point, measuring the match between the static and shifted sets: the time period corresponds to the highest ACFE lag. The pumping frequency (F) was then calculated as the period reciprocal value (Hz) and transformed in bpm by multiplying by 60.

Cross-correlation (Fig 3.4 B-D) between traces simultaneously recorded in different tracts of the same lymphatic network was performed by Cross-correlation function of Clampfit 10.2 Software. Also the Cross correlation function provides time series analysis, looking for regularities between two data sets: the first data set is shifted along the second one incrementally (in "lags"), in both directions, and the output is a "cross-correlation function estimate" (CCFE) calculated at each point, measuring the match between the two sets. Positive peaks ($0 < CCFE < 1$) indicate that the two waveforms are in phase, whereas negative peaks ($-1 < CCFE < 0$) indicate that they are out of phase; $CCFE = 1$ corresponds to complete identity between the two traces.

Cross-correlation differs from autocorrelation in that two or more data sets are compared with each other, and not with themselves.

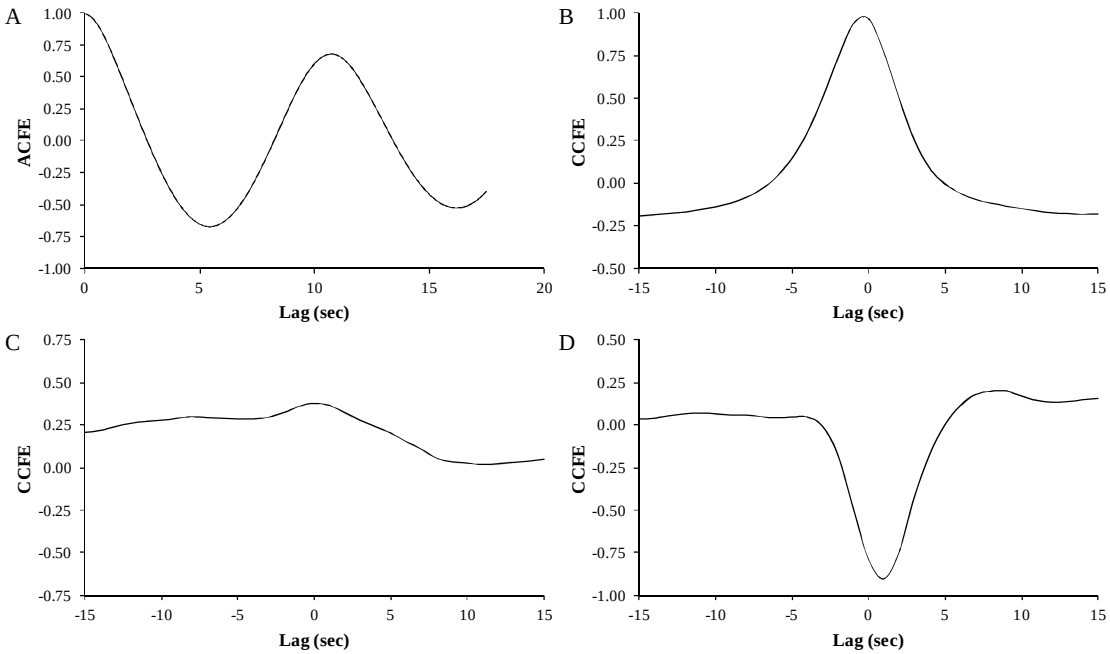

Figure 3.4 Examples of autocorrelation (**A**) and positive (**B**) or negative (**D**) cross-correlation plotted profiles. In **C** is reported the CCFE plot of two uncorrelated traces.

Lag period calculated with cross-correlation analysis was also used to calculate spread velocity (µm/sec) of contraction in active pumping vessels as indicated in eq. 3.1:

$$vel = \frac{\Delta_{lenghth}}{lag} \qquad (3.1)$$

where Δ_{lenght} (µm) is the distance between two adjacent actively pumping sites with no zero lag (sec).

The time constant, denoted by the Greek letter τ (tau), is the rise time characterizing the passive relaxation after lymphatic vessel constriction. The constant represents the time (sec) the vessel takes to reach 1-1/e ≈ approx 63.2% of its diastolic value: the larger the time constant is, the slower the vessel reaches its diastolic diameter. The time constant τ

(Fig 3.5) was found by fitting a single exponential function (eq. 3.2) to the acquire data using Clampfit 10.2 Software Fit Function, on a previously low-pass filtered diameter profile, using the exponential standard method (number of terms = 1):

$$f(t) = \sum_{i=1}^{n} A_i \, e^{-t/\tau_i} + C \qquad (3.2)$$

where A is the initial diameter length, t is time and C is an arbitrary vertical offset.

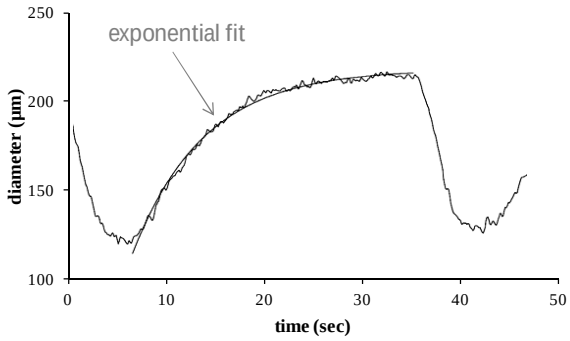

Figure 3.5 Example of tau exponential fitting performed using Fit function of Clampfit 10.2 Software.

The relationship between amplitude and frequency of contractions in actively pumping vessels was fitted by Sigma Plot 10.0 by Dynamic Fit Wizard as a rectangular hyperbola (eq. 3.3):

$$y = y_0 + \frac{a \cdot b}{b + x} \qquad (3.3)$$

The stroke volume (SV) indicates the volume of lymph (expressed in pL) pumped by an active or hybrid vessel at each contraction. SV is calculated using mean values of systolic and diastolic diameter lengths at each analyzed site over the full trace. Based on previous evidences which revealed that the cross-sectional area of diaphragmatic superficial lymphatics tends to be elliptical rather than cylindrical and the smaller radius in the plane perpendicular to the pleural surface is ~35% of the parallel one (77), SV

was estimated for a lymphatic segment of 10 µm length as [(diastolic cross-section – systolic cross-section) * 10 µm]

$$SV = \frac{\left\{\left[\left(\frac{d_D}{2}\right)\cdot\left(\frac{d_D}{2}\cdot 0.35\right)\cdot\pi\right]-\left[\left(\frac{d_S}{2}\right)\cdot\left(\frac{d_S}{2}\cdot 0.35\right)\cdot\pi\right]\right\}\cdot 10}{10^3}$$

where d_D (µm) and d_S (µm) are diastolic (peak value for hybrid vessels) and systolic diameters respectively, 0.35 is the smaller transverse to the larger in the plane radius ratio and 10^3 is the μm^3/pl conversion factor.

Similarly the diastolic volume load (DVL) indicates the volume of lymph (expressed in pL) accumulated into a lymphatic segment during the diastolic phase. DVL is calculated using mean values of fully expanded and diastolic diameters at each analyzed site over the full trace. DVL was also estimated for a lymphatic segment of 10 µm length as [(peak cross-section – diastolic cross-section) * 10 µm]

$$DVL = \frac{\left\{\left[\left(\frac{d_P}{2}\right)\cdot\left(\frac{d_P}{2}\cdot 0.35\right)\cdot\pi\right]-\left[\left(\frac{d_D}{2}\right)\cdot\left(\frac{d_D}{2}\cdot 0.35\right)\cdot\pi\right]\right\}\cdot 10}{10^3}$$

where d_P (µm) and d_s (µm) are fully expanded and systolic diameters respectively, 0.35 is the smaller transverse to the larger in the plane radius ratio and 10^3 is the μm^3/pl conversion factor.

SV and DVL are important determinants of lymph flow (LF, pL/min), which is the product of stroke/compliance volume and contraction frequency. They are also used to calculate ejection fraction (EF), which represents the volumetric fraction of lymph pumped by a lymphatic vessel at each pumping cycle and it is calculated as SV divided by diastolic volume or DVL divided by fully expanded vessel volume.

$$LF = SV \cdot F$$

$$EF = \frac{SV}{\left[\left(\frac{d_D}{2}\right) \cdot \left(\frac{d_D}{2} \cdot 0.35\right) \cdot \pi \cdot 10\right]} \qquad EF = \frac{DVL}{\left[\left(\frac{d_P}{2}\right) \cdot \left(\frac{d_P}{2} \cdot 0.35\right) \cdot \pi \cdot 10\right]}$$

Data are presented as mean ± SE. Differences between mean values have been statistically evaluated with *Student's t-test* or ANOVA after data normality distribution check.

Part II

3.4 *In vivo* experiments

Animals (mean body weight: 286 ± 5 g, n = 7) handling and surgical procedures were identical to the ones previously described. With the use of P-97 Flaming/Brown type Micropipette Puller (Sutter Instrument, Novato, USA), glass pipettes for microinjection were pulled from borosilicate glass capillaries (1B100-4, 1.0 mm outer diameter, 0.78 mm inner diameter, WPI Europe, Berlin, Germany) to tip diameters of ~25 μm and then they were beveled in order to reduce the damaging impact with the interstitial tissue. Pipettes were back-filled with mineral oil and mounted onto a mechanical microinjector (WPI Europe) set to deliver 9.2 nl/injection, at an injecting rate of 10 nl/sec. Under the stereomicroscope, pipettes were front filled with 1 μl of 1 M KCl solution (P9333 – Sigma Aldrich). With the use of a mechanical coarse/fine micromanipulator (Narishige), the pipette was placed next to the interstitium to be injected. Then, the pipette tip was gently advanced through the pleural diaphragmatic surface until it was placed under the mesothelial layer. A single injection of 9.2 nl of KCl 1 M was then triggered, and the pipette tip was immediately withdrawn from the diaphragmatic surface.

Before, during and after the injection maneuver intraluminal lymphatic pressure (P_{lymph}) was measured by the use of the micropuncture technique. P_{lymph} recordings were attained through glass micropipettes pulled by P-97 Flaming/Brown type Micropipette Puller (Sutter Instrument, Novato, USA) and then beveled to a tip diameter of ~2.5 μm. They were back-filled with 1 M NaCl solution and secured to a pipette holder filled with the same solution. The holder was connected to the dome of the motor driven pressure nulling system (Dual Servonull Pressure-Measuring System, Vista Electronics,

Ramona, CA)., in turn connected to a mineral oil-filled pressure transducer (Gould Instruments System). The pipette holder was mounted in a three-dimensional hydraulic micromanipulator (Joystick Micromanipulator MO-188 or MO-109, Narishighe) equipped with a fourth micromanipulator movement to drive the tip of the micropipette into the tissue. The pressure signal was relayed to an amplifier and a signal conditioner (model 6600, Gould Electronics), digitized with an analog-to-digital board, and displayed on the monitor using LabView software (National Instruments). Electrical zeroing of the recording system was performed before and immediately after each measurement by dipping the micropipette tip in a saline pool positioned at the same height of the pipette insertion point. Criteria for acceptance of the micropipette pressure recordings were a) an unchanged electrical zero of the system on withdrawal from the tissue compared with the pre-insertion value, b) a stable pressure reading for at least 10 sec, and c) repeated measurements from the same area were within ±1 cm H_2O.

3.5 Data analysis

The effect of diaphragmatic striated muscle fibers contraction due to KCl exposition on diaphragmatic lymphatics was evaluated as diameter and/or vessel lengths changes before and after tissue contraction in lymphatic vessels which were *perpendicular* or *parallel* with respect to the striated muscle fibers orientation. As more lymphatics were analyzed in the same video *in vivo* recorded, three frames from video data referring to each injection were selected. They represented a) the completely relaxed diaphragmatic striated muscle fibers preceding the KCl injection into the interstitium, b) the maximum contraction of striated fibers following the KCl injection and c) the striated fibers relaxation after at least ~ 30 seconds after *b*. Data were also normalized as percentage of resting diameter or early lymphatic length (l_0) in order to be better compared:

$$\Delta d = \left(\frac{d_{post,i}}{d_{pre,i}}\right) \cdot 100 \qquad \Delta d_{rel} = \left(\frac{d_{rel}}{d_{pre,i}}\right) \cdot 100$$

$$\Delta l = \left(\frac{l_1}{l_0}\right) \cdot 100$$

Where Δd is the effect of diaphragmatic striated muscle fibers contraction on lymphatic vessel diameter expressed as percentage of resting diameter, $d_{pre,i}$ (resting diameter) and $d_{post,i}$ are diameter lengths pre- and post-muscular tissue contraction, respectively, Δd_{rel} is lymphatic diameter after muscle relaxation, expressed as percentage of resting diameter and d_{rel} is diameter in *c*. Δl is linear lymphatic vessel shortening after diaphragm contraction (l_1), expressed as percentage of l_0.

In transverse linear lymphatic vessels stroke volume (SV, expressed in pL) was calculated using mean values of compressed and resting diameters of each analyzed vessel. Based on previous evidences which revealed that the cross-sectional area of

diaphragmatic lymphatics tends to be elliptical rather than cylindrical and the smaller radius in the plane perpendicular to the pleural surface is ~35% of the parallel one (77), it was estimated or a lymphatic segment of 10 μm length as [(diastolic cross-section – systolic cross-section) * 10 μm]

$$SV = \frac{\left\{\left[\left(\frac{d_{pre,i}}{2}\right)\cdot\left(\frac{d_{pre,i}}{2}\cdot 0.35\right)\cdot\pi\right]-\left[\left(\frac{d_{post,i}}{2}\right)\cdot\left(\frac{d_{post,i}}{2}\cdot 0.35\right)\cdot\pi\right]\right\}\cdot 10}{10^3}$$

where $d_{pre,i}$ and $d_{post,i}$ are diameters pre- and post-muscular tissue contraction respectively, 0.35 is the smaller transverse to the larger in the plane radius ratio and 10^3 is the μm^3/pl conversion factor.

Similarly, the diastolic volume load (DVL, expressed in pL) was calculated using mean values of expanded and resting diameter lengths at each analyzed vessel. Also DVL was estimated for a lymphatic segment of 10 μm length as [(diastolic cross-section – systolic cross-section) * 10 μm]

$$DVL = \frac{\left\{\left[\left(\frac{d_{post,i}}{2}\right)\cdot\left(\frac{d_{post,i}}{2}\cdot 0.35\right)\cdot\pi\right]-\left[\left(\frac{d_{pre,i}}{2}\right)\cdot\left(\frac{d_{pre,i}}{2}\cdot 0.35\right)\cdot\pi\right]\right\}\cdot 10}{10^3}$$

where $d_{pre,i}$ and $d_{post,i}$ are diameters pre- and post-muscular tissue contraction respectively, 0.35 is the smaller transverse to the larger in the plane radius ratio and 10^3 is the μm^3/pl conversion factor.

In longitudinal lymphatic vessels DVL (pL) was differently calculated, by using mean values of compressed and resting diameters and lengths of each analyzed vessel.

It was calculated as [(resting volume) – (compressed vessel volume)].

$$DVL = \frac{\left[\left(\frac{d_{pre,i}}{2}\right)\cdot\left(\frac{d_{pre,i}}{2}\cdot 0.35\right)\cdot\pi\cdot l_0\right] - \left[\left(\frac{d_{post,i}}{2}\right)\cdot\left(\frac{d_{post,i}}{2}\cdot 0.35\right)\cdot\pi\cdot l_1\right]}{10^3}$$

where $d_{pre,i}$ and $d_{post,i}$ are diameter pre- and post-muscular tissue contraction respectively, l_0 and l_1 are lymphatic vessel lengths pre- and post-muscular tissue contraction respectively, 0.35 is the smaller transverse to the larger in the plane radius ratio and 10^3 is the μm^3/pl conversion factor.

SV and DVL were also used to estimate ejection fraction (EF), which represents the volumetric fraction of lymph pumped by a lymphatic vessel at each compression and/or expansion due to extrinsic pump and it is calculated as SV divided by resting volume or DVL divided by expanded vessel volume.

$$EF = \frac{SV}{\left[\left(\frac{d_{pre,i}}{2}\right)\cdot\left(\frac{d_{prei}}{2}\cdot 0.35\right)\cdot\pi\cdot 10\right]} \qquad EF = \frac{DVL}{\left[\left(\frac{d_{post,i}}{2}\right)\cdot\left(\frac{d_{post,i}}{2}\cdot 0.35\right)\cdot\pi\cdot 10\right]}$$

Mean values of P_{lymph} were obtained from pressure recordings acquired with Labwiev custom software and analyzed by Clampfit 10.2 Software. Intraluminal pressure gradients (ΔP_{lymph}) due to diaphragmatic muscle contractions were calculated as difference between mean intraluminal lymphatic pressures measured pre- ($P_{lymph,1}$) and at the maximal muscle contraction ($P_{lymph,2}$):

$$\Delta P_{lymph} = P_{lymph,1} - P_{lymph,2}$$

The time interval between pressure pipette positioning and end-recording related to each injection was ~ 4 minutes. During this recording time, in order to avoid possible artifacts in P_{lymph} measure, rats were temporarily disconnected from the ventilator and

oxygenated with a continuous intra-tracheal flux of 50% O_2 in nitrogen at a continuous positive airway pressure of 7 mmHg,

Data are presented as mean ± SE, with n being the number of analyzed sites. Typically, only one site for any given experiment was obtained from one vessel. Statistical significance was evaluated by paired or unpaired *Student's t-test* or ANOVA after data normality distribution check, with $p < 0.05$ being considered significant.

4. Results and Discussion

Part I

4.1 *In vivo* experiments

4.1.1 In vivo diaphragmatic lymphatic network visualization

In vivo lymphatic vessels labeling by peritoneal dye injection is a common technique in order to better visualize lymphatics, which are usually transparent lymph filled. In fact, the diaphragmatic lymphatic network can be visualised under a stereomicroscope equipped with a white light epi-illuminator (Fig 4.1 A). In these conditions, lymphatics appear as darker-than-background vessels lined by white borders. This kind of visualization is very useful to better appreciate the lymphatic vessel orientation with respect to the diaphragmatic striated muscle fibers. On the other hand, the disadvantages of this method mainly consist in the few vessels which can be visualized, most laying on top of the pleural diaphragmatic surface, and the impossibility to use an automatic system to measure the lymphatic vessel diameter length. This is why the diaphragmatic lymphatic network was *in vivo* stained using a FITC-dextran conjugated dye (Fig 4.1 B), which allows a better vessel–to–background contrast and makes much more lymphatics detectable, even if they are not on the top of the pleural surface but immersed in the muscular tissue. The in *vivo staining* technique is based on the unique permeability of initial lymphatics to allow solutes larger than 70 kDa, such as the fluorescent dextrans, to cross their walls. By injecting FITC-conjugated 250 kDa dextrans in the peritoneal cavity, the only vessels which can be filled by these dextrans are lymphatics which drain the peritoneal cavity and the ones lying on the peritoneal surface of the diaphragm. Furthermore, the presence of intraluminal lymphatic valves is easier to identify in fluorescent-filled vessels, due to the inhomogeneous distribution of the tracer on the opposite sides of the valve.

On the other hand, under fluorescence epi-illumination the orientation of diaphragmatic muscle fibers is not always clearly detectable, as well as the presence of adipose tissue, which is primarily located in the extreme periphery of the muscular region.

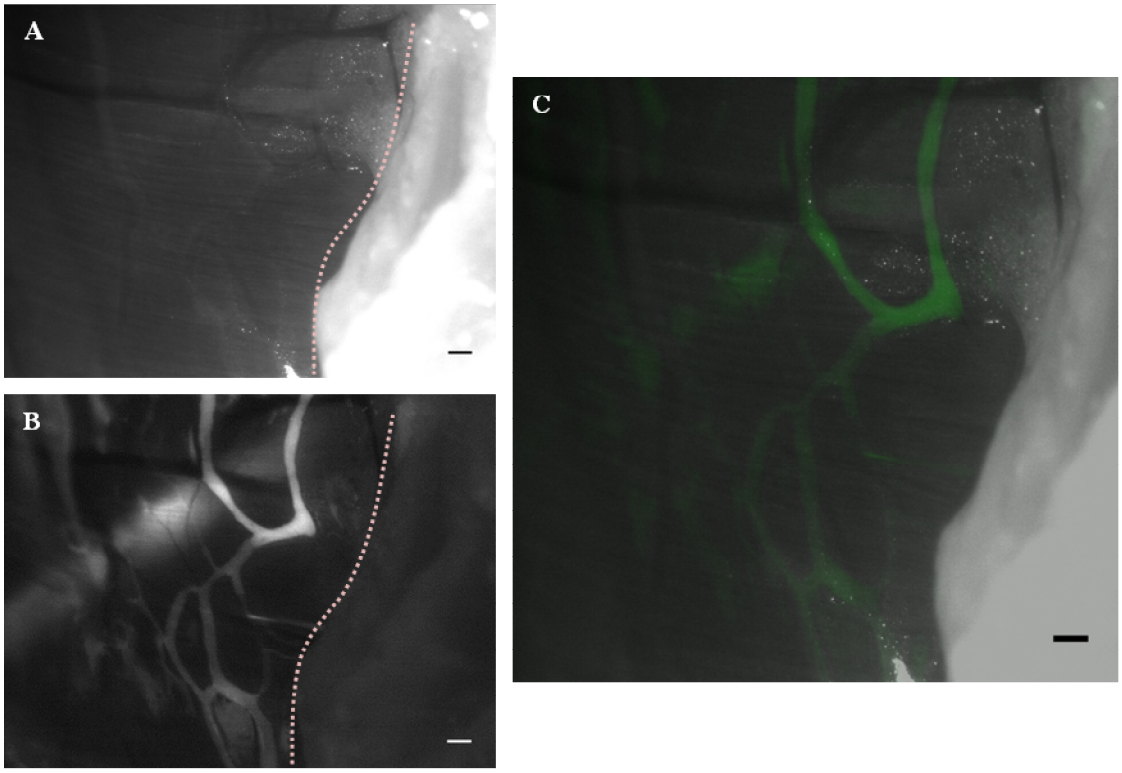

Figure 4.1 Pleural diaphragmatic lymphatic vessels. **A and B**: Diaphragmatic lymphatics can be visualized both in white epi-illumination (A) and fluorescence (B). Lymphatics which are distinguishable both in white light and fluorescence are superficial and mainly located in the muscular region of the diaphragm (pink dotted line), from the extreme periphery next to the ribs. **C** Merged image (green represents the FITC-fluorescent dye filled vessels). Scale bars 500 µm.

Most studies in which diaphragmatic lymphatics were *in vivo* stained, for example by not specific ink-staining (80), were then analyzed *ex vivo*. In experiments like the ones presented here, such a method would have caused too much background staining when the diaphragm would be epi-illuminated with white light. On the contrary, there are no reports about *in vivo* diaphragmatic lymphatics labeling with an intraperitoneal injection of a lymphatic-specific marker such as podoplanin or Lyve-1, which is a common

technique to stain lymphatics locally (219). This is primarily due to the possible negative effects of a systemic exposition to the antibody, which would trigger an immune reaction. Moreover, the high volume of conjugated-primary antibody which should be injected in order to correctly stain diaphragmatic lymphatics would make it a too much expensive technique. Both intrapleural and intraperitoneal fluorescent dye injections can be performed in order to *in vivo* stain diaphragmatic lymphatics. Lymphatic vessels (not specific) fluorescent staining is commonly performed by injecting fluorescent-conjugated high MW dextrans which, in this case, can be drained from the serous cavities only by lymphatics, due to their large size. Based on previous evidences, the intrapleural dye injection results in a better dye invasion into the diaphragmatic lymphatic network (82). In fact, 30 minutes after the pleural injection, ~90% of the fluorescent dye can be found deep in the diaphragm, as after crossing the entire diaphragm it reached the peritoneal side. On the contrary, 30 minutes after the peritoneal injection only a small fraction of the fluorescent dye has reached the pleural surface. Based on these evidences, an intrapleural dye injection would have been preferable to better stain the diaphragmatic lymphatic network. On the other hand the high background staining due to the entire mesothelial pleural surface exposition to the fluorescent dye would impair the automatic diameter measurement. Moreover, a smaller volume of FITC-conjugated dye can be injected in the pleural space, because an increase in pleural fluid volume, mirroring pleural effusion, compromises the respiratory function. This is why an intraperitoneal injection had been performed to *in vivo* stain diaphragmatic lymphatics, with a following longer period of *in vivo* incubation.

Mesenteric lymphatics are the most studied lymphatic vessels, mainly due to their great accessibility and the possibility to perform electrical, mechanical and pharmacological

in vivo and *ex vivo* studies on the full length vessels. Mesenteric lymphatics were found to be leaky to FITC-albumin (~ 4 nm in hydrodynamic radius, (220)), acting as exchange vessels which are able to extravasate solute and filter fluid (221). Unlike what was observed in those vessels, in our experiments diaphragmatic lymphatics were found not to be permeable to extravasation of FITC-fluorescent dextrans (~ 11 nm in hydrodynamic radius, (222; 223)) and microspheres mix injected into the peritoneal cavity. In fact, after 60 min of *in vivo* incubation and at least 150 min of video recording during the experiment, no fluorescent dye extravasated from the vessels lumen.

4.1.2 Determination of lymphatic pumping activity

I*n vivo* fluorescence staining of diaphragmatic lymphatic vessels (85; 83) allowed us to identify much more diaphragmatic lymphatics than we could see by white light epi-illumination. Diaphragmatic lymphatics fluorescence filling also allowed us to visualize both superficial vessels and deeper ones. Many of those fluorescent vessels were also found to be involved in active lymph propulsion, thus leading us to hypothesize that they could be strictly connected to parietal ones.

The FITC-dextran *in vivo* stained vessels were sometimes located more deeply than those previously extensively investigated (77; 224; 76), both in the tendineous region and among the muscle fibers. Those which lay in the extreme muscular periphery, next to the ribs, are mainly organized in complex loop structures, which are wider than others in the muscle (on the right side of Fig 4.2 A) and connected by linear tracts. On the contrary no loops were found in the tendineous (on the left side of Fig 4.2 A) region, but only linear vessels, most of them organized longitudinally with respect to the diaphragmatic muscle fibers. The most peripheral vessels showed rhythmic diameter

changes during the *in vivo* video recordings. In lymphatics immersed in soft tissues, such as mesenteric lymphatics, most of these changes are due to active contractions which depend upon the smooth muscle layer in their vessel wall, both as pacemaker sites and showing a coordinated pumping activity along the network.

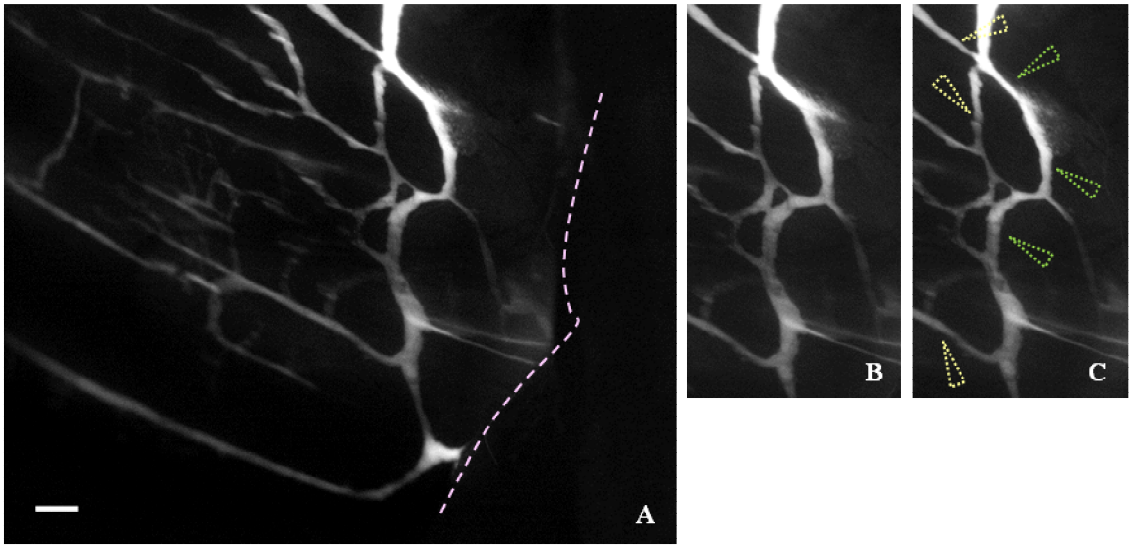

Figure 4.2 Diaphragmatic lymphatics pumping activity. Lymphatics located in the extreme periphery of the diaphragm showed pumping sites, affecting vessel diameter. **A** Overview of the pleural lymphatic network of the right part of the diaphragm, in which complex loops are clearly distinguishable next to the ribs (pink dashed line, scale bar 500 µm). **B and C** Image sequence showing lymphatic vessels diameter changes in distinct sites (green arrowheads), which can be recognized in some tracts of the same network, whereas adjacent sites exhibited no diameter changes during the recording time (yellow arrowheads).

Intrinsic pumping was extensively studied in mesenteric lymphatic vessels (156) and in the thoracic duct (225). However the thoracic duct and especially the diaphragm, are exposed to a physical environment that is very different from the one to which mesenteric lymphatics are exposed. Regarding diaphragmatic lymphatics, we found spontaneous changes in lymphatic vessels diameter only in those vessels which laid in the muscular peripheral region, next to the ribs, mainly in lymphatic loops. Indeed, diaphragmatic lymphatics running in the lateral to medial part of the muscular and tendineous diaphragm rely for their function only on the extrinsic mechanism (84; 83).

By modeling mechanical stresses affecting the diaphragmatic structure during cyclic respiratory movements, it was demonstrated that they are mostly located in the central stiffer tendineous region. On the contrary, minimal stresses appeared to be present in the peripheral muscle region (Negrini unpublished data). Thus, it is possible that smooth muscle elements in peripheral diaphragmatic lymphatics wall are required to supply the driving forces to sustain lymph formation and/or propulsion. Indeed, it is worth noting that inhibition of intrinsic contractile activity in the diaphragm reduces pleural lymphatic flow by ~ 40 % (81).

At present, there is no report of lymphatic vessels pumping activity in the muscular diaphragm, in which lymph drainage and propulsion have always been thought to be primarily affected by extrinsic forces generated by cardiac and respiratory movements. On the other hand, in a very recent study performed in our laboratory (226), it was found that in some loops the flow direction not always follows pressure gradients but instead is able to revert multiple times with an average frequency of ~ 4 times per minute. In these vessels lymph progression is oscillatory, both simultaneously or in sequence in the same and/or different tracts of the same loop, not dependent on cardiac or ventilatory frequency.

4.2 *In vitro* experiments

4.2.1 Localization of lymphatic smooth muscle

Immunostaining for smooth muscle alpha actin (α-SMC), which is one of the most used markers in order to stain lymphatic smooth muscle (121), led us to confirm that diaphragmatic lymphatics possess smooth muscle elements in their vessels wall (227). In fact, confocal analysis of the whole mount immunostainings for s α-SMC (red signal in Fig 4.3 B) of previously *in vivo* recorded diaphragmatic lymphatic networks strongly emphasized the presence of smooth muscle fibers in the wall of several diaphragmatic lymphatic vessels. In fact, similarly to skeletal muscle (228) and myocardial (229) lymphatics, smooth muscle cells are scanty in costal (84) and diaphragmatic (48) lymphatic vessels. Therefore, at least in initial lymphatics, lymphatic function seems to primarily depend upon extrinsic pumps (83; 82), maybe supplemented by lymphatic smooth muscle intrinsic contractility. Data showed α-SMC immunoreactivity in almost all vessels previously *in vivo* FITC-labelled in the lymphatic network.

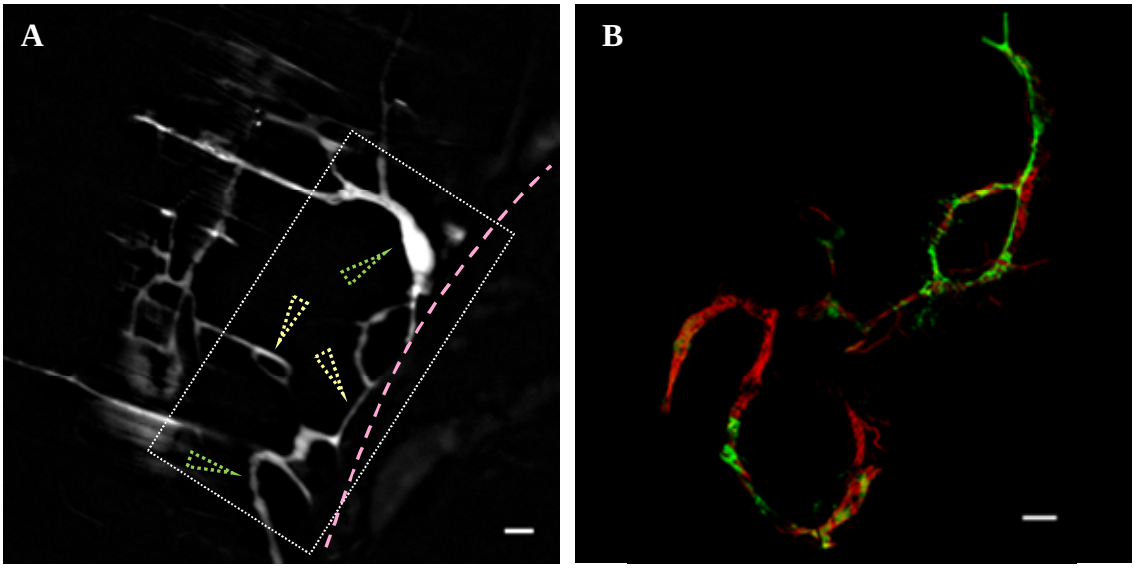

Figure 4.3 Smooth muscle α-actin lymphatic immunoreactivity. **A**: Peripheral lymphatics (green arrowheads) *in vivo* showing intrinsic pumping activity and not pumping vessels (yellow arrowheads). **B**: The whole mount staining for α-SMC, corresponding to the white dotted rectangle in A, highlights the presence of smooth muscle elements in the vessel wall of lymphatics of the entire network, whose disposition varies between contracting and not contracting sites (see text for details, green FITC-dextran dye, red α-SMC).(scale bars 500 μm).

On the other hand, it is worth noting that the distribution of the smooth muscle fibers surrounding lymphatic vessels are not homogenous. In fact, results showed that the smooth muscle mesh arrangement was extremely variable: in contracting sites (Fig 4.4 A and B) smooth muscle elements were organized in a dense mesh, completely encasing the lymphatic vessel (Fig 4.4 E), also visible in the inset showing the cross-sectional area (Fig 4.4 E inset) taken at the white line position. Conversely, in not pumping sites (Fig 4.4 C and D) smooth muscle elements were also present, but they were more sparsely organized, showing a lot of large gaps around the vessel wall, as illustrated by the cross-sectional images (Fig 4.4 F insets). They also generally ran longitudinally to the vessel major axis, a way not adequate to compress the vessel and correctly propel the lymph flux.

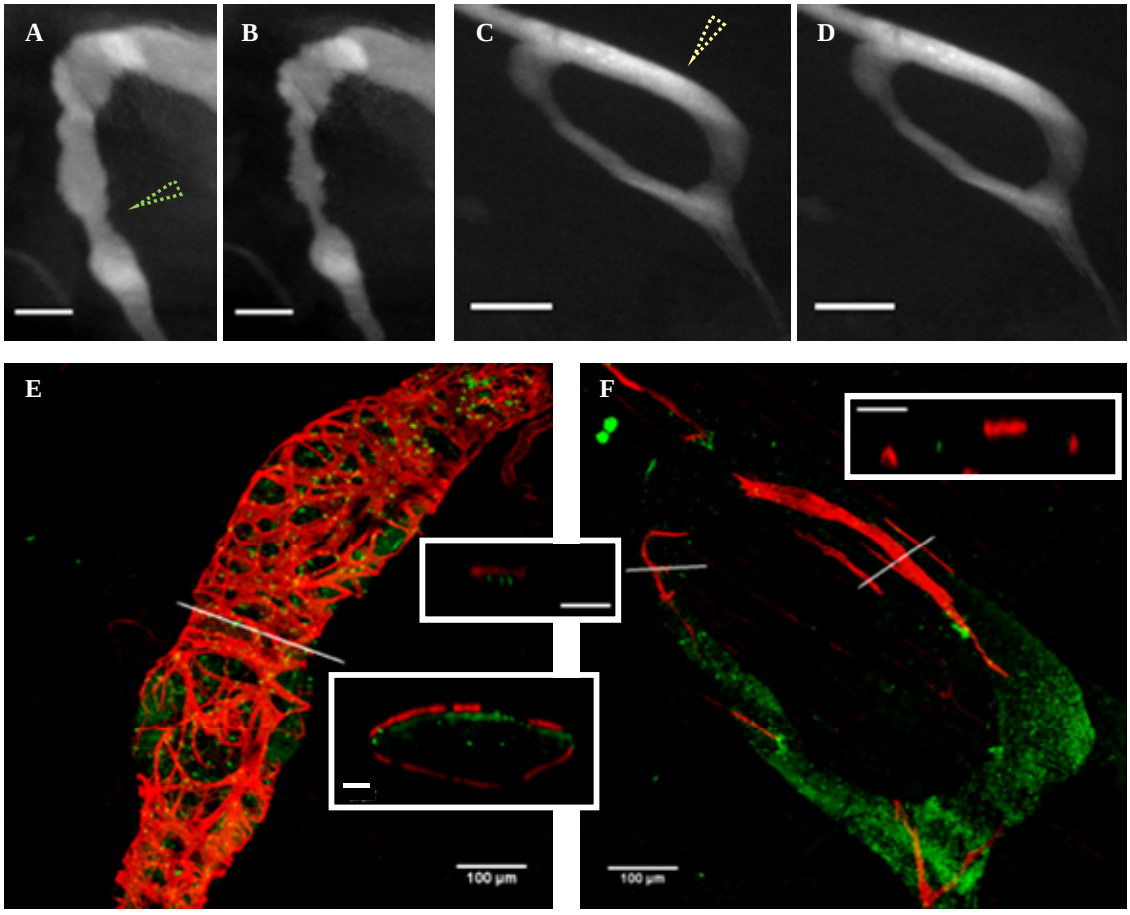

Figure 4.4 Smooth muscle elements in lymphatic vessels wall. **A and B** Still images showing an actively pumping lymphatic tract *in vivo* video recorded at different times. **C and D** Still images showing not pumping vessel *in vivo* video recorded at different times. (scale bars 250 µm). **E** α-SMC immunoreactivity of the same contracting site in A and B. **F** α-SMC immunoreactivity of the same loop in C and D (scale bars 100 µm). Insets show the cross-sections at the white lines in both panels E and F, (scale bars 25 µm). Green arrowhead pumping site, yellow arrowhead not contracting site.

By analyzing the complex organization of smooth muscle cells surrounding diaphragmatic lymphatics with respect to video *in vivo* recorded showing spontaneous pumping activity it was evident that the presence of smooth muscle elements was not sufficient *per se* to explain the lymphatics behavior, since smooth muscle elements were found both in spontaneous pumping vessels and not pumping ones. Looking at Fig 4.4 (E-F), it is clearly evident that the smooth muscle mesh organization in the lymphatic vessel wall is a key point in order to understand lymphatics function. In fact, in

spontaneously pumping sites, a well organized smooth muscle layer can be found, whereas in other sites smooth muscle elements are mainly arranged transversally or oblique than longitudinally with respect to the lymphatic orientation, suggesting that lymphatic smooth muscle cells are not arranged in clear longitudinal and circular layers as in the gastrointestinal tract (230) but may be made up of strongly interconnected bundles of cells running in many different directions setting up a complex mesh. On the other hand the longitudinal orientation of smooth muscle fibers in most of not pumping lymphatic vessels is not unusual, as smooth muscle cells longitudinally oriented can be found in rabbit arteries (231). In this study we found that longitudinally oriented smooth muscle fibers surrounding lymphatics were always scanty and dispersed, not completely encasing the lymphatic vessel but, on the contrary, forming many gaps in the muscle layer.

4.2.2 Detection of intraluminal lymphatic valves

Lymphatic intraluminal valves were observed in both linear vessels and loops, where they are probably involved in the control of both flow direction and fluid recirculation. Intraluminal valves detection relies on the different FITC-conjugated dye accumulation on the opposite sides of the valve, as shown in Fig 4.5 A. The FITC-dextran flow direction follows the lymph flow, as reported in the diagram in Fig 4.5 B and backflow is prevented by valve closure, avoiding lymph leakage from the loop structures. Moreover, the FITC-dextran accumulates as reported in Fig 4.5 B (green), allowing to obtain the three-dimensional views shown in Fig 4.5 C and D. They were obtained as “negatives”: in fact they correspond to the fluorescent dye accumulated in the vessel and not to the intraluminal valve itself. Then, a color-code was applied to better

appreciate the three-dimensional overview: the funnel, in particular (Fig 4.5 C), is clearly recognizable in the lateral view.

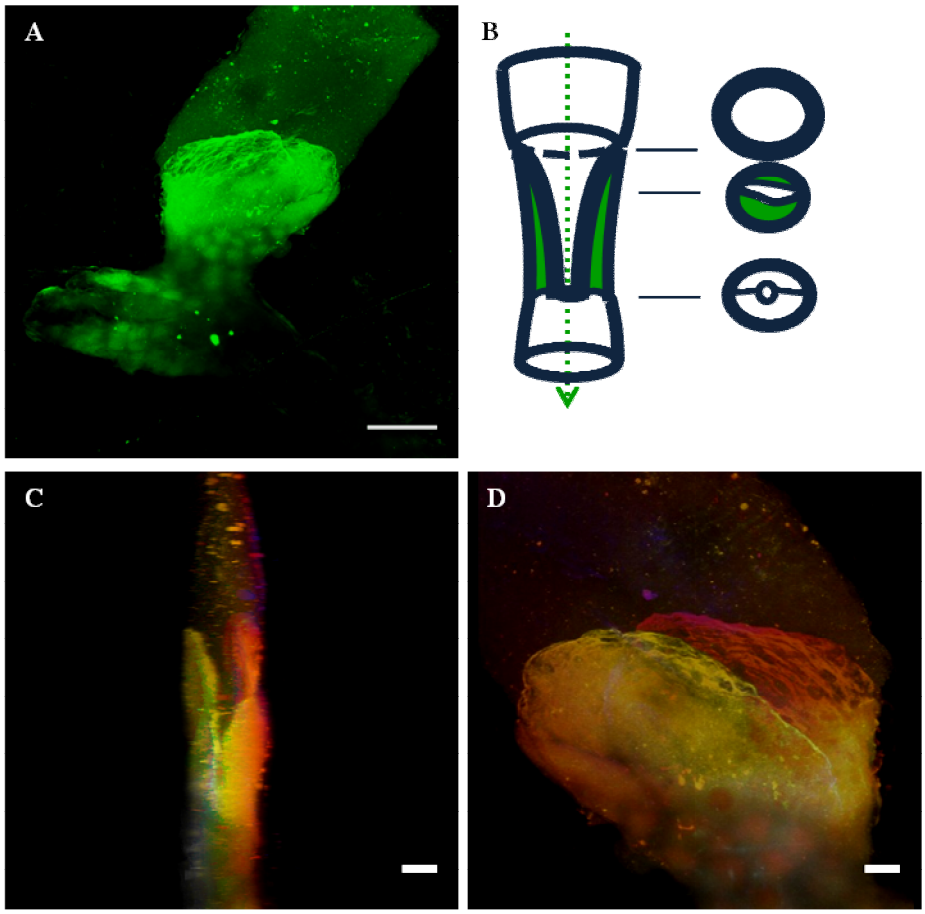

Figure 4.5 Lymphatic intraluminal valve. **A** The lymphatic valve is evident due to the different FITC-dextran accumulation profiles at the opposite sides of the valve itself (scalebar 100 µm). **B** Diagram showing lymph flow direction and FITC fluorescent dye accumulation next to the funnel. **C and D** 3D projection of the intraluminal valve showing lateral (C) and frontal (D) views (scale bars 25 µm). In C is particularly evident the valve funnel.

Intraluminal lymphatic valves gating depends on trans-valve pressure gradients, that allow lymph progression along the lymphatic network, which in turn depend on extrinsic and/or intrinsic forces acting on lymphatics. Particularly, in lymphatic vessels showing intrinsic contractility, during lymphatic systole the lymphatic smooth muscle cells contraction increases the intraluminal pressure. Given that the intraluminal

pressure increases and that all adjacent lymphangions do not contract at the exact same time but sequentially, some lymph flows in the retrograde direction, closing the input valve of the lymphangion during the beginning of systole (105; 140).

4.3 Functional behavior of diaphragmatic lymphatics

4.3.1 Lymphatics functional features

Temporal profiles of diaphragmatic lymphatics diameter changes, which modulate the resistance to lymph flow, led to highlight the existence of vessels which propel lymph either actively or passively. Fig. 4.6 shows examples of the changes over time of the diameter of diaphragmatic lymphatic vessels simultaneously measured at four different sites of the same loop. The systematic examination was performed on 15 loops *in vivo* video recorded from 11 rats at 201 sites and allowed to define four different classes of lymphatics. In traces of Fig. 4.6 the downward deflection from the steady value corresponds to an active stroke, whereas upward deflections from the baseline value correspond to passive vessel enlargements. The analysis of Fig. 4.6 allows to distinguish vessels segments presenting active contractions (Fig 4.6 A and B) and others characterized by *passive* enlargemnts only (Fig 4.6 C). In addition, the contracting segment of Fig. 4.6A do not show any sign of fluid accumulation during the diastolic phase, as from the relative constancy of the baseline diameter, whereas in case of segment depicted in Fig. 4.6 B, there is a clear increase in vessel diameter before the beginning of the active stroke. Therefore we defined the segments behaving like that in panel A as *pure actives* and those similar to that in panel B as *hybrids.* Finally, the segment of panel D showed no diameter change over time and was therefore defined *invariant* vessels (Fig 4.6 D).

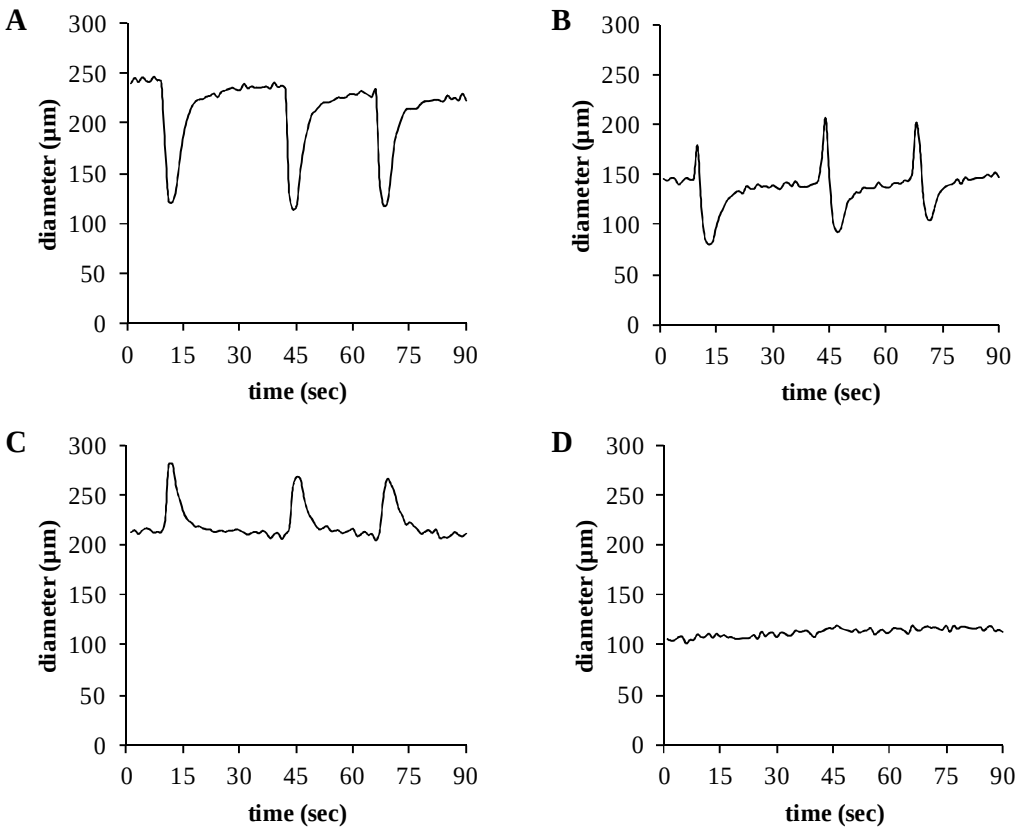

Figure 4.6 Different lymphatics behavior recognized based on the simultaneously recorded diameter changes vs time profiles. **A** Pumping site in which active spontaneous contractions were found. **B** Hybrid site showing a passive distension and a subsequent active contraction. **C** Passive compliant site. **D** Invariant not contracting site.

Most of actively pumping lymphatic vessels, as the mesenteric ones, show features like pure active diaphragmatic lymphatics (156), in which the stroke causes the diameter length shortening and then after the vessel relaxation it returns back to the initial diastolic length. Moreover, most of the analyzed diaphragmatic sites belonged to this class. This kind of contraction results in a rapid reduction of the lymphatic diameter length, a decrease in lymphatic compliance, an increase in the local lymph pressure, the closure of the upstream valve, the opening of the downstream valve, and the ejection of lymph into the next downstream lymphangion and can be explained by cardiac analogy (205) by dividing contracting period into lymphatic systole and diastole. This behavior

was encountered in lymphatic vessels investigated in this study, only located on the extreme periphery of the pleural surface of the diaphragm. Data related to the estimated compliance of deeper diaphragmatic vessels (224), which is similar to the one of mesenteric lymphatics (87), also suggests that in lymphatics not encased in a stiffer tissue (as the tendineous or muscular diaphragmatic ones) the smooth muscle layer also supplies the correct mechanical support, thus confirming the strong environmental effects on lymphatic functions.

On the other hand several diaphragmatic lymphatic sites showed a not pumping behavior, as their diameter never changed during the recording periods and they were classified as invariant sites. Since *in vivo* recordings were performed after blocking the respiratory movements, one cannot exclude that those invariant sites may exhibit a different behavior during spontaneous breathing. Unfortunately such a condition cannot be evaluated by the experimental setup used for this study performed in open chest. Indeed, since intrinsic pumping activity can be modulated by pharmacological or mechanical stresses too (129; 50; 232), one cannot exclude a similar effect on not-pumping vessel. In fact, very recent data from ongoing experiments seem to indicate that mechanical stimulation of diaphragmatic lymphatics, due to diaphragmatic skeletal muscle fibers contraction, induced pumping activity in invariant sites which were not directly mechanically stimulated, leading to hypothesize that pumping activity in those diaphragmatic lymphatics could at least in part be mediated by lymph flow.

Vessels belonging to different classes were interconnected in the very same loop. For example, in the network reported in Fig 4.7, the upper part of the loop was involved in the active lymph propulsion (violet line), whereas the lower part showed passive

compliant behavior, maybe acting as a passive lymph reservoir (green line). An hybrid tract (light blue line) was also present among them. Moreover, lymph entered the loop from the actively pumping upper input branch, running in parallel in both arms of the loop towards the invariant (pink line) lower output branches.

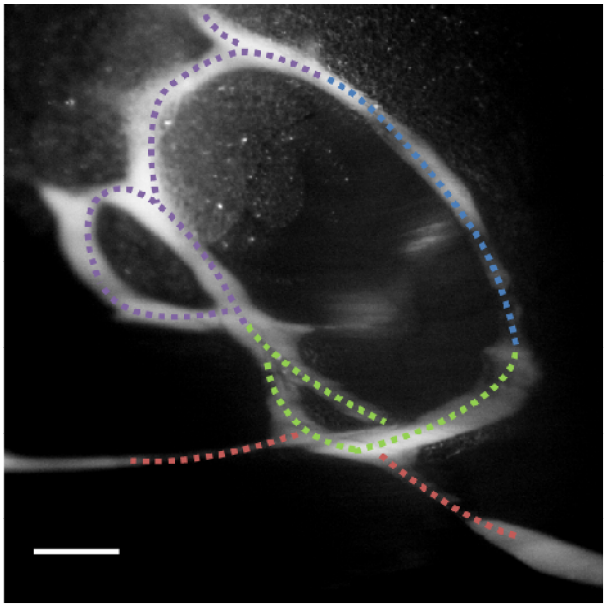

Figure 4.7 Different mechanical behavior of adjacent lymphatic tracts. Different regions belonging to the same network showed different mechanical behavior: an active pumping tract (violet line), a passive reservoir region (green line), a tract showing hybrid features (light blue line) and two invariant branches (pink line) were identified (scale bar 500 µm).

This kind of data analysis led us to understand that there is an extremely well structured functional organization in lymphatic loops and, in particular, that hybrid and/or pure passive regions are always in conjunction with pure active ones, as they also contract or enlarge with the same active sites frequency, forming functionally distinct regions which cooperate in order to correctly propel lymph fluid.

Most of active pumping sites, arranged in actively pumping regions are also surrounded by adipose tissue, as it is clearly evident in Fig 4.7. In fact, the violet dotted line highlights the active propelling tract which is the region of the lymphatic loop in which

adipose tissue can be extensively identified. Although the presence of lymphatic capillaries have not yet been completely clarified within adipose tissues, adipose tissue generally surrounds most of collecting lymphatic vessels and lymph nodes (233). Particularly, a study by Pond and colleagues (234) had defined this perilymphatic adipose tissue as being metabolically essential for proper immune responses and as a source of energy for immune activation and proliferation. Recent evidences indicating an increase in mesenteric lymphatic vessel contractility in the presence of oxidized low density lipoproteins (ox-LDL) suggest a direct effect of lipids on lymphatic contractility (235). However, the precise mechanisms by which this occurs and the impact of lipid metabolism on lymphatic functions are poorly understood. Moreover, as mesenteric lymphatics mainly drain nearly all lipids absorbed from nutrients, whether there is a causal relationship between lipid content in the lymph and fat deposition is not known.

Pure active lymphatics displayed periodic contractions alone and represent the major share of diaphragmatic lymphatics, with 52 % of analyzed sites falling therein. Their mean diastolic diameter was 161.98 ± 5.62 µm (n = 102) and no statistical differences were found between sexes. Vessel contraction made the systolic diameter significantly shorter than the diastolic, with a mean value of 74.55 ± 1.23 % ($p<0.01$ with respect to their diastolic diameter, paired t-test, n = 102; 120.16 ± 4.77 µm, $p<0.01$ with respect to their diastolic diameter, paired t-test, n = 102, Fig 4.8, violet bars). The mean contraction frequency of active vessels was 6.96 ± 0.37 bpm (n = 102).

Hybrid vessels showed a very complex behavior since the firstly expanded reaching a diameter peak value and subsequently contracted to a smaller systolic diameter . They represent the minor share of diaphragmatic lymphatics, with 4 % of analyzed sites

falling in this class. The mean value of their resting diameter was 147.16 ± 13.25 µm (n = 8), rising up to 123.86 ± 7.62 % of resting value ($p<0.01$, paired t-test, n = 8; 179.12 ± 13.35 µm, $p<0.01$ with respect to resting diameter, paired t-test, n = 8) and then falling to 66.02 ± 1.61 % ($p<0.01$, paired t-test, n = 8; 96.89 ± 8.58 µm, $p<0.01$ with respect to resting diameter, paired t-test, n = 8) of the diastolic diameter (Fig 4.8, light blue bars). The mean contraction frequency of hybrid vessels was 2.46 ± 0.13 bpm (n = 8). Relaxation time constant, τ was found to be significantly higher in active pumping vessels (2.66 ± 0.13 sec) than in hybrid lymphatics (1.73 ± 0.28 sec, unpaired t-test, $p<0.05$).

Passive compliant lymphatics represent 5 % of analyzed sites. Their mean diastolic diameter was 185.95 ± 32.16 µm (n = 9) and increased to 133.63 ± 7.32 % ($p<0.01$ with respect to diastolic diameter, paired t-test, n = 9) with respect to resting diameter (237.06 ± 36.96 µm, $p<0.01$ with respect to diastolic diameter, paired t-test, n = 9, Fig 4.8, green bars) due to lymph flow, with a relaxation frequency of 2.86 ± 0.51 bpm (n = 9).

Contraction frequency and/or vessels enlargement frequency were not affected both by respiratory cycle (71 ± 3 breaths/min) and heart rate (118 ± 9 bpm, at 122 ± 7 cm H_2O blood pressure measured at the carotid artery with the chest wall open).

Invariant lymphatics showed a diastolic diameter never changing during the recording periods, with 40% of analyzed sites falling therein. Their mean diameter was 154.37 ± 7.40 µm (n = 78), not statistically different from the diastolic diameter of all the other classes ($p = 0.448$, one way ANOVA, 196 d.f, Fig 4.8, pink bars).

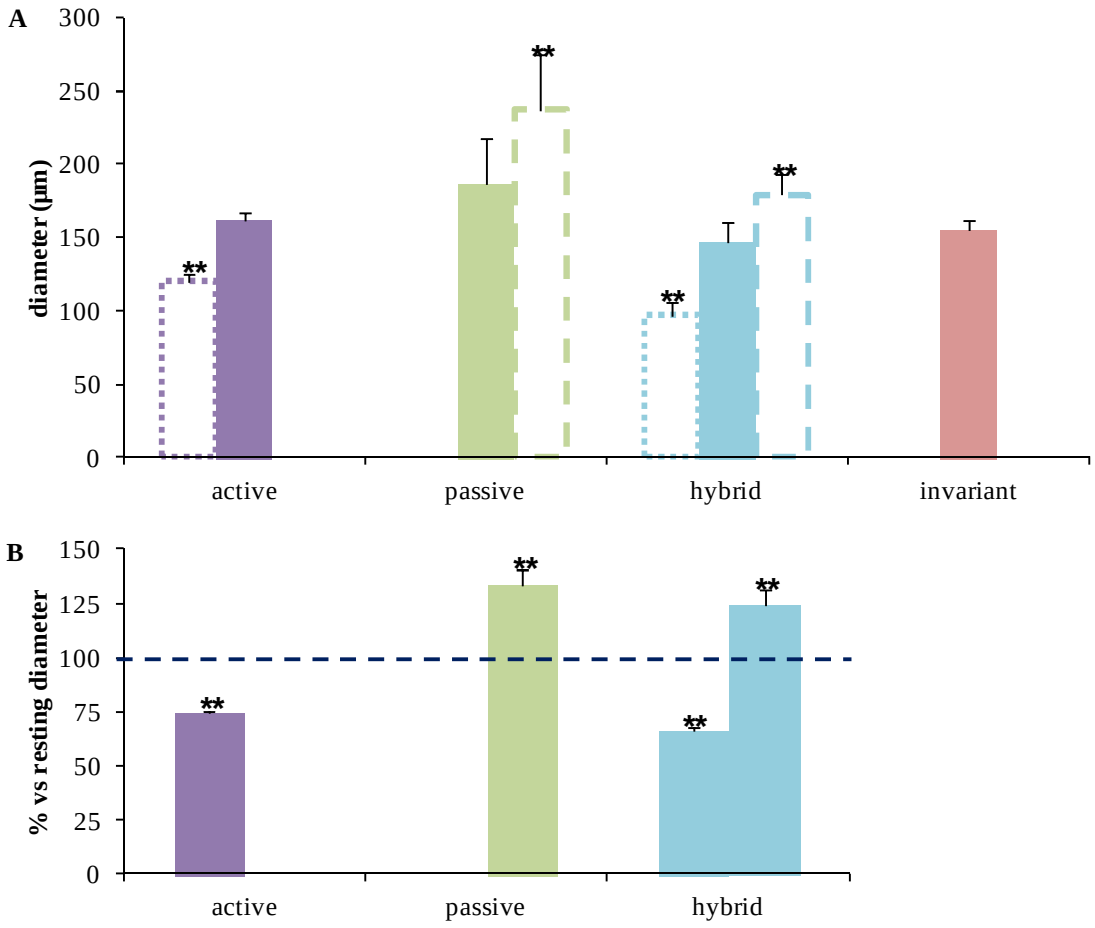

Figure 4.8 Diaphragmatic lymphatics diameter changes. **A** Mean resting diameter length for the four classes of lymphatics (solid color bars) compared with systolic (hollow dotted bars) and fully expanded (hollow dashed bars) diameter (** $p<0.01$ vs resting diameter). **B** Systolic and fully expanded diameter-vs diastolic difference, expressed as percentage, with respect to 100% (diastolic diameter, ** $p<0.01$).

Despite we found no difference in lymphatic mean diastolic diameter (Fig 4.8) between the four analyzed classes of diaphragmatic lymphatics, more than 90% of them belonged to pure active or invariant classes. Interestingly, active and invariant sites seems to be the stiffest lymphatics if compared to the other classes.

4.3.2 Relationship between amplitude of contractions and resting diameter in active vessels

Looking at active pumping vessels, Δ contraction (diastolic – systolic diameter, expressed as percentage of diastolic diameter) in each site was found to be different from each other. In fact, the analysis of all 102 actively pumping sites highlighted an extreme variability among their contraction amplitudes, ranging from 4.8 % to 66.5 % of their diastolic diameter. It was then investigated the possible existence of a Δ contraction dependence on the resting diameter and data were grouped based on the diastolic diameter in classes of 50 µm increments. As reported in the graph showed in Fig 4.9, concerning Δ contraction, no significant differences were found among all groups ($p = 0.257$, one way ANOVA, 100 d.f.), thus allowing to conclude that Δ contraction of active pumping sites is independent from diastolic vessel diameter.

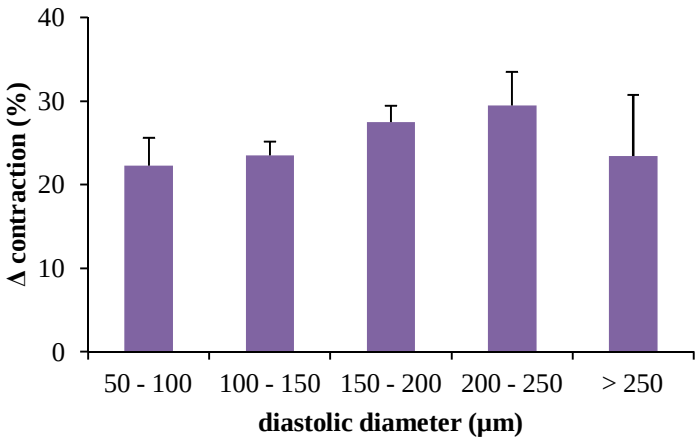

Figure 4.9 Δ contraction of active pumping sites which varied in size.

It is interesting to note that hybrid sites contract and/or enlarge with a contraction amplitude not different from pure active or passive sites. The same contraction amplitude (~ 25% with respect to resting diameter) was also reported in actively

pumping adult rat mesenteric lymphatics, which was found to be slightly reduced by aging (~ 20% with respect to resting diameter, (236)).

Generally, the frequency and amplitude of lymphatic contractions vary significantly (237). Benoit and colleagues (101) found that the mesenteric lymphatics showing phasic contractions had mean resting diameter of ~ 70 µm and a contraction amplitude of ~ 43% of diastolic resting diameter. In another paper, the same authors found that lymphatics with mean resting diameters of ~ 110 µm had a contraction amplitude of ~ 35% of diastolic resting diameter (186). Galanzha and colleagues (238) found that lymphatics which had mean resting diameters of ~ 150 µm had an amplitude of ~30%. Hence, these data indicate that generally larger lymphatics have smaller amplitude of phasic contractions. Conversely, in diaphragmatic lymphatics we found that the contraction amplitude of actively pumping vessels is independent on the lymphatics diameter.

Notwithstanding no contraction amplitude variability was found among actively pumping sites of different size, they were extremely variable in both their diastolic and systolic radii (Table 4.1). Fluid flux (J) in an ideal vessel is given by Poiseuille's Law

$$J = \frac{\Delta P \cdot \pi \cdot r^4}{8 \cdot \eta \cdot l}$$

where ΔP represents the pressure hydraulic gradient which drives fluid flux, η is fluid viscosity and l is the vessel tract length. Thus, an extreme variability in diameter would greatly affect lymph flux, therefore lymphatic vessels diameter appears quite homogenous within the same loop structure, even if their diameters also vary between adjacent loops.

interval (µm)	n	mean d (µm)	Δ contraction (%)	p value	mean r (µm)	systolic r (µm)
50 - 100	14	80.65 ± 3.36	22.31 ± 3.31	no	40.33 ± 1.68	31.45 ± 1.31
100 – 150	34	129.95 ± 2.41	23.54 ± 1.64	no	64.97 ± 1.20	50.03± 0.93
150 - 200	31	173.02 ± 2.37	27.51 ± 1.97	no	86.51 ± 1.19	63.15 ± 0.87
200 - 250	15	222.02 ± 3.26	29.48 ± 4.02	no	111.01 ± 1.63	78.82 ± 1.16
> 250	8	285.10 ± 6.56	23.45 ± 7.30	no	142.55 ± 3.28	109.77 ± 2.53

Table 4.1 Summary of Δ contraction mean values of active pumping sites which were grouped based on their diastolic diameter (d) in steps of 50 µm. Mean diastolic radius (r) and systolic r are also reported.

4.3.3 Relationship between amplitude and frequency of contractions in active vessels

The variability of contraction amplitudes among actively pumping sites was also investigated in order to identify its possible dependence on contraction frequency. In fact, a great variability in contraction frequencies was also found in this class of vessels, ranging from 2.2 bpm to 17.4 bpm, even if contraction frequency was found to be independent from vessel size (data not shown).

Δ diameters (systolic - diastolic diameter change) were plotted (Fig 4.10) as a function of contraction frequency.

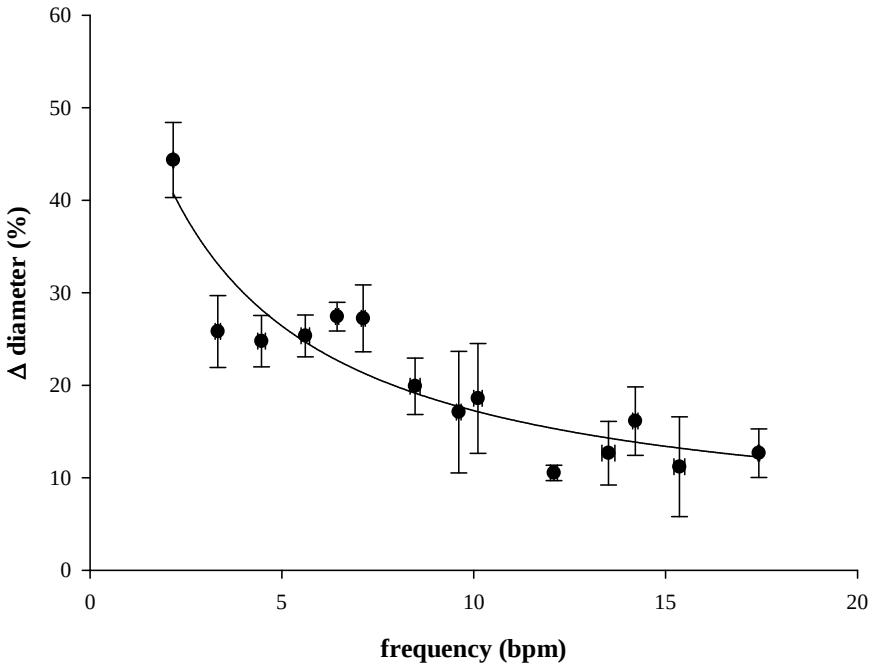

Figure 4.10 Dependence of vessel Δ systolic - diastolic diameter as a function of corresponding contraction frequency in active lymphatic vessels: data were classified based on contraction frequency and plotted as mean values of each resulting group (see the text for further details).

The pooled data were best fitted by a rectangular hyperbola of the following type:

$$y = y_0 + \frac{a \cdot b}{b + x}$$

where (y_0 = 3.94, a = 71.92, b = 2.27). Although quite dispersed, data tended to significantly (n = 14, r^2= 0.84, $p < 0.01$) decrease with increasing frequency, indicating that the relationship between diameter change and contraction frequency tended to keep the flux at a steady value inside the same structure (see paragraph 4.3.5).

Such a kind of inverse relationship was also described by Amerini and colleagues (239) by investigating the modulatory effects of substance P administration to rat mesenteric lymphatics. In that study, SP increased basal tone and chronotropy but reduced both systolic and resting diameter lengths, leading to a reduction in spontaneous contraction amplitude. Also Gasheva and colleagues (225) found a positive chronotropic effect

compensating the reduction of contraction amplitude by testing the modulatory effect of l-NAME on spontaneously pumping lymphatics, since fractional pump flow (EF · CF) did not significantly changed during the NO synthase blockade.

It is worth noting that Δ diameter and frequency heterogeneity were encountered also within the same lymphatic network. For example, plotting data related to a single network in a Δ diameter vs frequency graph resulted in the identification of two separated classes, both in Δ diameter and cycle frequency (Fig 4.11). The low frequency class (n = 8) had a mean contraction frequency of 5.7 ± 0.3 bpm and a mean value of Δ diameter of 28.0 ± 1.5 %, whereas the high frequency class (n = 7) had a mean contraction frequency of 13.5 ± 0.5 bpm (unpaired t-test, $p<0.01$) and a mean value of Δ diameter of 7.9 ± 1.1 % (unpaired t-test, $p<0.01$), thus confirming existence of two functionally distinct loops which cooperated in the same lymphatic network.

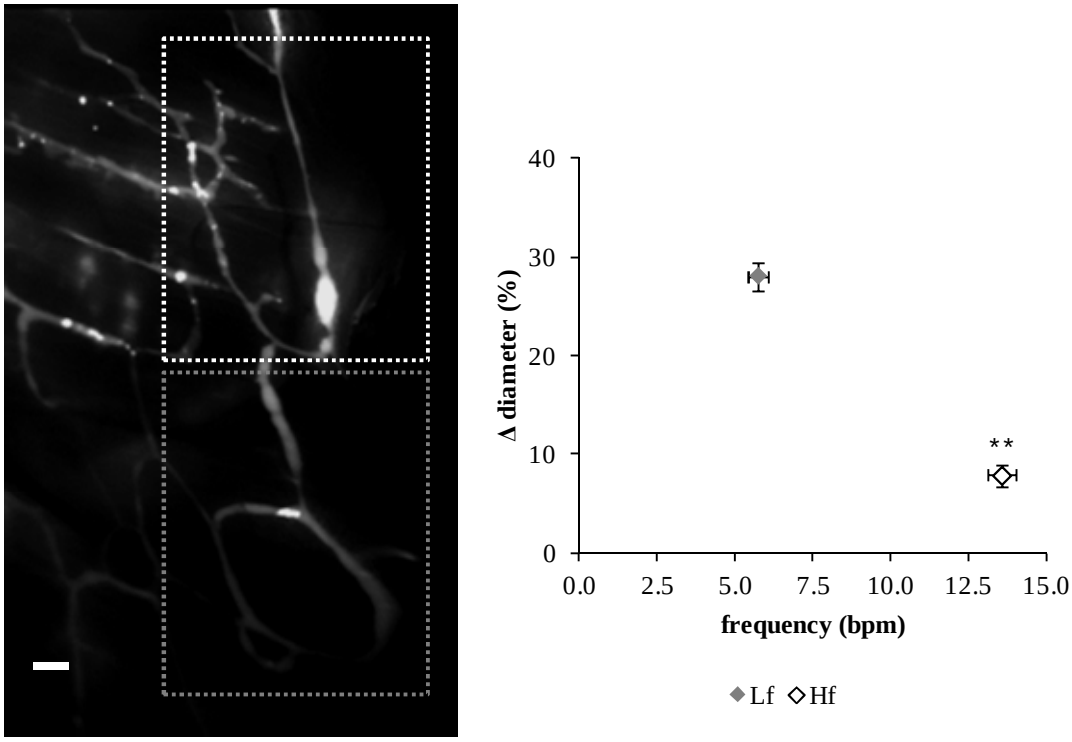

Figure 4.11 Different regions in the same lymphatic network show-significantly different Δ diameter vs frequency values. In regions of the loop where the contraction frequency is low (Lf), Δ diameter is large, (grey dotted rectangle) whereas where contraction frequency is high (Hf) Δ diameter is about three fold lower (white dotted rectangle). Scale bar 500 µm.

In general, the functional diversity of smooth muscle elements is characterized by the different contractile activity: phasic smooth muscle cells which can be found in gastrointestinal tract exhibit rhythmic rapid shortening and relaxing cycles, whereas tonic smooth muscle cells which are found in blood vessels wall have slower shortening velocities and prolonged contraction (240). We found that mean value of contraction frequency of pure active peripheral pumping lymphatics of adult rats was ~ 6 bpm, a value in close agreement with that of Benoit (101) and Akl (236) (~ 6 - 9 bpm). As lymphatic vessels actively contract to regulate lymph fluid transport, the lymphatic contractions which drive lymph propulsion (phasic brief contractions) and the ones that alter flow-resistance (tonic, long-lasting contractions) coexist (156; 241) in the same

lymphatic network, thus probably explaining the existence of, respectively, high- and low-frequency active pumping sites.

4.3.4 Functional parameters in lymphatics

In order to standardize data obtained from vessels of different lengths and based on the evidence previously reported (77) that in diaphragmatic lymphatics the ratio between the diameter perpendicular to the pleural surface and the superficial one is 0.35, it had been possible to calculate SV, DVL, EF and LF in a vessel tract arbitrarily set 10 µm long.

	Stroke Volume (pL)	Diastolic Volume Load (pL)	Ejection Fraction (%)	Contraction/expansion frequency (bpm)	Lymph Flux ($pL min^{-1}$)
active	34.9 ± 3.0	n.a.	43 ± 2	6.96 ± 0.37	199.3 ± 13.9
invariant	n.a.	n.a.	n.a.	n.a.	n.a.
hybrid	64.4 ± 9.7	28.7 ± 6.7	70 ± 3	2.46 ± 0.13	152.6 ± 20.5
passive	n.a.	66.7 ± 24.4	40 ± 6	2.86 ± 0.51	106.7 ± 50.6
p value	$p < 0.01$	no	$p < 0.01$	-	no

Table 4.2 Lymphatics mechanical parameters. Stroke volume (SV, for contracting vessels) and diastolic volume load (DVL for vessels which underwent to an enlargement) were normalized and expressed as ejection fractions, i.e. as % of the end-diastolic volume . SV and CV were also used to estimate lymph flux.

SVs of active pumping sites were normalized with respect to diastolic volumes whereas SVs and DVLs of hybrid and passive sites were normalized with respect to fully expanded vessel volumes and expressed as EFs. The EF represents the average volumetric fraction of lymph propelled with each vessel contraction or accommodated with each passive vessel enlargement. As reported in Table 4.2, the EF was similar ($p = 0.667$, unpaired t-test) in active pumping sites and adjacent passive ones, whereas hybrid sites had an higher EF with respect to both active ($p<0.01$, unpaired t-test) and passive ($p<0.01$, unpaired t-test) sites due to the vessel enlargement which preceded the active stroke, allowing a great volume of lymph to be accommodated and subsequently propelled.

Focusing on the EF of the major class of diaphragmatic lymphatics sites (i.e active pumping ones) which corresponds to 43 % of lymphatic diastolic volume, it is worth noting that it is significantly lower than mesenteric lymphatics one (~ 67 %, (101)), thus suggesting that diaphragmatic lymphatic function efficiency may be improved by the cooperation with extrinsic forces that can affect the very same vessels.

Moreover, it is worth to remind that hybrid, passive or purely active segments, all belonged to the same loops . Most of these peripheral loops are composed of purely active and invariant segments: in these loops the purely active segments display the highest frequency of contraction (up to 17 bpm, mean value of all active pumping sites is about 7 bpm). In fewer loops, purely active segments are accompanied by passive and hybrid ones: in this cases the purely active contractile frequency is lower (about 3 bpm) and the hybrid segments contraction and relaxation of the passive segments follows the contraction frequency of the pure active ones to which they are in close proximity.

4.3.5 Lymph flux

The analysis of 8 loops in 7 lymphatic networks (n = 68 active pumping sites) pointed out that lymph flux was almost constant in each loop structure. In fact, as in diaphragmatic lymphatics the contraction amplitude of actively pumping vessels is independent on the lymphatics size but it is dependent on the vessels contraction frequency, the product of diameter change times frequency lead to an almost constant flow.

Particularly, two analyzed loops showed the same contraction frequency in the whole structure, whereas in six loops contraction frequency but not lymph flux (Fig 4.12) varied in adjacent segments of the same loop.

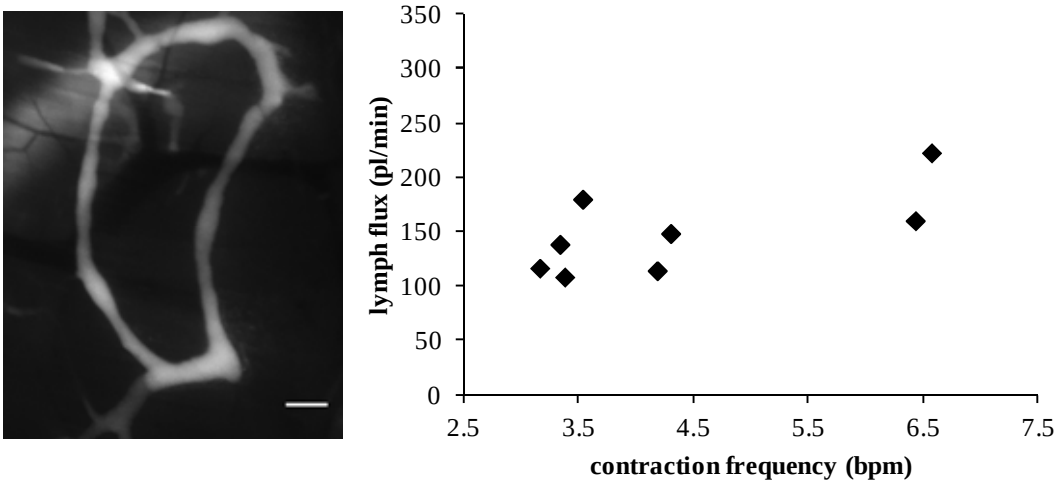

Figure 4.12 Diaphragmatic lymphatic loop in which eight active pumping sites showed different contraction frequencies but lymph flow was found to be relatively constant (scale bar 500 μm).

The only exception found was a double loop structure in which lymph flux was significantly different (Fig 4.13). In fact in a loop (corresponding to the Low contracting frequency structure in Fig 4.11) lymph flux was 145.28 ± 16.78 pL/min (n = 8) whereas in the adjacent one (corresponding to the High contracting frequency structure in Fig 4.11) lymph flux was significantly lower, 58.56 ± 7.29 pL/min ($p < 0.01$, unpaired t-test, n = 7).

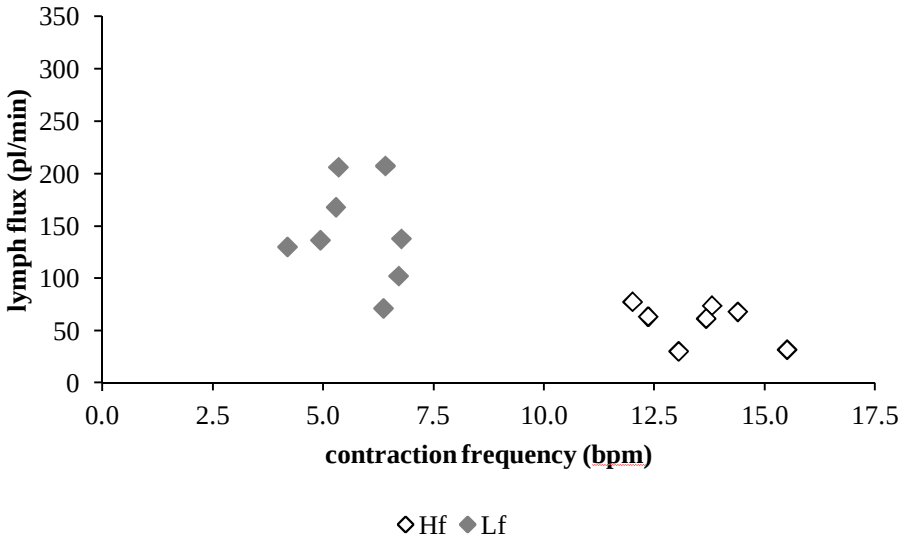

Figure 4.13 Different segments of the same loop (dark grey or white symbols) maintain a roughly homogenous lymph flux within itp. However, adjacent loops in the same lymphatic network show a significantly different lymph flux.

To understand the features of fluid movements, lymph propulsion along the network was calculated in different regions of the same loop. For example, as reported in Fig 4.14 A, lymph flux was estimated in each pumping site (white circles) and in external branches connected to the loop (light blue circles). For each analyzed site lymph flux (pL/min) is indicated next to the site itself. *In vivo* video recordings allowed to detect fluid recirculation in the complex loop structure, which is represented in Fig 4.14 B by the arrow colors: fluid moved and reflowed from the light blue top left loop to the violet top right one and finally to the lower left blue loop. The graph reported in Fig 4.14 C shows the lymph flux (J_l) in the three adjacent and correlated structures (same colors as in B), highlighting the existence of a J_l variability of ~ 150 pL/min among different adjacent loops. Pooling together data from the entire network allows to identify different tracts acting as input (Fig 4.14 B, yellow arrowheads) or output (Fig 4.14 B, orange arrowhead) branches. The existence of transverse ducts departing from

superficial vessels and running perpendicularly to them, thus explaining the presence of J_l variability in some loop tracts, cannot be excluded. On the other hand, the fluorescence epi-illumination of diaphragmatic lymphatics used in this kind of experiments does not permit their eventual detection.

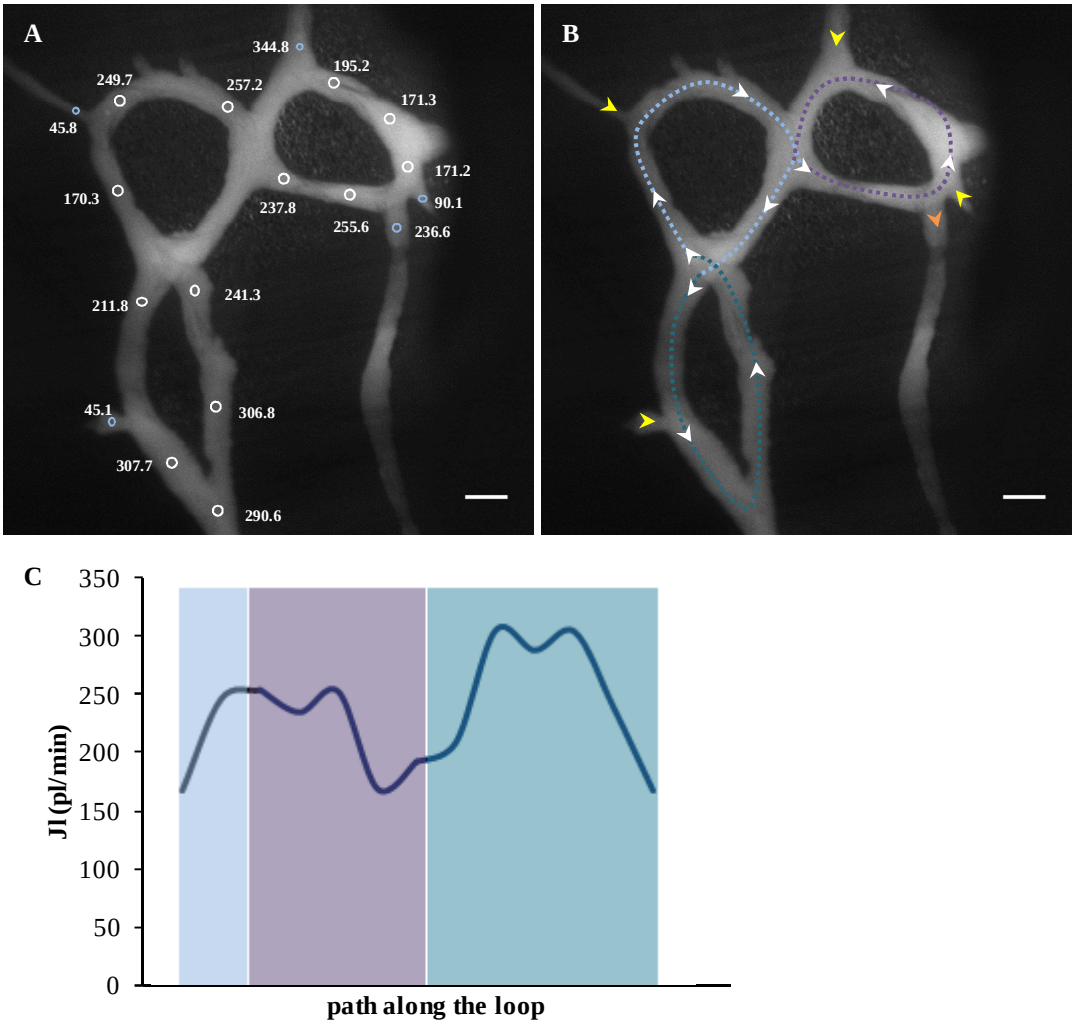

Figure 4.14 Lymph flux in a lymphatic loop. **A** Lymph flux was estimated both in loop pumping sites (white circles) and external branches (light blue circles). Lymph flux data are reported next to the site and are expressed as pL/min. **B** Lymph flow direction in three adjacent loops (depicted with different colors) is indicated by white arrowheads. The picture also shows input (yellow arrowheads) and output (orange arrowhead) branches. (scale bars 250 µm). **C** the graph show lymph flow (J_l) in the same three adjacent regions of the complex loop (key color as in B).

Notwithstanding in the same loop lymphatic sites with different pumping properties coexist, they all collaborate to attain a steady flux in the closed loop structure. This could point to the fact that even when an apparent disorganization exists, there must be a sort of order which keeps lymph flux almost constant.

4.4 Temporal analysis

4.4.1 Temporal correlation among sites belonging to the same lymphatic network

Although lymphatics diameter, contraction amplitude and contraction frequency affect lymph flow, only two parameters characterize the coordination between different pumping sites and the resulting contraction waves: a) the time delay between the onset of contractions of adjacent sites (for synchronous contractions) and b) the relative contraction frequency between adjacent sites (for asynchronous contractions).

As explained above, vessels belonging to the four different classes can be identified in the same lymphatic structure; therefore we performed a temporal analysis of the local activity of a lymphatic segment with respect to the immediately adjacent sites. To this aim a cross-correlation analysis of simultaneously recorded diameter changes over time was performed. For example, a zero lag was found between a passive compliant site and the adjacent active or hybrid one. Moreover, zero lag was also found between all passive compliant adjacent sites, thus confirming the existence of a region showing passive mechanical features (lower right region of the loop in Fig 4.15) which was functionally defined as a passive reservoir (see also Fig 4.7). In fact, passive vessels enlargement was strictly connected to the active pumping of other sites in close proximity to them.

On the other hand, several actively pumping sites can coexist in the same loop structure, as reported in Fig 4.15 (b, c and d). In this loop structure, sites ‘b’ and ‘c’ displayed a strongly correlated intrinsic pumping activity, with the same contraction frequency of 3.1 bpm and a lag of 0.5 sec (c vs b), underling the trigger role of site ‘b’. Also the passive compliant site ‘a’ had the same contraction frequency, with a 0.95 sec delay with respect to site ‘b’, being farther away from the trigger site. A higher frequency

contracting site was also found in the same loop, since site 'd' showed a contraction frequency of 5.4 bpm, which was also found to be uncorrelated to other regions in the same loop structure.

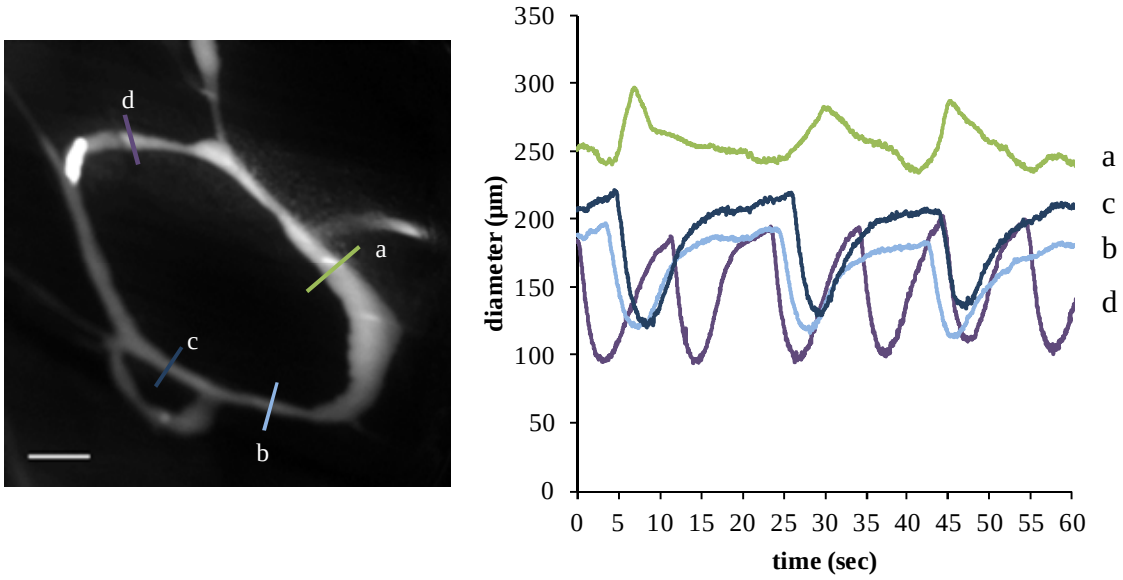

Figure 4.15 Diameter profiles simultaneously recorded in different sites of the same lymphatic loop . **a** passive compliant vessel, **b and c** correlated actively pumping sites (b is the command site). **d** uncorrelated active pumping site (scalebar 500 µm).

Results indicate that coordination among active pumping sites exists in diaphragmatic lymphatics, a well organized functional mechanism also previously described in mesenteric (106) lymphatic vessels, which allows the correct lymph flux along the network. In fact, all active pumping sites contributed to the ordered propulsion of the lymph in the network, as highlighted by the image sequence reported in Fig 4.16, in which a fluorescent aggregate (see image sequence below), as expected on the analysis presented in Fig. 4.15, moved counterclockwise along the network several times.

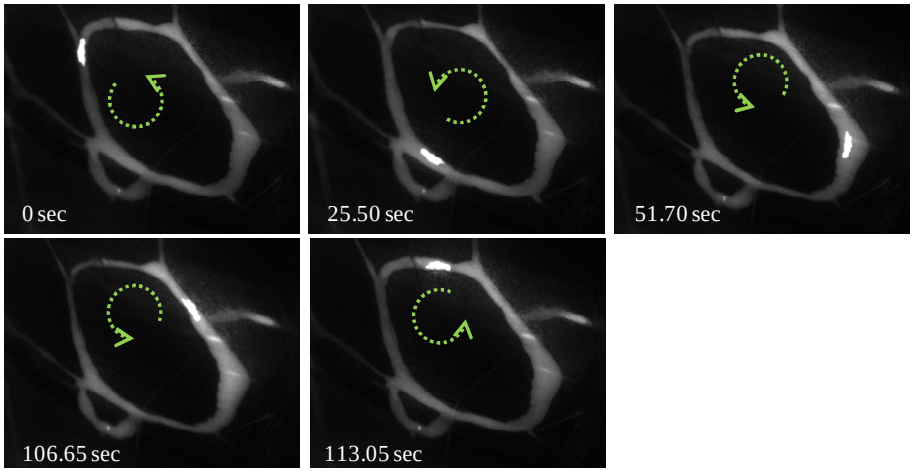

Figure 4.16 Image sequence of a fluorescent microspheres aggregate reflowing counterclockwise along the lymphatic loop during the recording period.

Pooling together data from different loops in which adjacent sites had the same contraction frequency and no zero lag between them, it had been possible to calculate the apparent "spread" of the contraction wave along the network, by dividing their distance by the time lag of contractions. This computation gave a mean spreading velocity of the contraction wave of 1.31 ± 0.34 mm/sec (n = 5 loop structures). In spite of an high spread velocity of contraction waves in mesenteric lymphatics (4 – 8 mm/sec), in diaphragmatic lymphatics active contractions propagate slowly, probably due to the complex organization of the lymphatic network. In fact, low propagation velocity may favor lymph recirculation along the whole network and particularly in the loops, whereas mesenteric lymphatics are mainly linear.

Lastly, it had been reported that the coordination of lymphatic contractions can be modulated, for example, by temperature. In fact, by changing the temperature of the lymphatic tract, it is possible to cause contraction waves to propagate in both an "orthograde" direction (following flow direction) and a "retrograde" direction (opposite to flow direction, (135)). This finding represents a key point for future perspectives, as

both modulatory drugs and mechanical stimuli should be tested in order to evaluate their effect on diaphragmatic lymphatics function.

4.4.2 Identification of lymphatic pacemaker sites

The determination of the general characteristics of the contractile waves propagation along the lymphatic network provides important information of the role of the pacemaker in the coordination of the pumping activity through lymphatics. Such information are necessary to clarify the potential role of the disorder affecting lymphatic electrical events in the pathogenesis of various diseases, which can lead to diminished lymph flow and formation of local edema. Based on temporal correlation analysis, multiple pacemaker sites can be identified in different diaphragmatic lymphatic network tracts. Following Akl and colleagues (236), the time delay between the contractile waveforms from two consecutive axial positions along the vessel can be measured and used to calculate the propagation velocity. If a vessel has a single pacemaker site near the middle, the contractile waves propagate away from the pacemaker site in opposite directions and the propagation velocity changes from negative (to the left of the pacemaker site), to positive (to the right of the pacemaker site, type I zero crossing). If instead a vessel has two pacemaker sites, then two contractile waves propagate in opposite directions toward each other resulting in a collision site, where the velocity changes from positive to negative (type II zero crossing).

The graph in Fig 4.17 shows the average contraction wave velocity (mm/sec) of five consecutive contractions in adjacent sites along a lymphatic tract of about 1800 μm (left panel of Fig. 4.17). The contraction wave velocity changes sign two times from negative to the positive direction, which correspond to the zero-crossings visible in the

graph reported in Fig 4.17. The former was identified between sites 1 and 2 in Fig 4.17, leading to hypothesize the possible presence of a pacemaker site located between 364 and 859 μm from the site arbitrarily set to zero. The second change of contraction wave velocity from negative to positive direction was identified between sites 3 and 4 of Fig 4.17, thus we hypothesized the presence of another pacemaker site located between 1320 μm and 1711 μm.

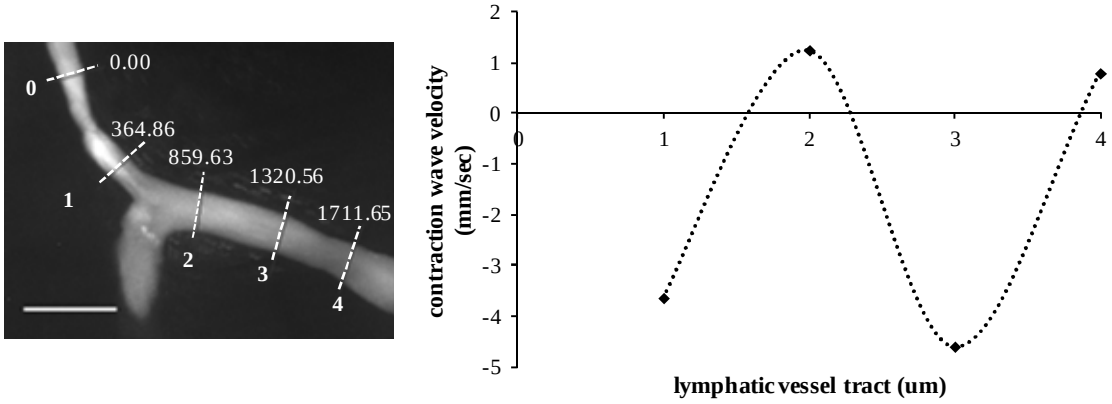

Figure 4.17 Contraction wave propagation velocity in four adjacent lymphatic tracts (regions 1-4), corresponding to the ones reported on the left. The figure also shows the distance of four different sites from a reference site arbitrarily set to 0.00 μm (scalebar 500 μm).

Temporal analysis between diameter profiles led us to assess that at least two pacemaker sites cooperate to sustain fluid flux in the observed loop. In fact, the image sequence reported in Fig 4.18, referring to the *in vivo* video recording of about sixty seconds of the active pumping activity in this lymphatic network tract, highlights the presence of two pacemaker sites (Fig 4.18 arrowheads, panels C and G) and the collision site in between them (Fig 4.18 arrow, panel M). It is worth noting that the two pacemaker sites acted in a coordinated manner but not simultaneously to correctly propel the lymph fluid. Particularly, the not FITC-stained dark lymph entered from the lower input branch and it was propelled to the right when the first pacemaker site

contracted (Fig 4.18 panel C), whereas it was pushed in the reverse direction when the second pacemaker site contracted (Fig 4.18 panel G).

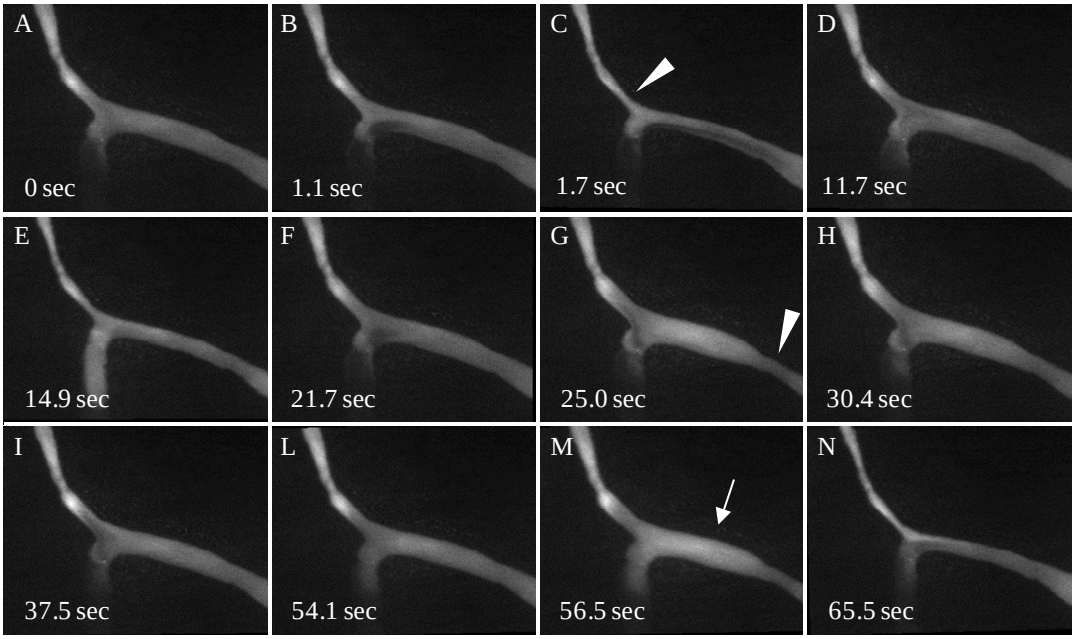

Figure 4.18 Image sequence showing the coordinated pumping activity of two pacemaker sites (arrowheads) flanking the collision site (arrow, see text for further details), over a period of about sixty seconds.

It is well known that actively pumping lymphatic vessels, independently on their location in the body or on their main functional involvement, transport lymph fluid by rhythmic constrictions of the lymphatic smooth muscle cells in their vessel walls. Particularly, studies on mesenteric lymphatics of the guinea pig demonstrated the existence of the pacemaker mechanism (137), underlying that the generation of L-type Ca^{2+} channel-mediated action potentials and associated constrictions are due to a summation of spontaneous transient depolarizations (STDs). L-type Ca^{2+}-channels are voltage-gated and open in response to the suprathreshold depolarization of the smooth muscle membrane, which is generated by an electrical event, named pacemaker potential. Despite further analysis are required to determine electrical features of

diaphragmatic lymphatic smooth muscle cells (and their associated endothelial cells) in order to understand the pacemaker behavior of some of them, the present study indicates that lymphatic pacemaker sites exist in the peripheral portion of the diaphragmatic lymphatic network.

Part II

4.5 Preliminary results

This Part II of the research work, still ongoing, aims at investigating the contribution of diaphragmatic striated muscle fibers active contractions in lymphatic function. The effect of diaphragmatic muscle contraction during the active respiratory cycle on diaphragmatic lymphatics was mimicked by KCl 1 M injection into the interstitium next to the very same vessel. Pleural lymphatic loops previously investigated from a functional point of view mainly displayed intrinsic pumping activity during the *in vivo* experiments. On the contrary, KCl 1M effect was evaluated in *parallel* and *perpendicular* lymphatics (relative to the diaphragmatic skeletal muscle fibers orientation), which were found to be mostly invariant vessels and also less peripheral than lymphatic loops. By locally injecting 2.3 nl of KCl 1M solution (KCl from now onwards) no effect was found on those lymphatic vessels (data not shown) and then multiple injection into the interstitium were performed. Occasional muscle contractions were found by injecting 6.9 nl of KCl, whereas maximal local effects were found after 9.2 nl of KCl injection. Thus this KCl volume had been used to perform the experiments described in Part II.

4.5.1 Diaphragmatic muscle contraction effect on perpendicular lymphatics

To distinguish between different components contributing to the extrinsic pump, the effect of diaphragmatic muscle contraction was evaluated by selective contraction induced by KCl exposition. KCl application is often used as a tool to activate muscle contraction by changing the K^+ equilibrium potential and causing a membrane

depolarization which increases cell membrane potential at some value above the resting level (242). Membrane depolarization increases intracellular calcium concentration $[Ca^{2+}]_i$: which regulates muscle contraction of both striated and smooth muscles, albeit with significant intracellular differences, which are however not relevant to the present work (243; 244).

In our analysis we considered long diaphragmatic vessels belonging to lymphatic loops and running either parallel or perpendicular to the skeletal diaphragmatic underlying fibers: vessels exhibiting a pumping-like activity were excluded from the analysis.

Muscle contraction effect on perpendicular lymphatics was found to be dependent both on the distance from the KCl injection site and on the functional features of the lymphatic vessel itself. As shown in Fig. 4.19, striated muscle contraction next to the vessel (distance < ~ 300 µm) produced a marked constriction of the lymphatic vessel (violet arrow, Fig.6.1, 12.). On the contrary, striated muscle contraction far from the vessel (distance > ~ 900 µm) pulled one side of the vessel, thus causing an increase of the apparent vessel diameter (Fig 4.19, green arrow). Muscle contraction initiated by KCl administration at distances in between 300 and 900 µm gave mixed results, probably due to a very variable spatial extent of muscle activation with the present technique.

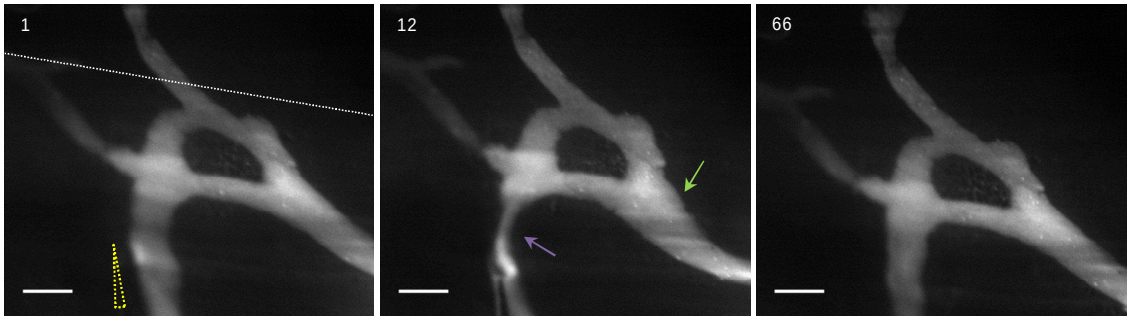

Figure 4.19 Timeframe showing the effect of diaphragmatic muscle contraction on perpendicular lymphatics (striated muscle fibers orientation highlighted by white dotted line) next (contraction) or far (expansion) to the injection site: 1 sec corresponds to the injection frame, 12 sec to the maximal striated muscle fibers contraction and 66 sec to the diaphragm relaxation. KCl was injected into the interstitium as indicated by yellow arrowhead. Violet arrow indicates the effect of diaphragm contraction on the closer site whereas green arrow indicates the effect on the far site. Scalebar 250 µm.

Two population of compressing perpendicular lymphatics were found, which showed a greater (Fig 4.19 violet arrow) or less (Fig 4.20 violet arrow) sensitivity to skeletal muscle contraction.

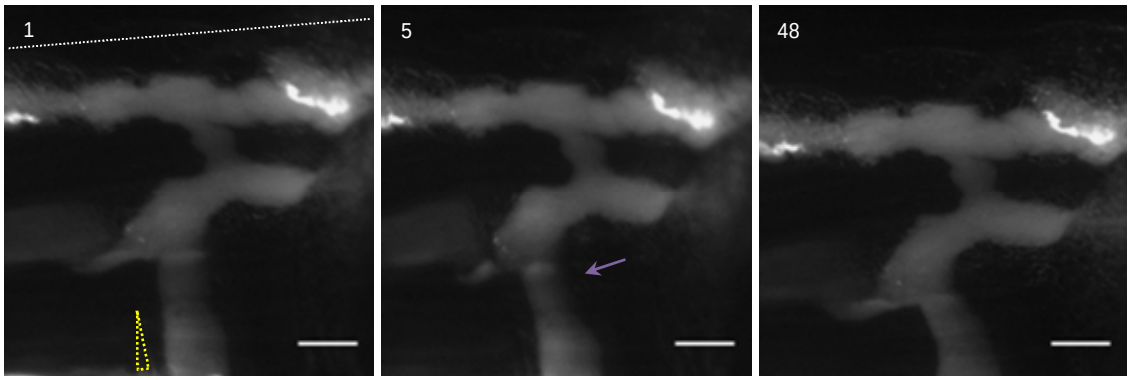

Figure 4.20 Timeframe showing the effect of diaphragmatic muscle contraction on a perpendicular lymphatic (striated muscle fibers orientation highlighted by white dotted line) next (contraction) to the injection site: 1 sec corresponds to the injection frame, 5 sec to the maximal striated muscle fibers contraction and 48 sec to the diaphragm relaxation. KCl was injected into the interstitium as indicated by yellow arrowhead. Violet arrow indicates the effect of diaphragm contraction. Scalebar 250 µm.

The extrinsic pump effect on perpendicular compressing lymphatics is reported in Fig 4.21 and 4.22. As clearly evident, two population of perpendicular vessels were found. The most significant effect (Fig 4.21) was found in lymphatics with mean resting diameter of 165.12 ± 10.38 µm which decreased to 89.48 ± 7.68 µm ($p < 0.01$, paired t-test vs resting diameter, n = 13) after skeletal muscle contraction After diaphragm relaxation lymphatic diameter reached 150.11 ± 9.28 µm, a value significantly higher ($p < 0.01$, paired t-test, n=13) than that observed at maximum skeletal muscle contraction. On average, lymphatic vessel diameter decreased to 53.6 ± 2.3 % of resting diameter (Δd, $p < 0.01$, paired t-test vs the respective resting diameter set to 100%, n = 13) and returned to 91.3 ± 2.2 % of resting diameter (Δd_{rel}, $p < 0.01$, paired t-test vs the respective minimum diameter, n = 13) after relaxation. In most of the lymphatics analyzed, diaphragm relaxation did not cause the vessel diameter to return back to 100% of their respective resting diameter. This is due to the fact that wash-out of KCl with a gentle flush of warm saline was performed only after the video recording was stopped, in order to avoid possible artifacts.

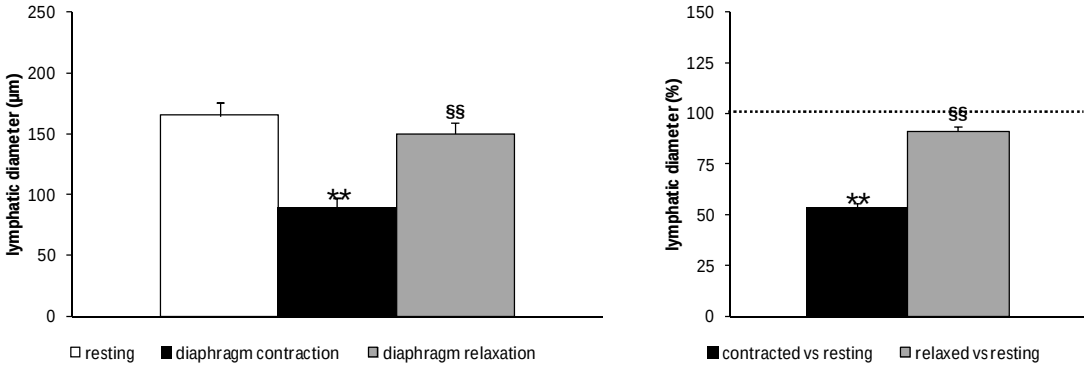

Figure 4.21 Effect of diaphragmatic muscle contraction on perpendicular lymphatics next to the KCl injection site, which compressed showing greater sensitivity to the extrinsic pump. Panel on the left shows mean diameter before and after striated diaphragmatic muscle fibers contraction and then after muscle relaxation. Panel on the right shows the extrinsic pump effect on lymphatic diameter , expressed as percentage of resting diameter. (** $p < 0.01$ vs resting diameter; §§ $p < 0.01$ vs lymphatic tone corresponding to the maximal diaphragm contraction)

A lower but significant effect (Fig 4.22) was found in larger perpendicular lymphatics with mean resting diameter of 186.67 ± 25.59 µm (no significant differences in diastolic diameter were found between the two populations of lymphatics) which decreased to 143.85 ± 21.58 µm ($p < 0.01$, paired t-test vs resting diameter, $n = 7$) due to muscle contraction. After diaphragm relaxation lymphatic diameter reached 178.81 ± 26.59 µm ($p < 0.01$, paired t-test vs lymphatic diameter corresponding to the muscle contraction, $n = 7$). In those lymphatic vessels, on average, diameter decreased to 76.25 ± 2.4 % of resting diameter (Δd, $p < 0.01$, paired t-test vs the respective resting diameter set to 100%, $n = 7$) and returned to 94.9 ± 1.9 % of resting diameter (Δd_{rel}, $p < 0.01$, paired t-test vs the respective minimum diameter, $n = 7$) after relaxation.

Therefore, changes in lymphatic diameter were found to be two fold in the most sensitive perpendicular lymphatics (Hs, 100 - Δd = 46.4 ± 2.3 %) compared to the less sensitive ones (Ls, 100 – Δd = 23.5 ± 2.4 %, $p < 0.01$, unpaired t-test), probably due to different stiffness of the wall of lymphatic vessels, assuming that diaphragmatic muscular tissue is isotropic (224).

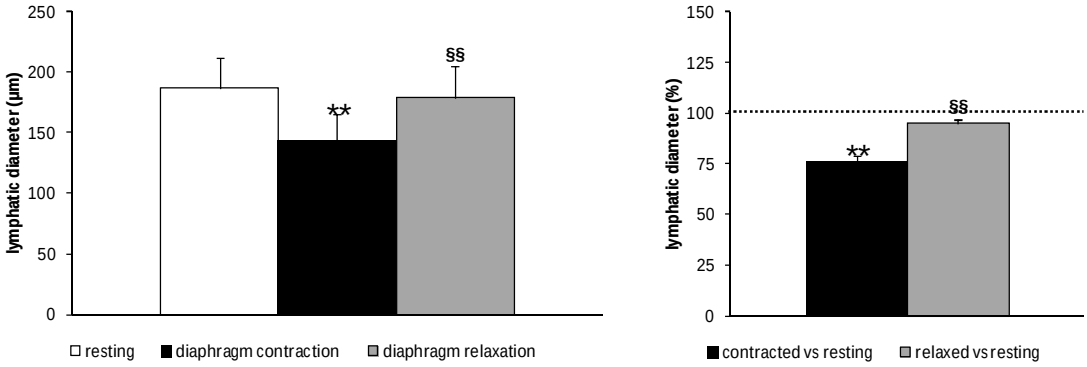

Figure 4.22 Effect of diaphragmatic muscle contraction on perpendicular lymphatics next to the KCl injection site, which constricted showing less sensitivity to the extrinsic pump. Panel on the left shows mean diameter before and after striated diaphragmatic muscle fibers contraction and then after muscle relaxation. Panel on the right shows the extrinsic pump effect on lymphatic tone, expressed as percentage of resting diameter. (** $p < 0.01$ vs resting diameter; §§ $p < 0.01$ vs lymphatic tone corresponding to the maximal diaphragm contraction)

Perpendicular lymphatic vessels which were located far from the diaphragmatic contracting skeletal muscle fibers showed opposite behavior, expanding rather than compressing (Fig 4.19 green arrow, Fig 4.23). They had mean resting diameter of 134.70 ± 20.70, not statistically different from the diastolic diameter of all the other perpendicular lymphatics ($p = 0.172$, one way ANOVA, 27 d.f.). Their mean diameter increased to 182.89 ± 28.27 µm ($p < 0.01$, paired t-test vs resting diameter, $n = 8$) and after skeletal diaphragmatic fiber relaxation lymphatic diameter decreased to 151.20 ± 21.65 µm ($p < 0.01$, paired t-test vs lymphatic diameter corresponding to the muscle contraction, $n = 8$). On average, lymphatic diameter increased up to 135.8 ± 2.3 % of resting diameter (Δd, $p < 0.01$, paired t-test vs the respective resting diameter set to 100%, $n = 8$) and then stepped back at 115.5 ± 5.5 % of resting diameter (Δd_{rel}, $p < 0.01$, paired t-test vs the respective expanded diameter, $n = 8$).

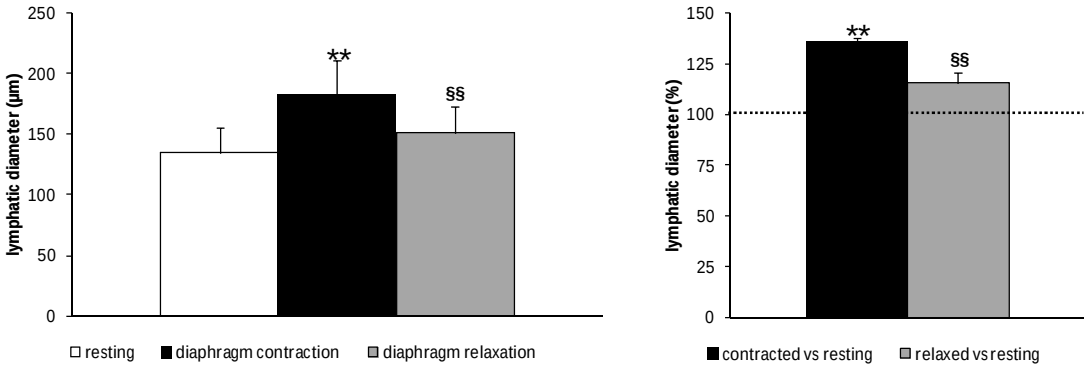

Figure 4.23 Effect of diaphragmatic muscle contraction on perpendicular lymphatics next to the KCl injection site, which expanded due to the extrinsic pump. Panel on the left shows mean diameter before and after striated diaphragmatic muscle fibers contraction and then after muscle relaxation. Panel on the right shows the extrinsic pump effect on lymphatic tone, expressed as percentage of resting diameter. (** $p < 0.01$ vs resting diameter; §§ $p < 0.01$ vs lymphatic tone corresponding to the maximal diaphragm contraction)

4.5.2 Diaphragmatic muscle contraction effect on parallel lymphatics

Similar to what observed for perpendicularly oriented vessels (Fig 4.19 – 4.23), skeletal diaphragmatic muscle contraction effect on longitudinally oriented lymphatics was also found to be dependent on the distance from the contracting site; however the effect on lymphatic segments was different. Indeed, as shown in Fig 4.24, the contraction of striated muscle next to the vessel caused shortening and distortion of the lymphatic vessel, with simultaneous enlargement of the lymphangions (Fig 4.24, orange arrow).

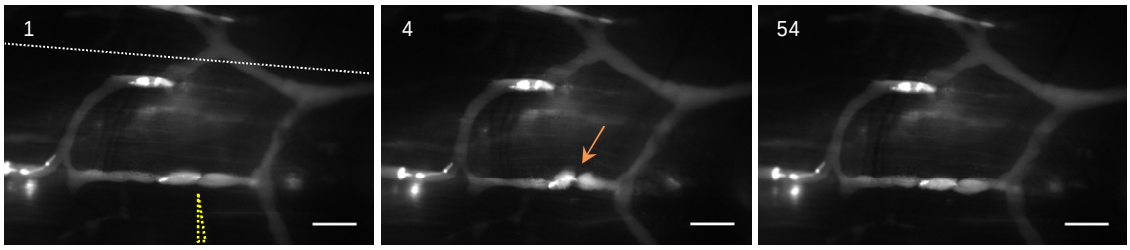

Figure 4.24 Timeframe showing the effect of diaphragmatic muscle contraction on a parallel lymphatic (striated muscle fibers orientation highlighted by white dotted line) next to the injection site:1 sec corresponds to the injection frame, 4 sec to the maximal striated muscle fibers contraction and 54 sec to diaphragm relaxation. KCl was injected into the interstitium as indicated by yellow arrowhead. Orange arrow indicates the effect of diaphragmatic contraction on the vessel which expanded and shortened. Scalebar 500 µm.

Pictures in Fig 4.25 highlight the selective effect of diaphragm contraction. In fact, as the lymphatic vessel next to the injecting site (orange arrow) shortened and expanded again, distant vessels (pink arrow) were not affected by local skeletal muscle contraction.

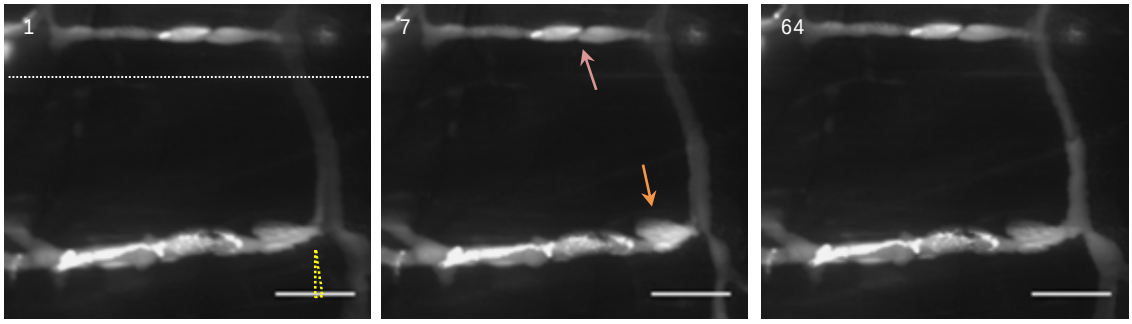

Figure 4.25 Timeframe showing the effect of diaphragmatic muscle contraction on parallel lymphatics (striated muscle fibers orientation highlighted by white dotted line) next or far to the injection site:1 sec corresponds to the injection frame, 7 sec to the maximal striated muscle fibers contraction and 64 sec to diaphragm relaxation. KCl was injected into the interstitium as indicated by yellow arrowhead. Orange arrow indicates the effect of diaphragmatic contraction on the vessel next to the contracting site, which expanded and shortened. On the contrary no effect was found in the far site as indicated by pink arrow. Scalebar 500 µm.

The effect of local skeletal muscle contraction on parallel lymphatics is reported in Fig 4.26 and 4.27. on average, lymphatic length between two reference points decreased to 66.9 ± 3.0 % of resting one (Δl, $p < 0.01$, paired t-test vs the respective l_0 set to 100%, n = 9) and thereafter returned to 81.8 ± 3.6 % of its resting length ($p < 0.05$, paired t-test vs the respective shortened length, n = 9) after skeletal muscle relaxation (Fig 4.26).

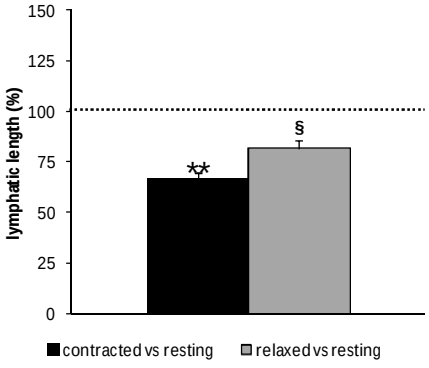

Figure 4.26 Effect of skeletal diaphragmatic muscle contraction on parallel lymphatics next to the KCl injection site, which shortened due to the extrinsic pump. The graph shows the extrinsic pump effect on lymphatic length, expressed as percentage of resting one. (** $p < 0.01$ vs pre-contraction length, § $p < 0.05$ vs lymphatic length corresponding to the maximal diaphragmatic fibers contraction).

The mean resting diameter of parallel lymphatics was 117.71 ± 20.49 µm and expanded to 148.69 ± 23.31 µm ($p < 0.01$, paired t-test vs resting diameter, n = 11), decreasing back to 133.64 ± 23.86 µm ($p < 0.05$, paired t-test vs lymphatic diameter corresponding to the muscle contraction, n = 11) after diaphragmatic relaxation (Fig 4.27). On average, lymphatic diameter increased to 129.2 ± 3.6 % of resting diameter (Δd, $p < 0.01$, paired t-test vs the respective resting diameter set to 100%, n = 11) and then returned back to 115.4 ± 6.1 % of resting diameter (Δd_{rel}, $p < 0.05$, paired t-test vs the respective expanded diameter, n = 11).

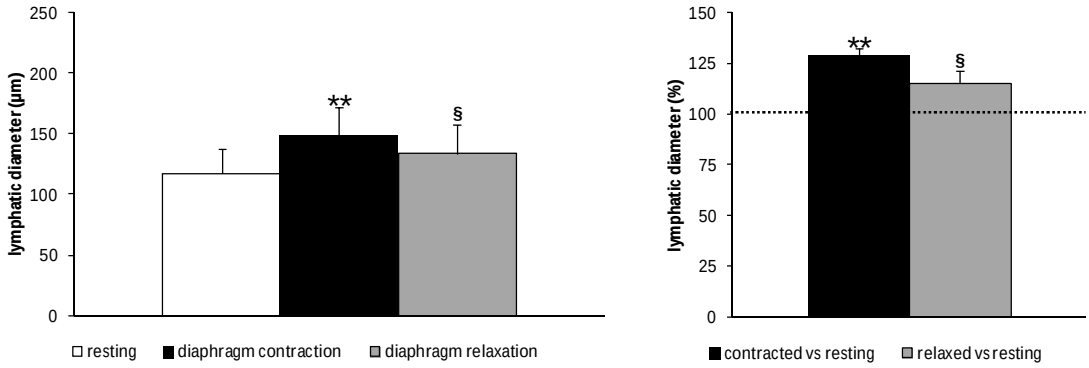

Figure 4.27 Effect of diaphragmatic muscle contraction on parallel lymphatics next to the KCl injection site, which expanded their cross-section due to the extrinsic pump. Panel on the left shows mean diameter length before and after striated diaphragmatic muscle fibers contraction and then after muscle relaxation. Panel on the right shows the extrinsic pump effect on lymphatic tone, expressed as percentage of resting diameter. (** $p < 0.01$ vs pre-contraction length; § $p < 0.05$ vs lymphatic length corresponding to the maximal diaphragmatic fibers contraction).

Taken together these preliminary data indicate that local diaphragmatic skeletal muscle contractions actually modulate lymphatic function, by compressing and expanding segmental vessel diameter and/or length. Conversely to selective muscle contraction induced by local perivascular KCl injection, all the diaphragmatic striated fibers contract during spontaneous respiratory cycle. Thus, it is conceivable that each lymphatic vessel is hypothetically compressed by adjacent muscle fibers but

simultaneously stretched by far ones as the diaphragmatic skeletal muscle contracts during inspiration One may hypothesize that perpendicular lymphatics which expand or, if any, only slightly compress (Ls) when perivascular fibers contract belong to the same class of vessel, whereas more compressing lymphatics (Hs) belong to a different class, probably distinguishable on the basis of the mechanical stiffness of the vessel wall, which still requires further investigations.

4.5.3 Functional parameters in lymphatics

Mean resting diameter was significantly greater (161.82 ± 10.20 µm, $p < 0.05$, $n = 28$) in perpendicular lymphatics compared to parallel ones (117.71 ± 20.49 µm, $n = 11$).

	perpendicular lymphatics			parallel lymphatics	p value
mean resting diameter (µm)	161.82 ± 10.20			117.71 ± 20.49	p < 0.05
	Hs compress	**Ls compress**	**expand**		
Stroke Volume (pL)	54.52 ± 6.37	42.00 ± 10.87	-	-	no
Diastolic Volume Load(pL)	-		49.18 ± 14.78	1961.51 ± 766.42	no
Ejection Fraction (%)	71 ± 2**	41 ± 4	46 ± 2	64 ± 2[§§]	p < 0.01

Table 4.3 Lymphatics functional parameters. Stroke volume (SV) and diastolic volume load (DVL)) were normalized and also expressed as ejection fraction (EF). Compressing lymphatics are reported as Hs (more sensitive) and Ls (less sensitive) with respect to extrinsic pump effect on vessel tone.

In perpendicular vessels SVs and DVLs were estimated (Table 4.3) in order to be compared with those of intrinsic propelling vessel (see Part I). No significant differences were found between SVs of perpendicular compressed lymphatics which

showed greater (Hs) or less (Ls) sensitivity to the extrinsic pump although the latter seem to be lower. Also vessels which expanded had comparable DVLs. On the contrary, EFs of Hs lymphatics was significantly higher than those of both constricted Ls ($p < 0.01$, unpaired t-test) and expanded ($p < 0.01$, unpaired t-test) lymphatic vessels.

If we compare the EFs of actively pumping lymphatics (43 ± 2 %) with those of Hs (71 ± 2 %) and Ls (41 ± 4 %) perpendicular lymphatics it is conceivable that intrinsic and extrinsic mechanisms support the whole lymph propulsion almost to the same extent, which is in good agreement with the reported amiloride induced reduction of pleura lymphatic flux of 40 %.

4.5.4 Diaphragmatic muscle contraction effect on lymphatics intraluminal pressure

As previously described, thoracic tissues are subjected to external influences which also affect lymphatic functions. Lymph drainage from serous cavities and lymph propulsion to the bloodstream by diaphragmatic lymphatics are affected by cardiac and respiratory cycles. In fact, local tissue displacement associated with cardiogenic oscillations plays a key role in promoting lymph formation and propulsion (54), as the active contraction of respiratory muscles is required to support an efficient lymphatic drainage from the thoracic tissues (56). Micropuncture experiments performed on rodents diaphragmatic lymphatics demonstrated that there are in- or out-of-phase cardiogenic swings of intraluminal lymphatic pressure ranging from ~ -20 to ~ + 10 cm H_2O (66; 54) affecting intralymphatic pressure gradients. Also during spontaneous inspiration mechanical stresses arise in intercostals and diaphragmatic tissues resulting in P_{lymph} and P_{in}, oscillations which are transmitted to the lymphatic vessel lumen as pressure gradients (56).

At present, intrinsic intraluminal pressure oscillation have been recorded only occasionally (85). We had been able to measure intaluminal pressure only in lymphatic tracts adjacent to ones showing intrinsic pumping activity. In fact, one cannot exclude that the pipette insertion maneuver might hinder the intrinsic contractile capacity of the vessel wall. This is why Fig 4.28 (violet arrowhead) shows the damped pressure oscillation profile due to the intrinsic pumping activity in the lymphangion adjacent to the analyzed one, thus confirming the cyclic effect of the intrinsic pump on lymphatic function.

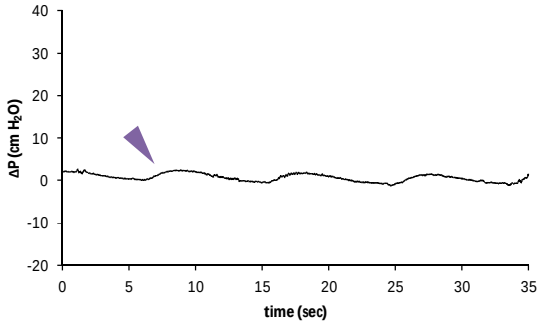

Figure 4.28 Example of intraluminal pressure changes due to intrinsic pumping activity (violet arrowhead) in an adjacent lymphangion to the one in which the micropipette has been inserted. In this case.

Diaphragm contraction can either induce an increase or a decrease in intraluminal lymphatic pressure, as reported in Fig 4.29 (green arrowheads). Data reported refer to intraluminal pressure recordings in two perpendicular lymphatic vessels which were not distinguishable from an anatomical point of view. Pressure data represent the early part of a still ongoing work, which requires further analysis to better evaluate the complete functional behavior of the extrinsic pump. As the animals were temporarily disconnected from the mechanical ventilator no respiratory effect can be observed in

pressure traces and the high frequency oscillations are of cardiogenic origin (Fig 4.29 red arrows).

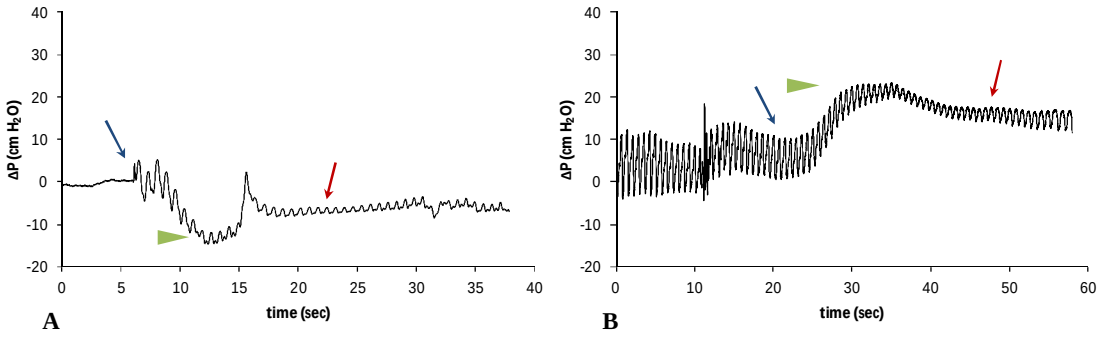

Figure 4.29 Example of intraluminal pressure changes due to extrinsic pump (green arrowheads) after diaphragmatic muscle contraction (blue arrows indicate the KCl injections time into interstitium) next to perpendicular lymphatic vessels. In **A** diaphragm contraction induced a ΔP decrease of -14.37 cmH_2O, whereas in B the diaphragm contraction induced a ΔP increase of + 14.95 cmH_2O. Red arrows indicate the cardiogenic effect on lymphatic intraluminal pressure.

Intraluminal pressure changes externally induced by diaphragmatic striated muscle contraction and resulting as perpendicular lymphatics expansion and/or contraction were plotted in a ΔP vs Δd graph, distinguishing between data grouped as Hs (Fig 4.30 B) and Ls or expanding (Fig 4.30 A) lymphatics. Both populations were fitted by a linear trend (A: $y = 0.37x - 5.44$, $r^2 = 0.58$, $n = 7$; B: $y = 0.17 – 27.00$, $r^2 = 0.54$, $n = 7$), suggesting the existence of two separated populations. In fact, the Ls and expanding lymphatics (Fig 4.30 A) had an extreme variability in intraluminal pressure changes and data were fitted by a linear trend which had a greater slope, indicating that small changes in diameter induced a major shift in intraluminal lymphatic pressure. On the contrary, data from Hs lymphatics (Fig 4.30 B) were fitted by a linear trend which had a smaller slope, thus resulting in weak changes in intraluminal lymphatic pressure induced by larger diameter length reductions. Particularly, these vessels also showed only negative pressure changes, mainly in the -20 – -10 cmH_2O interval.

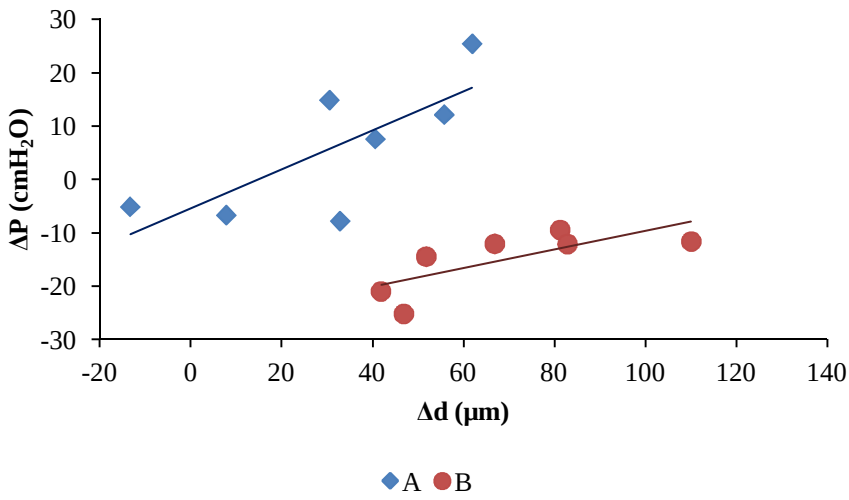

Figure 4.30 Relationship between changes in intraluminal lymphatic pressure (ΔP) and diameter (Δd) in perpendicular lymphatics. The pressure data were plotted vs Δd. A correspond to lLs or expanding lymphatic vessels, whereas B represent ΔP changes in Hs vessels.

Early results from preliminary intraluminal pressure changes recorded during diaphragmatic muscle contraction suggest the existence of two separated population of perpendicular lymphatics, as previously hypothesized in Paragraph 4.5.1. The ΔP/Δd ratio is proportional to the reciprocal value of the vessel compliance (ΔV/ΔP) which is an intrinsic feature of the vessel wall. According to what previously published (224) these data confirm the existence of perpendicular diaphragmatic lymphatics which are undistinguishable from a morphological point of view but may possess lower (Fig 6.12 A) or higher (Fig 6.12 B) compliance.

Data from intraluminal pressure recordings of parallel lymphatics also showed a single population fitted by a linear trend (Fig 4.31, $y = 0.24x - 25.87$, $r^2 = 0.63$, $n = 6$) with intermediate slope.

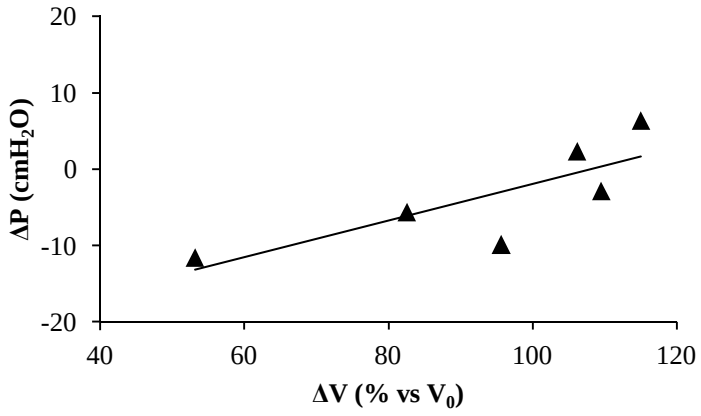

Figure 4.31 Relationship between changes in intraluminal lymphatic pressure (ΔP) and volume changes (ΔV) in parallel lymphatics.

In conclusion, lymph formation in initial lymphatics and its propulsion along the initial lymphatic network are mainly sustained by hydrostatic pressure gradients, as lymphatics offer no resistance to fluid and macromolecules to enter the lumen, which are strongly affected by extrinsic and/or intrinsic forces. Further experiments will be required to understand the relative role and the interaction between the intrinsic and extrinsic mechanism by treating the vessels and the perivascular interstitium with either acetylcholine or noreprinephrine. In fact acetylcholine is able to evoke skeletal muscle contraction (245), whereas it causes hyperpolarization in lymphatic smooth muscle cells, while noreprinephrine only induces lymphatic smooth muscle depolarization (246), thus allowing a more precise dissection of the role of the extrinsic mechanism alone.

5. *Conclusions*

The identification of spontaneous contractile activity in lymphatic vessels of the diaphragm, a muscular tissue always subjected to rhythmical movements, is somehow surprising. Indeed, these active vessels are mostly located at the far periphery of the diaphragm, in a region in close continuity with the abdominal wall. Moreover, these lymphatic loops are endowed with at least four kinds of vessel. Nevertheless, this active pumping mechanism is not the only responsible for the whole pleural lymphatic flux, given that most of the lymphatic diaphragmatic network is located in the more central muscular and tendineous regions, whose movements are more accentuated than those of the far periphery during the respiratory cycle. Indeed, these lymphatics are mostly subjected to the extrinsic pumping mechanism due to the contraction of the striated muscle fibers surrounding them. In conclusion, at least in the diaphragm, the two different strategies of lymph propulsion (intrinsic and extrinsic mechanisms) do coexist, but their relative importance seems to be spatially segregated: the intrinsic mechanism seems to be confined to those lymphatic loops in the periphery, while in more central lymphatic vessels, seldom organized into loops, the extrinsic mechanism prevails.

6. References

1. **Yoffey JM, Courtice FC.** *Lymphatics, Lymph and the Lymphomyeloid Complex.* London: Academic, 1970.

2. **Jeltsch M, Tammela T, Alitalo K, Wilting J.** Genesis and pathogenesis of lymphatic vessels. *Cell Tissue Res.* 2003, Vol. 314, 1, pp. 69-84.

3. **Alitalo K.** The lymphatic vasculature in disease. *Nat. Med.* 2011, Vol. 17, pp. 1371-1380.

4. **Sabin FR.** On the origin of the lymphatic system from the veins, and the development of the lymph hearts and thoracic duct in the pig. *Am. J. Anat.* 1902, Vol. 1, pp. 367–389.

5. **Sabin FR**. On the development of the superficial lymphatics in the skin of the pig. *Am.J. Anat.* 1904, Vol. 3, pp. 183-195.

6. **Risau W, Flamme I.** Vasculogenesis. *Annu Rev Cell Dev Biol.* 1995, Vol. 11, pp. 73-91.

7. **Folkman J, Shing Y.** Angiogenesis. *J Biol Chem.* 1992, Vol. 267, pp. 10931-10934.

8. **Risau W.** Mechanisms of angiogenesis. *Nature.* 1997, Vol. 386, pp. 671-674.

9. **Ferrara N.** Role of vascular endothelial growth factor in regulation of physiological angiogenesis. *Am J Physiol Cell Physiol.* 2001, 280, pp. 1358-1366.

10. **Folkman J.** Angiogenesis in cancer, vascular, rheumatoid and other disease. *Nat Med.* 1995, Vol. 1, pp. 27-31.

11. **Huntington GS, McClure CFW.** The anatomy and development of the jugular lymph sac in the domestic cat (Felis domestica). *Am. J. Anat.* 1910, Vol. 10, pp. 177–312.

12. **Carmeliet P, Ferreira V, Breier G, Pollefeyt S, Kieckens L, Gertsenstein M, Fahrig M, Vandenhoeck A, Harpal K, Eberhardt C, Declercq C, Pawling J, Moons L, Collen D, Risau W, Nagy A.** Abnormal blood vessel development and lethality in embryos lacking a single VEGF allele. *Nature.* 1996, Vol. 380, pp. 435-439.

13. **Ferrara N.** Vascular endothelial growth factor: molecular and biological aspects. *Curr Top Microbiol Immunol.* 1999, Vol. 237, pp. 1-30.

14. **Ferrara N, Carver-Moore K, Chen H, Dowd M, Lu L, O'Shea KS, Powell-Braxton L, Hillan KJ, Moore MW.** Heterozygous embryonic lethality induced by targeted inactivation of the VEGF gene. *Nature.* 1996, Vol. 380, pp. 439-442.

15. **Shalaby F, Rossant J, Yamaguchi TP, Gertsenstein M, Wu XF, Breitman ML, Schuh AC.** Failure of blood-island formation and vasculogenesis in Flk-1-deficient mice. *Nature.* 1995, Vol. 376, pp. 62-66.

16. **Lawson ND, Scheer N, Pham VN, Kim CH, Chitnis AB, Campos-Ortega JA, Weinstein BM.** Notch signaling is required for arterial-venous differentiation during embryonic vascular development. *Development.* 2001, Vol. 128, pp. 3675-3683.

17. **Zhong TP, Childs S, Leu JP, Fishman MC.** Gridlock signalling pathway fashions the first embryonic artery. *Nature.* 2001, Vol. 414, pp. 216-220.

18. **Adams RH, Wilkinson GA, Weiss C, Diella F, Gale NW, Deutsch U, Risau W, Klein R.** Roles of ephrinB ligands and EphB receptors in cardiovascular development: demarcation of arterial/venous domains, vascular morphogenesis, and sprouting angiogenesis. *Genes Dev.* 1999, Vol. 13, pp. 295-306.

19. **Harvey NL, Oliver G.** Choose your fate: artery, vein or lymphatic vessel? *Curr Opin Genet Dev.* 2004, Vol. 14, pp. 499-505.

20. **Banerji S, Ni J, Wang SX, Clasper S, Su J, Tammi R, Jones M, Jackson DG.** LYVE-1, a new homologue of the CD44 glycoprotein, is a lymph-specific receptor for hyaluronan. *J Cell Biol.* 1999, Vol. 144, pp. 789-801.

21. **Oliver G.** Lymphatic vasculature development. *Nat Rev Immunol.* 2004, Vol. 4, pp. 35-45.

22. **Wigle JT, Oliver G.** Prox1 function is required for the development of the murine lymphatic system. *Cell.* 1999, Vol. 98, pp. 769-778.

23. **Wigle JT, Harvey N, Detmar M, Lagutina I, Grosveld G, Gunn MD, Jackson DG, Oliver G.** An essential role for Prox1 in the induction of the lymphatic endothelial cell phenotype. *EMBO J.* 2002, Vol. 21, pp. 1505-1513.

24. **Hong YK, Harvey N, Noh YH, Schacht V, Hirakawa S, Detmar M, Oliver G.** Prox1 is a master control gene in the program specifying lymphatic endothelial cell fate. *Dev Dyn.* 2002, Vol. 225, pp. 351-357.

25. **Petrova TV, Mäkinen T, Mäkelä TP, Saarela J, Virtanen I, Ferrell RE, Finegold DN, Kerjaschki D, Ylä-Herttuala S, Alitalo K.** Lymphatic endothelial reprogramming of vascular endothelial cells by the Prox-1 homeobox transcription factor. *EMBO J.* 2002, Vol. 21, pp. 4593-4599.

26. **Dumont DJ, Jussila L, Taipale J, Lymboussaki A, Mustonen T, Pajusola K, Breitman M, Alitalo K.** Cardiovascular failure in mouse embryos deficient in VEGF receptor-3. *Science.* 1998, Vol. 282, pp. 946-949.

27. **Kaipainen A, Korhonen J, Mustonen T, van Hinsbergh VW, Fang GH, Dumont D, Breitman M, Alitalo K.** Expression of the fms-like tyrosine kinase 4 gene

becomes restricted to lymphatic endothelium during development. *Proc Natl Acad Sci U S A.* 1995, Vol. 92, pp. 3566-3570.

28. **Hamada K, Oike Y, Takakura N, Ito Y, Jussila L, Dumont DJ, Alitalo K, Suda T.** VEGF-C signaling pathways through VEGFR-2 and VEGFR-3 in vasculoangiogenesis and hematopoiesis. *Blood.* 2000, Vol. 96, pp. 3793-3800.

29. **Abtahian F, Guerriero A, Sebzda E, Lu MM, Zhou R, Mocsai A, Myers EE, Huang B, Jackson DG, Ferrari VA, Tybulewicz V, Lowell CA, Lepore JJ, Koretzky GA, Kahn ML.** Regulation of blood and lymphatic vascular separation by signaling proteins SLP-76 and Syk. *Science.* 2003, Vol. 299, pp. 247-251.

30. **Saharinen P, Tammela T, Karkkainen MJ, Alitalo K.** Lymphatic vasculature: development, molecular regulation and role in tumor metastasis and inflammation. *Trends Immunol.* 2004, Vol. 25, pp. 387-395.

31. **Oliver G, Alitalo K.** The lymphatic vasculature: recent progress and paradigms. *Annu Rev Cell Dev Biol.* 2005, Vol. 21, pp. 457-483.

32. **Witte MH, Bernas MJ, Martin CP, Witte CL.** Lymphangiogenesis and lymphangiodysplasia: from molecular to clinical lymphology. *Microsc Res Tech.* 2001, Vol. 55, pp. 122-145.

33. **Grey, H.** *Anatomy of the human body, by Henry Gray.* 20th ed. Philadelphia: Lea & Febiger, 1918. http://www.bartleby.com/107/.

34. **Karpanen T, Alitalo K.** Molecular biology and pathology of lymphangiogenesis. *Annu Rev Pathol.* 2008, Vol. 3, pp. 367-397.

35. **Leak LV.** Studies on the permeability of lymphatic capillaries. *J Cell Biol.* 1971, Vol. 50, pp. 300-323.

36. **Leak LV.**. The structure of lymphatic capillaries in lymph formation. *Fed Proc.* 1976, Vol. 35, pp. 1863-1871.

37. **Marchetti C, Poggi P, Piacentini C, Calligaro A.** Scanning and transmission electron microscopy of rabbit heart lymphatic capillaries. *Lymphology.* 1991, Vol. 24, pp. 26-31.

38. **Cornford ME, Oldendorf WH.** Terminal endothelial cells of lymph capillaries as active transport structures involved in the formation of lymph in rat skin. *Lymphology.* 1993, Vol. 26, pp. 67-78.

39. **Leak LV, Burke JF.** Fine structure of the lymphatic capillary and the adjoining connective tissue area. *Am J Anat.* 1966, Vol. 118, pp. 785-809.

40. **Leak LV, Burke JF.**. Ultrastructural studies on the lymphatic anchoring filaments. *J Cell Biol.* 1968, Vol. 36, pp. 129-149.

41. **Gerli R, Ibba L, Fruschelli C.** Morphometric analysis of elastic fibers in human skin lymphatic capillaries. *Lymphology.* 1989, Vol. 22, pp. 167-172.

42. **Gerli R, Ibba L, Fruschelli C.**. A fibrillar elastic apparatus around human lymph capillaries. *Anat Embryol (Berl).* 1990, Vol. 181, pp. 281-286.

43. **Gerli R, Ibba L, Fruschelli C.**. Ultrastructural cytochemistry of anchoring filaments of human lymphatic capillaries and their relation to elastic fibers. *Lymphology.* 1991, Vol. 24, pp. 105-112.

44. **Schmid-Schönbein GW.** Microlymphatics and lymph flow. *Physiol Rev.* 1990, Vol. 70, pp. 987-1028.

45. **Aukland K, Reed RK.** Interstitial-lymphatic mechanisms in the control of extracellular fluid volume. *Physiol Rev.* 1993, Vol. 73, pp. 1-78.

46. **Vainionpää N, Bützow R, Hukkanen M, Jackson DG, Pihlajaniemi T, Sakai LY, Virtanen I.** Basement membrane protein distribution in LYVE-1-immunoreactive lymphatic vessels of normal tissues and ovarian carcinomas. *Cell Tissue Res.* 2007, Vol. 328, pp. 317-328.

47. **Hogan RD, Unthank JL.** Mechanical control of initial lymphatic contractile behavior in bat's wing. *Am J Physiol.* 1986, Vol. 251, pp. H357-H363.

48. **Grimaldi A, Moriondo A, Sciacca L, Guidali ML, Tettamanti G, Negrini D.** Functional arrangement of rat diaphragmatic initial lymphatic network. *Am J Physiol Heart Circ Physiol.* 2006, Vol. 291, pp. H876-H885.

49. **Petrova TV, Karpanen T, Norrmén C, Mellor R, Tamakoshi T, Finegold D, Ferrell R, Kerjaschki D, Mortimer P, Ylä-Herttuala S, Miura N, Alitalo K.** Defective valves and abnormal mural cell recruitment underlie lymphatic vascular failure in lymphedema distichiasis. *Nat Med.* 2004, Vol. 10, pp. 974-981.

50. **von der Weid PY, Zawieja DC.** Lymphatic smooth muscle: the motor unit of lymph drainage. *Int J Biochem Cell Biol.* 2004, Vol. 36, pp. 1147-1153.

51. **Mäkinen T, Norrmén C, Petrova TV.** Molecular mechanisms of lymphatic vascular development. *Cell Mol Life Sci.* 2007, Vol. 64, pp. 1915-1929.

52. **Alitalo K, Carmeliet P.** Molecular mechanisms of lymphangiogenesis in health and disease. *Cancer Cell.* 2002, Vol. 1, pp. 219-227.

53. **Yin X, Truty J, Lawrence R, Johns SC, Srinivasan RS, Handel TM, Fuster MM.** A critical role for lymphatic endothelial heparan sulfate in lymph node metastasis. *Mol. Cancer.* 2010, Vol. 9:316.

54. **Mazzoni MC, Skalak TC, Schmid-Schönbein GW.** Effects of skeletal muscle fiber deformation on lymphatic volumes. *Am J Physiol.* 1990, Vol. 259, pp. H1860-H1868.

55. **Levick JR, Michel CC.** Microvascular fluid exchange and the revised Starling principle. *Cardiovasc Res.* 2010, Vol. 87, pp. 198-210.

56. **Reed RK, Rubin K.** Transcapillary exchange: role and importance of the interstitial fluid pressure and the extracellular matrix. *Cardiovasc Res.* 2010, Vol. 87, pp. 211-217.

57. **Starling, EH.** On the Absorption of Fluids from the Connective Tissue Spaces. *J Physiol.* 1896, Vol. 19, pp. 312-326.

58. **Scallan, JP.** *Capillary Fluid Exchange, Regulation Functions and Pathology.* Morgan & Claypool Life Sciences,San Rafael (CA), 2010.

59. **Yuan SY, Rigor RR.** Regulation of Endothelial Barrier Function. San Rafael (CA): Morgan & Claypool Life Sciences, 2010.

60. **Schulte-Merker S, Sabine A, Petrova TV.** Lymphatic vascular morphogenesis in development, physiology, and disease. *J Cell Biol.* 2011, Vol. 193, pp. 607-618.

61. **Le Double AF.** Diaphragme. *Traité des variations du système musculaire de l'homme et leur signification au point de vue de l'anthropologie zoologique.* s.l. : Schleicher Frères publishers, Paris, France, 1897, Vol. 1, pp. 297–309.

62. **Mead J.** Functional significance of the area of apposition of diaphragm to rib cage [proceedings]. *Am Rev Respir Dis.* 1979, Vol. 119, pp. 31-32.

63. **Urmey WF, De Troyer A, Kelly KB, Loring SH.** Pleural pressure increases during inspiration in the zone of apposition of diaphragm to rib cage. *J Appl Physiol.* 1988, Vol. 65, pp. 2207-2212.

64. **Hostettler A, Nicolau SA, Rémond Y, Marescaux J, Soler L.** A real-time predictive simulation of abdominal viscera positions during quiet free breathing. *Prog Biophys Mol Biol.* 2010, Vol. 103, pp. 169-184.

65. **Boriek AM, Hwang W, Trinh L, Rodarte JR.** Shape and tension distribution of the active canine diaphragm. *Am J Physiol Regul Integr Comp Physiol.* 2005, Vol. 288, pp. R1021-1027.

66. **Loring SH, Mead J.** Action of the diaphragm on the rib cage inferred from a force-balance analysis. *J Appl Physiol.* 1982, Vol. 53, pp. 756-760.

67. **Mead J, Loring SH.** Analysis of volume displacement and length changes of the diaphragm during breathing. *J Appl Physiol.* 1982, Vol. 53, pp. 750-755.

68. **De Troyer A, Loring SH.** Actions of the respiratory muscles. Roussos C (Ed). *The Thorax, Lung Biology in Health and Disease Series.* Marcel Dekker, New York, USA, 1995, Vol. 85, pp. 535–564.

69. **Miserocchi G, Mariani E, Negrini D.** Role of the diaphragm in setting liquid pressure in serous cavities. *Respir Physiol.* 1982, Vol. 50, pp. 381-392.

70. **Negrini D, Pistolesi M, Miniati M, Bellina R, Giuntini C, Miserocchi G.** Regional protein absorption rates from the pleural cavity in dogs. *J Appl Physiol.* 1985, Vol. 58, pp. 2062-2067.

71. **Miserocchi G, Negrini D, Mukenge S, Turconi P, Del Fabbro M.** Liquid drainage through the peritoneal diaphragmatic surface. *J Appl Physiol.* 1989, Vol. 66, pp. 1579-1585.

72. **Negrini D, del Fabbro M, Venturoli D.** Fluid exchanges across the parietal peritoneal and pleural mesothelia. *J Appl Physiol.* 1993, Vol. 74, pp. 1779-1784.

73. **Negrini D, Mukenge S, Del Fabbro M, Gonano C, Miserocchi G.** Distribution of diaphragmatic lymphatic stomata. *J Appl Physiol.* 1991, Vol. 70, pp. 1544-1549.

74. **Wang NS.** Anatomy of the pleura. *Clin Chest Med.* 1998, Vol. 19, pp. 229-240.

75. **Negrini D, Del Fabbro M, Gonano C, Mukenge S, Miserocchi G.** Distribution of diaphragmatic lymphatic lacunae. *J Appl Physiol.* 1992, Vol. 72, pp. 1166-1172.

76. **Negrini D, Moriondo A.** Lymphatic anatomy and biomechanics. *J Physiol.* 2011, Vol. 589, pp. 2927-2934.

77. **Moriondo A, Bianchin F, Marcozzi C, Negrini D.** Kinetics of fluid flux in the rat diaphragmatic submesothelial lymphatic lacunae. *Am J Physiol Heart Circ Physiol.* 2008, Vol. 295, pp. H1182-H1190.

78. **Engelson ET, Skalak TC, Schmid-Schönbein GW.** The microvasculature in skeletal muscle. I. Arteriolar network in rat spinotrapezius muscle. *Microvasc Res.* 1985, Vol. 30, pp. 29-44.

79. **Skalak T, Schmid-Schöenbein G, Zweifach BW.** Lymph transport in skeletal muscle. *Tissue Nutrition and Viability.* New York: Springer-Verlag, 1986, pp. 243–261.

80. **Shinohara H.** Lymphatic system of the mouse diaphragm: morphology and function of the lymphatic sieve. *Anat Rec.* 1997, Vol. 249, pp. 6-15.

81. **Negrini D, Ballard ST, Benoit JN.** Contribution of lymphatic myogenic activity and respiratory movements to pleural lymph flow. *J Appl Physiol.* 1994, Vol. 76, pp. 2267-2274.

82. **Moriondo A, Grimaldi A, Sciacca L, Guidali ML, Marcozzi C, Negrini D.** Regional recruitment of rat diaphragmatic lymphatics in response to increased pleural or peritoneal fluid load. *J Physiol.* 2007, Vol. 579, pp. 835-847.

83. **Negrini D, Moriondo A, Mukenge S.** Transmural pressure during cardiogenic oscillations in rodent diaphragmatic lymphatic vessels. *Lymphat Res Biol.* 2004, Vol. 2, pp. 69-81.

84. **Moriondo A, Mukenge S, Negrini D.** Transmural pressure in rat initial subpleural lymphatics during spontaneous or mechanical ventilation. *Am J Physiol Heart Circ Physiol.* 2005, Vol. 289, pp. H263-H269.

85. **Negrini D, Del Fabbro M.** Subatmospheric pressure in the rabbit pleural lymphatic network. *J Physiol.* 1999, Vol. 520, pp. 761-769.

86. **Miserocchi G, Pistolesi M, Miniati M, Bellina CR, Negrini D, Giuntini C.** Pleural liquid pressure gradients and intrapleural distribution of injected bolus.J Appl Physiol. *1984.* 56, pp. 526-532.

87. **Zhang RZ, Gashev AA, Zawieja DC, Davis MJ.** Length-tension relationships of small arteries, veins, and lymphatics from the rat mesenteric microcirculation. *Am J Physiol Heart Circ Physiol.* 2007, Vol. 292, pp. H1943-H1952.

88. **Sakai LY, Keene DR, Morris NP, Burgeson RE.** Type VII collagen is a major structural component of anchoring fibrils. *J Cell Biol.* 1986, Vol. 103, pp. 1577-1586.

89. **Keene DR, Sakai LY, Lunstrum GP, Morris NP, Burgeson RE.** Type VII collagen forms an extended network of anchoring fibrils. *J Cell Biol.* 1987, Vol. 104, pp. 611-621.

90. **Burgeson RE, Lunstrum GP, Rokosova B, Rimberg CS, Rosenbaum LM, Keene DR.** The structure and function of type VII collagen. *Ann N Y Acad Sci.* 1990, Vol. 580, pp. 32-43.

91. **Chen M, Marinkovich MP, Veis A, Cai X, Rao CN, O'Toole EA, Woodley DT.** Interactions of the amino-terminal noncollagenous (NC1) domain of type VII collagen with extracellular matrix components. A potential role in epidermal-dermal adherence in human skin. *J Biol Chem.* 1997, Vol. 272, pp. 14516-14522.

92. **Rousselle P, Keene DR, Ruggiero F, Champliaud MF, Rest M, Burgeson RE.** Laminin 5 binds the NC-1 domain of type VII collagen. *J Cell Biol.* 1997, Vol. 138, pp. 719-728.

93. **Wiig H, Swartz MA.** Interstitial fluid and lymph formation and transport: physiological regulation and roles in inflammation and cancer. *Physiol Rev.* 2012, Vol. 92, pp. 1005-1060.

94. **Schad H, Flowaczny H, Brechtelsbauer H, Birkenfeld G.** The significance of respiration for thoracic duct flow in relation to other driving forces of lymph flow. *Pflugers Arch.* 1978, Vol. 378, pp. 121-125.

95. **Swartz MA, Berk DA, Jain RK.** Transport in lymphatic capillaries. I. Macroscopic measurements using residence time distribution theory. *Am J Physiol.* 1996, Vol. 270, pp. H324-H329.

96. **Parsons RJ, McMaster PD.** The effect of the pulse upon the formation and flow of lymph. *J Exp Med.* 1938, Vol. 68, pp. 353-376.

97. **Olszewski WL, Engeset A.** Intrinsic contractility of prenodal lymph vessels and lymph flow in human leg. *Am J Physiol.* 1980, Vol. 239, pp. H775-H783.

98. **McGeown JG, McHale NG, Thornbury KD.** Effects of varying patterns of external compression on lymph flow in the hindlimb of the anaesthetized sheep. *J Physiol.* 1988, Vol. 397, pp. 449-457.

99. **Mortimer PS, Simmonds R, Rezvani M, Robbins M, Hopewell JW, Ryan TJ.** The measurement of skin lymph flow by isotope clearance-reliability, reproducibility, injection dynamics, and the effect of massage. *J Invest Dermatol.* 1990, Vol. 95, pp. 677-682.

100. **Ikomi E, Zweifach BW, Schmid-Schonbein GW.** Fluid pressures in the rabbit popliteal afferent lymphatics during passive tissue motion. *Lymphology.* 1997, Vol. 30, pp. 13-23.

101. **Benoit JN, Zawieja DC, Goodman AH, Granger HJ.** Characterization of intact mesenteric lymphatic pump and its responsiveness to acute edemagenic stress. *Am J Physiol.* 1989, Vol. 257, pp. H2059-H2069.

102. **Li B, Silver I, Szalai JP, Johnston MG.** Pressure-volume relationships in sheep mesenteric lymphatic vessels in situ: response to hypovolemia. *Microvasc Res.* 1998, Vol. 56, pp. 127-138.

103. **Mendoza E, Schmid-Schönbein GW.** A model for mechanics of primary lymphatic valves. *J Biomech Eng.* 2003, Vol. 125, pp. 407-414.

104. **Swartz MA.** The physiology of the lymphatic system. *Adv Drug Deliv Rev.* 2001, Vol. 50, pp. 3-20.

105. **McHale NG, Roddie IC.** The effect of transmural pressure on pumping activity in isolated bovine lymphatic vessels. *J Physiol.* 1976, Vol. 261, pp. 255-269.

106. **Zawieja DC, Davis KL, Schuster R, Hinds WM, Granger HJ.** Distribution, propagation, and coordination of contractile activity in lymphatics. *Am J Physiol.* 1993, Vol. 264, pp. H1283-H1291.

107. **Armenio S, Cetta F, Tanzini G, Guercia C.** Spontaneous contractility in the human lymph vessels. *Lymphology.* 1981, Vol. 14, pp. 173-178.

108. **Davis MJ, Scallan JP, Wolpers JH, Muthuchamy M, Gashev AA, Zawieja DC.** Intrinsic increase in lymphangion muscle contractility in response to elevated afterload. *Am J Physiol Heart Circ Physiol.* 2012, Vol. 303, pp. H795-H808.

109. **Gnepp, DR.** Lymphatics. *Edema.* New York: Raven Press, 1984, pp. 263-298.

110. **Casley-Smith JR.** How the lymphatic system works. *Lymphology.* 1968, Vol. 1, pp. 77-80.

111. **Webb R.** Behavior of lymphatic vessels in the living bat. *Anat Rec.* 1944, Vol. 88, pp. 351-367.

112. **Barrowman JA.** *Physiology of the Gastrointestinal Lymphatic System.* London: Cambridge University Press, 1978.

113. **Schipp R.** Structure and ultrastructure of mesenteric lymphatic vessels. *New Trends in Basic Lymphology, Experentia Supplementum.* Collette J Birkhauser, Basel, Stuttgart, 1967, pp. 50-67.

114. **Breiteneder-Geleff S, Soleiman A, Kowalski H, Horvat R, Amann G, Kriehuber E, Diem K, Weninger W, Tschachler E, Alitalo K, Kerjaschki D.** Angiosarcomas express mixed endothelial phenotypes of blood and lymphatic capillaries: podoplanin as a specific marker for lymphatic endothelium. *Am J Pathol.* 1999, Vol. 154, pp. 385-394.

115. **Hosking B, Makinen T.** Lymphatic vasculature: a molecular perspective. *Bioessays.* 2007, Vol. 29, pp. 1192-1202.

116. **Hungerford JE, Little CD.** Developmental biology of the vascular smooth muscle cell: building a multilayered vessel wall. *J Vasc Res.* 1999, Vol. 36, pp. 2-27.

117. **Bergwerff M, Verberne ME, DeRuiter MC, Poelmann RE, Gittenberger-de Groot AC.** Neural crest cell contribution to the developing circulatory system: implications for vascular morphology? *Circ Res.* 1998, Vol. 82, pp. 221-231.

118. **Ohtani Y, Ohtani O.** Postnatal development of lymphatic vessels and their smooth muscle cells in the rat diaphragm: a confocal microscopic study. *Arch Histol Cytol.* 2001, Vol. 64, pp. 513-522.

119. **Mikawa T, Gourdie RG.** Pericardial mesoderm generates a population of coronary smooth muscle cells migrating into the heart along with ingrowth of the epicardial organ. *Dev Biol.* 1996, Vol. 174, pp. 221-232.

120. **Wilting J, Neeff H, Christ B.** Embryonic lymphangiogenesis. *Cell Tissue Res.* 1999, Vol. 297, pp. 1-11.

121. **Muthuchamy M, Gashev A, Boswell N, Dawson N, Zawieja D.** Molecular and functional analyses of the contractile apparatus in lymphatic muscle. *FASEB J.* 2003, Vol. 17, pp. 920-922.

122. **Rovner AS, Thompson MM, Murphy RA.** Two different heavy chains are found in smooth muscle myosin. *Am J Physiol.* 1986, Vol. 250, pp. C861-C870.

123. **Babij P, Periasamy M.** Myosin heavy chain isoform diversity in smooth muscle is produced by differential RNA processing. *J Mol Biol.* 1989, Vol. 210, pp. 673-679.

124. **Nagai R, Kuro-o M, Babij P, Periasamy M.** Identification of two types of smooth muscle myosin heavy chain isoforms by cDNA cloning and immunoblot analysis. *J Biol Chem.* 1989, Vol. 264, pp. 9734-9737.

125. **White S, Martin AF, Periasamy M.** Identification of a novel smooth muscle myosin heavy chain cDNA: isoform diversity in the S1 head region. *Am J Physiol.* 1993, Vol. 264, pp. C1252-1258.

126. **Khromov AS, Somlyo AV, Somlyo AP.** Nucleotide binding by actomyosin as a determinant of relaxation kinetics of rabbit phasic and tonic smooth muscle. *J Physiol.* 1996, Vol. 492, pp. 669-673.

127. **Lauzon AM, Tyska MJ, Rovner AS, Freyzon Y, Warshaw DM, Trybus KM.** A 7-amino-acid insert in the heavy chain nucleotide binding loop alters the kinetics of smooth muscle myosin in the laser trap. *J Muscle Res Cell Motil.* 1998, Vol. 19, pp. 825-837.

128. **Sweeney HL, Rosenfeld SS, Brown F, Faust L, Smith J, Xing J, Stein LA, Sellers JR.** Kinetic tuning of myosin via a flexible loop adjacent to the nucleotide binding pocket. *J Biol Chem.* 1998, Vol. 273, pp. 6262-6270.

129. **von der Weid PY, Muthuchamy M.** Regulatory mechanisms in lymphatic vessel contraction under normal and inflammatory conditions. *Pathophysiology.* 2010, Vol. 17, pp. 263-276.

130. **van Helden D F, von der Weid PY, Crowe MJ.** Electrophysiology of lymphatic smooth muscle. *Interstitium, Connective Tissue, and Lymphatics.* London: Portland Press, 1995, pp. 221-236.

131. **Azuma T, Ohhashi T, Sakaguchi M.** Electrical activity of lymphatic smooth muscles. *Proc Soc Exp Biol Med.* 1977, Vol. 155, pp. 270-273.

132. **Allen JM, McHale NG, Rooney BM.** Effect of norepinephrine on contractility of isolated mesenteric lymphatics. *Am J Physiol.* 1983, Vol. 244, pp. H479-H486.

133. **McHale NG, Allen JM.** The effect of external Ca^{2+} concentration on the contractility of bovine mesenteric lymphatics. *Microvasc Res.* 1983, Vol. 26, pp. 182-192.

134. **Atchison DJ, Rodela H, Johnston MG.** Intracellular calcium stores modulation in lymph vessels depends on wall stretch. *Can J Physiol Pharmacol.* 1998, Vol. 76, pp. 367-372.

135. **McHale NG, Meharg MK.** Co-ordination of pumping in isolated bovine lymphatic vessels. *J Physiol.* 1992, Vol. 450, pp. 503-512.

136. **McCloskey KD, Toland HM, Hollywood MA, Thornbury KD, McHale NG.** Hyperpolarisation-activated inward current in isolated sheep mesenteric lymphatic smooth muscle. *J Physiol.* 1999, Vol. 521, pp. 201-211.

137. **van Helden DF.** Pacemaker potentials in lymphatic smooth muscle of the guinea-pig mesentery. *J Physiol.* 1993, Vol. 471, pp. 465-479.

138. **van Helden DF, von der Weid PY, Crowe MJ.** Intracellular Ca^{2+} release: a basis for electrical pacemaking in lymphatic smooth muscle. *Smooth Muscle Excitation.* London: Academic Press, 1996, pp. 355-373.

139. **Toland HM, McCloskey KD, Thornbury KD, McHale NG, Hollywood MA.** Ca(2+)-activated Cl(-) current in sheep lymphatic smooth muscle. *Am J Physiol Cell Physiol.* 2000, Vol. 279, pp. C1327-C1335.

140. **Hargens AR, Zweifach BW.** Contractile stimuli in collecting lymph vessels. *Am J Physiol.* 1977, Vol. 233, pp. H57-H65.

141. **Ohhashi T, Takahashi N.** Acetylcholine-induced release of endothelium-derived relaxing factor from lymphatic endothelial cells. *Am J Physiol.* 1991, Vol. 260, pp. H1172-H1178.

142. **Ferguson MK, DeFilippi VJ.** Nitric oxide and endothelium-dependent relaxation in tracheobronchial lymph vessels. *Microvasc Res.* 1994, Vol. 47, pp. 308-317.

143. **von der Weid PY, Crowe MJ, Van Helden DF.** Endothelium-dependent modulation of pacemaking in lymphatic vessels of the guinea-pig mesentery. *J Physiol.* 1996, Vol. 493, pp. 563-575.

144. **von der Weid PY, Van Helden DF.** Beta-adrenoceptor-mediated hyperpolarization in lymphatic smooth muscle of guinea pig mesentery. *Am J Physiol.* 1996, Vol. 270, pp. H1687-H1695.

145. **Serbeniuk TsV, Lelekova TV.** [Participation of cGMP in inhibitory mechanisms of the center of amphibian lymph hearts]. *Fiziol Zh SSSR Im I M Sechenova.* 1997, Vol. 73, pp. 506-511.

146. **Rayner SE, Van Helden DF.** Evidence that the substance P-induced enhancement of pacemaking in lymphatics of the guinea-pig mesentery occurs through endothelial release of thromboxane A2. *Br J Pharmacol.* 1997, Vol. 121, pp. 1589-1596.

147. **von der Weid, PY.** Review article: lymphatic vessel pumping and inflammation-the role of spontaneous constrictions and underlying electrical pacemaker potentials. *Aliment Pharmacol Ther.* 2001, Vol. 15, pp. 1115-1129.

148. **Gashev AA, Davis MJ, Zawieja DC.** Inhibition of the active lymph pump by flow in rat mesenteric lymphatics and thoracic duct. *J Physiol.* 2002, Vol. 540, pp. 1023-1037.

149. **McHale NG, Roddie IC.** Pumping activity in isolated segments of bovine mesenteric lymphatics. *J Physiol.* 1975, Vol. 244, pp. 70P-72P.

150. **Ohhashi T, Azuma T, Sakaguchi M.** Active and passive mechanical characteristics of bovine mesenteric lymphatics. *Am J Physiol.* 1980, Vol. 239, pp. H88-H95.

151. **Reddy NP, Staub NC.** Intrinsic propulsive activity of thoracic duct perfused in anesthetized dogs. *Microvasc Res.* 1981, Vol. 21, pp. 183-192.

152. **Hayashi A, Johnston MG, Nelson W, Hamilton S, McHale NG.** Increased intrinsic pumping of intestinal lymphatics following hemorrhage in anesthetized sheep. *Circ Res.* 1987, Vol. 60, pp. 265-272.

153. **Eisenhoffer J, Lee S, Johnston MG.** Pressure-flow relationships in isolated sheep prenodal lymphatic vessels. *Am J Physiol.* 1994, Vol. 267, pp. H938-H943.

154. **Gashev AA, Orlov RS, Zawieja DC.** [Contractions of the lymphangion under low filling conditions and the absence of stretching stimuli. The possibility of the sucking effect]. *Ross Fiziol Zh Im I M Sechenova.* 2001, Vol. 87, pp. 97-109.

155. **Gashev AA.** [The pump function of the lymphangion and the effect on it of different hydrostatic conditions]. *Fiziol Zh SSSR Im I M Sechenova.* 1989, Vol. 75, pp. 1737-1743.

156. **Zawieja DC.** Contractile physiology of lymphatics. *Lymphat Res Biol.* 2009, Vol. 7, pp. 87-96.

157. **Lewis GP, Winsey NJ.** The action of pharmacologically active substances on the flow and composition of cat hind limb lymph. *Br J Pharmacol.* 1970, Vol. 40, pp. 446-460.

158. **Haddy FJ, Scott JB, Grega GJ.** Effects of histamine on lymph protein concentration and flow in the dog forelimb. *Am J Physiol.* 1972, Vol. 223, pp. 1172-1177.

159. **Amelang E, Prasad CM, Raymond RM, Grega GJ.** Interactions among inflammatory mediators on edema formation in the canine forelimb. *Circ Res.* 1981, Vol. 49, pp. 298-306.

160. **Svensjö E, Adamski SW, Su K, Grega GJ.** Quantitative physiological and morphological aspects of microvascular permeability changes induced by histamine and inhibited by terbutaline. *Acta Physiol Scand.* 1982, Vol. 116, pp. 265-273.

161. **Dobbins DE, Swindall BT, Haddy FJ, Dabney JM.** Blockade of histamine-mediated increases in microvascular permeability by H1- and H2-receptor antagonists. *Microvasc Res.* 1981, Vol. 21, pp. 343-350.

162. **Ferguson MK, Shahinian HK, Michelassi F.** Lymphatic smooth muscle responses to leukotrienes, histamine and platelet activating factor. *J Surg Res.* 1988, Vol. 44, pp. 172-177.

163. **Edery H, Lewis GP.** Kinin-forming activity and gistamine in lymph after tissue injury. *J Physiol.* 1963, Vol. 169, pp. 568-583.

164. **Ohhashi T, Kawai Y, Azuma T.** The response of lymphatic smooth muscles to vasoactive substances. *Pflugers Arch.* 1978, Vol. 375, pp. 183-188.

165. **Takahashi N, Kawai Y, Ohhashi T.** Effects of vasoconstrictive and vasodilative agents on lymphatic smooth muscles in isolated canine thoracic ducts. *J Pharmacol Exp Ther.* 1990, Vol. 254, pp. 165-170.

166. **Hashimoto S, Kawai Y, Ohhashi T.** Effects of vasoactive substances on the pig isolated hepatic lymph vessels. *J Pharmacol Exp Ther.* 1994, Vol. 269, pp. 482-488.

167. **Ferguson MK, Williams UE, Leff AR, Mitchell RW.** Heterogeneity of tracheobronchial lymphatic smooth muscle responses to histamine and 5-hydroxytryptamine. *Lymphology.* 1993, Vol. 26, pp. 113-119.

168. **Miyahara H, Kawai Y, Ohhashi T.** 5-Hydroxytryptamine-2 and -4 receptors located on bovine isolated mesenteric lymphatics. *J Pharmacol Exp Ther.* 1994, Vol. 271, pp. 379-385.

169. **Hollywood MA, Hutchinson SP, Aiken J, McHale NG.** Inhibition of spontaneous contractility of sheep lymphatics by serotonin. *J Physiol.* 1993, Vol. 459, p. 262P.

170. **Hollywood MA, McHale NG.** Serotonin has both inhibitory and excitatory effects on spontaneous contractility in isolated sheep mesenteric lymphatics. *J Physiol.* 1993, Vol. 467, p. 305P.

171. **Ferguson MK.** Modulation of lymphatic smooth muscle contractile responses by the endothelium. *J Surg Res.* 1992, Vol. 52, pp. 359-363.

172. **Yokoyama S, Ohhashi T.** Effects of acetylcholine on spontaneous contractions in isolated bovine mesenteric lymphatics. *Am J Physiol.* 1993, Vol. 264, pp. H1460-H1464.

173. **Reeder LB, Yang LH, Ferguson MK.** Modulation of lymphatic spontaneous contractions by EDRF. *J Surg Res.* 1994, Vol. 56, pp. 620-625.

174. **Mizuno R, Koller A, Kaley G.** Regulation of the vasomotor activity of lymph microvessels by nitric oxide and prostaglandins. *Am J Physiol.* 1998, Vol. 274, pp. R790-R796.

175. **Shirasawa Y, Ikomi F, Ohhashi T.** Physiological roles of endogenous nitric oxide in lymphatic pump activity of rat mesentery in vivo. *Am J Physiol Gastrointest Liver Physiol.* 2000, Vol. 278, pp. G551-G556.

176. **Ziegler-Heitbrock, HW.** The biology of the monocyte system. *Eur J Cell Biol.* 1989, Vol. 49, pp. 1-12.

177. **Johnston MG, Gordon JL.** Regulation of lymphatic contractility by arachidonate metabolites. *Nature.* 1981, Vol. 293, pp. 294-297.

178. **Johnston MG, Feuer C.** Suppression of lymphatic vessel contractility with inhibitors of arachidonic acid metabolism. *J Pharmacol Exp Ther.* 1983, Vol. 226, pp. 603-607.

179. **Rayner SE, Van Helden DF.** Evidence that the substance P-induced enhancement of pacemaking in lymphatics of the guinea-pig mesentery occurs through endothelial release of thromboxane A2. *Br J Pharmacol.* 1997, Vol. 121, pp. 1589-1596.

180. **Gao J, Zhao J, Rayner SE, Van Helden DF.** Evidence that the ATP-induced increase in vasomotion of guinea-pig mesenteric lymphatics involves an endothelium-dependent release of thromboxane A2. *Br J Pharmacol.* 1999, Vol. 127, pp. 1597-1602.

181. **Johnston MG, Kanalec A, Gordon JL.** Effects of arachidonic acid and its cyclo-oxygenase and lipoxygenase products on lymphatic vessel contractility in vitro. *Prostaglandins.* 1983, Vol. 25, pp. 85-98.

182. **Elias RM, Johnston MG.** Modulation of fluid pumping in isolated bovine mesenteric lymphatics by a thromboxane/endoperoxide analogue. *Prostaglandins.* 1988, Vol. 36, pp. 97-106.

183. **Chan AK, Vergnolle N, Hollenberg MD, von der Weid PY.** Proteinase-activated receptor 2 activation modulates guinea-pig mesenteric lymphatic vessel pacemaker potential and contractile activity. *J Physiol.* 2004, Vol. 560, pp. 563-576.

184. **Yokoyama S, Benoit JN.** Effects of bradykinin on lymphatic pumping in rat mesentery. *Am J Physiol.* 1996, Vol. 270, pp. G752-G756.

185. **Lobov GI, Pan'kova MN.** Heparin inhibits contraction of smooth muscle cells in lymphatic vessels. *Bull Exp Biol Med.* 2010, Vol. 149, pp. 4-6. 186. **Benoit JN.** Effects of alpha-adrenergic stimuli on mesenteric collecting lymphatics in the rat. *Am J Physiol.* 1997, Vol. 273, pp. R331-R336.

187. **Baluk P, Fuxe J, Hashizume H, Romano T, Lashnits E, Butz S, Vestweber D, Corada M, Molendini C, Dejana E, McDonald DM.** Functionally specialized junctions between endothelial cells of lymphatic vessels. *J Exp Med.* 2007, Vol. 204, pp. 2349-2362.

188. **Taylor AE, Gaar KA, Gibson H.** Effect of tissue pressure on lymph flow. *Biophys J.* 1970, Vol. 10, p. 45A.

189. **Guyton AC.** Interstitial fluid pressure. II. Pressure-volume curves of interstitial space. *Circ Res.* 1965, Vol. 16, pp. 452-460.

190. **Taylor AE, Gibson WH, Granger HJ, Guyton AC.** The interaction between intracapillary and tissue forces in the overall regulation of interstitial fluid volume. *Lymphology.* 1973, Vol. 6, pp. 192-208.

191. **Rockson SG.** Lymphedema. *Am J Med.* 2001, Vol. 110, pp. 288-295.

192. **Witte MH, Bernas MJ, Martin CP, Witte CL.** Lymphangiogenesis and lymphangiodysplasia: from molecular to clinical lymphology. *Microsc Res Tech.* 2001, Vol. 55, pp. 122-145.

193. **Wang Y, Oliver G.** Current views on the function of the lymphatic vasculature in health and disease. *Genes Dev.* 2010, Vol. 24, pp. 2115-2126.

194. **Karkkainen MJ, Saaristo A, Jussila L, Karila KA, Lawrence EC, Pajusola K, Bueler H, Eichmann A, Kauppinen R, Kettunen MI, Yla-Herttuala S, Finegold DN, Ferrell RE, Alitalo K.** A model for gene therapy of human hereditary lymphedema. *Proc Natl Acad Sci U S A.* 2001, Vol. 98, pp. 12677-12682.

195. **Saaristo A, Tammela T, Timonen J, Yla-Herttuala S, Tukiainen E, Asko-Seljavaara S, Alitalo K.** Vascular endothelial growth factor-C gene therapy restores lymphatic flow across incision wounds. *FASEB J.* 2004, Vol. 18, pp. 1707-1709.

196. **Saaristo A, Tammela T, Farkkilā A, Kärkkäinen M, Suominen E, Yla-Herttuala S, Alitalo K.** Vascular endothelial growth factor-C accelerates diabetic wound healing. *Am J Pathol.* 2006, Vol. 169, pp. 1080-1087.

197. **Saaristo A, Veikkola T, Tammela T, Enholm B, Karkkainen MJ, Pajusola K, Bueler H, Ylä-Herttuala S, Alitalo K.** Lymphangiogenic gene therapy with minimal blood vascular side effects. *J Exp Med.* 2002, Vol. 196, pp. 719-730.

198. **Brice G, Child AH, Evans A, Bell R, Mansour S, Burnand K, Sarfarazi M, Jeffery S, Mortimer P.** Milroy disease and the VEGFR-3 mutation phenotype. *J Med Genet.* 2005, Vol. 42, pp. 98-102.

199. **Finegold DN, Kimak MA, Lawrence EC, Levinson KL, Cherniske EM, Pober BR, Dunlap JW, Ferrell RE.** Truncating mutations in FOXC2 cause multiple lymphedema syndromes. *Hum Mol Genet.* 2001, Vol. 10, pp. 1185-1189.

200. **Ferrell RE.** Research perspectives in inherited lymphatic disease. *Ann N Y Acad Sci.* 2002, Vol. 979, pp. 39-51. discussion 76-79.

201. **Negrini D, Passi A, De Luca G, Miserocchi G.** Pulmonary interstitial pressure and proteoglycans during development of pulmonary edema. *Am J Physiol.* 1996, Vol. 270, pp. H2000-H2007.

202. **Negrini D, Tenstad O, Wiig H.** Interstitial exclusion of albumin in rabbit lung measured with the continuous infusion method in combination with the wick technique. *Microcirculation.* 2003, Vol. 10, pp. 153-165.

203. **Dreyer G, Norões J, Figueredo-Silva J, Piessens WF.** Pathogenesis of lymphatic disease in bancroftian filariasis: a clinical perspective. *Parasitol Today.* 2000, Vol. 16, pp. 544-548.

204. **Granger HJ.** Role of the interstitial matrix and lymphatic pump in regulation of transcapillary fluid balance. *Microvasc Res.* 1979, Vol. 18, pp. 209-216.

205. **Granger HJ, Kovalcheck S, Zweifach BW, Barnes GE.** Quantitative analysis of active lymphatic pumping. *Proceedings of VII Summer Computer Simulation Conference.* La Jolla, CA: Simulation Council, 1977.

206. **McHale NG, Roddie IC.** The effects of catecholamines on pumping activity in isolated bovine mesenteric lymphatics. *J Physiol.* 1983, Vol. 338, pp. 527-536.

207. **Zawieja DC, Greiner ST, Davis KL, Hinds WM, Granger HJ.** Reactive oxygen metabolites inhibit spontaneous lymphatic contractions. *Am J Physiol.* 1991, Vol. 260, pp. H1935-H1943.

208. **Padera TP, Stoll BR, So PT, Jain RK.** Conventional and high-speed intravital multiphoton laser scanning microscopy of microvasculature, lymphatics, and leukocyte-endothelial interactions. *Mol Imaging.* 2002, Vol. 1, pp. 9-15.

209. **Intaglietta M, Tompkins WR.** On-line measurement of microvascular dimensions by television microscopy. *J Appl Physiol.* 1972, Vol. 32, pp. 546-551.

210. **Halpern W, Kelley M.** In vitro methodology for resistance arteries. *Blood Vessels.* 1991, Vol. 28, pp. 245-251.

211. **Yip CY, Aggarwal SJ, Diller KR, Bovik AC.** Simultaneous multiple site arteriolar vasomotion measurement using digital image analysis. *Microvasc Res.* 1991, Vol. 41, pp. 73-83.

212. **Lee J, Jirapatnakul AC, Reeves AP, Crowe WE, Sarelius IH.** Vessel diameter measurement from intravital microscopy. *Ann Biomed Eng.* 2009, Vol. 37, pp. 913-926.

213. **Vas R, Eigler N, Miyazono C, Pfaff JM, Resser KJ, Weiss M, Nivatpumin T, Whiting J, Forrester J.** Digital quantification eliminates intraobserver and interobserver variability in the evaluation of coronary artery stenosis. *Am J Cardiol.* 1985, Vol. 56, pp. 718-723.

214. **Hoogeveen RM, Bakker CJ, Viergever MA.** MR phase-contrast flow measurement with limited spatial resolution in small vessels: value of model-based image analysis. *Magn Reson Med.* 1999, Vol. 41, pp. 520-528.

215. **Beux F, Carmassi S, Salvetti MV, Ghiadoni L, Huang Y, Taddei S, Salvetti A.** Automatic evaluation of arterial diameter variation from vascular echographic images. *Ultrasound Med Biol.* 2001, Vol. 27, pp. 1621-1629.

216. **Andriotis A, Zifan A, Gavaises M, Liatsis P, Pantos I, Theodorakakos A, Efstathopoulos EP, Katritsis D.** A new method of three-dimensional coronary artery reconstruction from X-ray angiography: validation against a virtual phantom and multislice computed tomography. *Catheter Cardiovasc Interv.* 2008, Vol. 71, pp. 28-43.

217. **Simons MA, Bastian BV, Bray BE, Dedrickson DR.** Comparison of observer and videodensitometric measurements of simulated coronary artery stenoses. *Invest Radiol.* 1987, Vol. 22, pp. 562-568.

218. **Fischer MJ, Uchida S, Messlinger K.** Measurement of meningeal blood vessel diameter in vivo with a plug-in for ImageJ. *Microvasc Res.* 2010, Vol. 80, pp. 258-266.

219. **McElroy M, Hayashi K, Garmy-Susini B, Kaushal S, Varner JA, Moossa AR, Hoffman RM, Bouvet M.** Fluorescent LYVE-1 antibody to image dynamically lymphatic trafficking of cancer cells in vivo. *J Surg Res.* 2009, Vol. 151, pp. 68-73.

220. **Unterberg A, Wahl M, Baethmann A.** Effects of bradykinin on permeability and diameter of pial vessels in vivo. *J Cereb Blood Flow Metab.* 1984, Vol. 4, pp. 574-585.

221. **Scallan JP, Huxley VH.** In vivo determination of collecting lymphatic vessel permeability to albumin: a role for lymphatics in exchange. *J Physiol.* 2010, Vol. 588, pp. 243-254.

222. **Armstrong JK, Wenby RB, Meiselman HJ, Fisher TC.** Armstrong JK, Wenby RB, Meiselman HJ, Fisher TC. *Biophys J.* 2004, Vol. 87, pp. 4259-4270.

223. **Lee AG, Arena CP, Beebe DJ, Palecek SP.** Development of macroporous poly(ethylene glycol) hydrogel arrays within microfluidic channels. *Biomacromolecules.* 2010, Vol. 11, pp. 3316-3324.

224. **Moriondo A, Boschetti F, Bianchin F, Lattanzio S, Marcozzi C, Negrini D.** Tissue contribution to the mechanical features of diaphragmatic initial lymphatics. *J Physiol.* 2010, Vol. 588, pp. 3957-3969.

225. **Gasheva OY, Zawieja DC, Gashev AA.** Contraction-initiated NO-dependent lymphatic relaxation: a self-regulatory mechanism in rat thoracic duct. *J Physiol.* 2006, Vol. 575, pp. 821-832.

226. **Bianchin F, Moriondo A, Marcozzi C, Solari E, Lattanzio S, Negrini D.** Dynamic recruitment of diaphragmatic submesothelial lymphatics. *Acta Physiologica.* 2010, Vol. 200, p. Supplement 681 :P104.

227. **Ohtani O, Ohtani Y.** Organization and developmental aspects of lymphatic vessels. *Arch Histol Cytol.* 2008, Vol. 71, pp. 1-22.

228. **Skalak TC, Schmid-Schönbein GW, Zweifach BW.** New morphological evidence for a mechanism of lymph formation in skeletal muscle. *Microvasc Res.* 1984, Vol. 28, pp. 95-112.

229. **Mehlhorn U, Davis KL, Burke EJ, Adams D, Laine GA, Allen SJ.** Impact of cardiopulmonary bypass and cardioplegic arrest on myocardial lymphatic function. *Am J Physiol.* 1995, Vol. 268, pp. H178-H183.

230. **Grider JR.** Reciprocal activity of longitudinal and circular muscle during intestinal peristaltic reflex. *Am J Physiol Gastrointest Liver Physiol.* 2003, Vol. 284, pp. G768-G775.

231. **Kockx MM, Wuyts FL, Buyssens N, Van Den Bossche RM, De Meyer GR, Bult H, Herman AG.** Longitudinally oriented smooth muscle cells in rabbit arteries. *Virchows Arch A Pathol Anat Histopathol.* 1993, Vol. 422, pp. 293-299.

232. **von der Weid PY, Rehal S, Dyrda P, Lee S, Mathias R, Rahman M, Roizes S, Imtiaz MS.** Mechanisms of VIP-induced inhibition of the lymphatic vessel pump. *J Physiol.* 2012, Vol. 590, pp. 2677-2691.

233. **Bohlen HG, Wang W, Gashev A, Gasheva O, Zawieja D.** Phasic contractions of rat mesenteric lymphatics increase basal and phasic nitric oxide generation in vivo. 2009, Am J Physiol Heart Circ Physiol., Vol. 297, pp. H1319-H1328.

234. **Pond CM.** Adipose tissue and the immune system. *Prostaglandins Leukot Essent Fatty Acids.* 2005, Vol. 73, pp. 17-30.

235. **Wang W, Hein TW, Zhang C, Zawieja DC, Liao JC, Kuo L.** Oxidized low-density lipoprotein inhibits nitric oxide-mediated coronary arteriolar dilation by up-regulating endothelial arginase I. *Microcirculation.* 2011, Vol. 18, pp. 36-45.

236. **Akl TJ, Nepiyushchikh ZV, Gashev AA, Zawieja DC, Cot GL.** Measuring contraction propagation and localizing pacemaker cells using high speed video microscopy. *J Biomed Opt.* 2011. 026016.

237. **Galanzha EI, Brill GE, Aizu Y, Ulyanov SS, Tuchin VV.** Speckle and Doppler Methods of Blood and Lymph Flow Monitoring. *Handbook of Optical Biomedical Diagnostics.* s.l. : Bellingham: SPIE Press, 2002, pp. 875-937.

238. **Galanzha EI, Tuchin VV, Zharov VP.** In vivo integrated flow image cytometry and lymph/blood vessels dynamic microscopy. *J Biomed Opt.* 2005, Vol. 10. 054018.

239. **Amerini S, Ziche M, Greiner ST, Zawieja DC.** Effects of substance P on mesenteric lymphatic contractility in the rat. *Lymphat Res Biol.* 2004, Vol. 2, pp. 2-10.

240. **Babu GJ, Warshaw DM, Periasamy M.** Smooth muscle myosin heavy chain isoforms and their role in muscle physiology. *Microsc Res Tech.* 2000, Vol. 50, pp. 532-540.

241. **Wang W, Nepiyushchikh Z, Zawieja DC, Chakraborty S, Zawieja SD, Gashev AA, Davis MJ, Muthuchamy M.** Inhibition of myosin light chain phosphorylation decreases rat mesenteric lymphatic contractile activity. *Am J Physiol Heart Circ Physiol.* 2009, Vol. 297, pp. H726-H734.

242. **Bolton TB.** Mechanisms of action of transmitters and other substances on smooth muscle. *Physiol Rev.* 1979, Vol. 59, pp. 606-718.

243. **Gordon AM, Homsher E, Regnier M.** Regulation of contraction in striated muscle. *Physiol Rev.* 2000, Vol. 80, pp. 853-924.

244. **Webb RC.** Smooth muscle contraction and relaxation. *Adv Physiol Educ.* 2003, Vol. 27, pp. 201-206.

245. **Elmqvist D, Thesleff S.** A study of acetylcholine induced contractures in denervated mammalian muscle. *Acta Pharmacol Toxicol (Copenh).* 1960, Vol. 17, pp. 84-93.

246. **Crowe MJ, von der Weid PY, Brock JA, Van Helden DF.** Co-ordination of contractile activity in guinea-pig mesenteric lymphatics. *J Physiol.* 1997, Vol. 500, pp. 235-244.

247. **Granger H, Laine G, Barnes G, Lewis R.** Dynamics and control of transmicrovascular fluid exchange. *Edema.* s.l. : New York: Raven Press, 1984, pp. 189-228.

248. **Olszewski, WL.** The lymphatic system in body homeostasis: physiological conditions. *Lymphat Res Biol.* 2003, Vol. 1, pp. 11-21.

249. **Alitalo K, Tammela T, Petrova TV.** Lymphangiogenesis in development and human disease. *Nature.* 2005, Vol. 438, pp. 946-953.

250. **Harvey NL.** The link between lymphatic function and adipose biology. *Ann N Y Acad Sci.* 2008, Vol. 1131, pp. 82-88.

251. **Allen L, Weatherford T.** Role of fenestrated basement membrane in lymphatic absorption from peritoneal cavity. *Am J Physiol.* 1959, Vol. 197, pp. 551-554.

252. **Leak LV, Rahil K.** Permeability of the diaphragmatic mesothelium: the ultrastructural basis for "stomata". *Am J Anat.* 1978, Vol. 151, pp. 557-593.

253. **Ohtani Y, Ohtani O, Nakatani T.** Microanatomy of the rat diaphragm: a scanning electron and confocal laser scanning microscopic study. *Arch Histol Cytol.* 1993, Vol. 56, pp. 319-328.

254. **Margaris KN, Black RA.** Modelling the lymphatic system: challenges and opportunities. *J R Soc Interface.* 2012, Vol. 9, pp. 601-612.

255. **Davis MJ, Rahbar E, Gashev AA, Zawieja DC, Moore JE Jr.** Determinants of valve gating in collecting lymphatic vessels from rat mesentery. *Am J Physiol Heart Circ Physiol.* 2011, Vol. 301, pp. H48-H60.

256. **Gashev AA, Davis MJ, Gasheva OY, Nepiushchikh ZV, Wang W, Dougherty P, Kelly KA, Cai S, Von Der Weid PY, Muthuchamy M, Meininger CJ, Zawieja DC.** Methods for lymphatic vessel culture and gene transfection. *Microcirculation.* 2009, Vol. 16, pp. 615-628.

257. **Gashev AA.** Physiologic aspects of lymphatic contractile function: current perspectives. *Ann N Y Acad Sci.* 2002, Vol. 979, pp. 178-187.

258. **Gashev AA, Davis MJ, Delp MD, Zawieja DC.** Regional variations of contractile activity in isolated rat lymphatics. *Microcirculation.* 2004, Vol. 11, pp. 477-492.